mechanism) with the microthermometry findings of Cooper and Lloyd [99, 100]. This fact appears to have influenced Voutsinos and Judd towards the ready acceptance of these results and towards the rejection of Judd's earlier work. The reasons for this rejection are in fact inadequately argued. The phrase 'failure of the optical filter to properly isolate the (mercury yellow) spectral lines ... from the remainder of the spectrum' could imply the presence of transmission side-bands in the filter; this could, analogously to white-light illumination, have given a reduction in the number of fringes, but it seems unlikely that such a filter could have been used. Alternatively, the words could imply a filter of too high a bandwidth; this (as shown in Section 6.3.4) would have given successively weaker fringes in the inner (thinner) microlayer region only; no such effect was, however, observed.

The monochromaticity defects here discussed were certainly absent in the present study. Side-bands in the filter were blocked to less than 0,001 per cent transmittance, and the bandwidth (as analysed in Section 6.3.4 and Appendix 9) was sufficient for fringes to be visible with essentially undiminished contrast up to a microlayer thickness of 1 μm and to be detectable up to a thickness of approximately 4 μm. If the microlayer in the present study had had an edge thickness of the order of 10 μm (as Voutsinos and Judd's remarks imply), then six fully bright fringes would have occurred close to the inner microlayer edge, a further 18 of successively diminishing visibility would have occurred in the inner region (less than half-way to the edge), and none would have been visible in the outer region. Strong and roughly equally spaced fringes (typically four maxima) were, however, observed over the entire microlayer area.

Similar reasoning dismisses an argument favouring thick microlayer which might be derived from the interference study of Katto and Shoji [175]. The study dealt with liquid

layers formed beneath injected, flattened air bubbles and revealed irregular fringe spacing such that some fringes appeared to stand out more clearly than others. It occurred to the author that a similar effect might have arisen in the present study and that only the clearest fringes were recorded and possibly numerous intermediate ones lost. Had this been the case, however, the fringe visibility would (with a now thick layer) still have been limited to the region near the inner microlayer edge. Since this was not observed the argument is ruled out.

No other reasons for a reduction in the number of maximum-reflectance fringes from 60 (the figure required for a microlayer thickness of 10 μm) to four can be found to apply in the present study.

Faced with this dilemma, the author turned for an opinion to an optics consultant, Dr J H Talbot [207]. Talbot, after a brief examination of the present work could similarly find no obvious optical defect that would have led to the suggested erroneously low fringe count. Concerning the study of Voutsinos and Judd, however, he expressed reservations on the laser technique and in particular on the evident omission of a spatial filter. The laser used by Voutsinos and Judd, the Spectra Physic Model 125A, was in his experience incapable of unimodal operation, irrespective of tuning; thus in the absence of spatial filtration, multimode interference would have occurred and additional and confusing fringes could have been present (see Figure 9.14). The correct procedure for obtaining a clean interferometry beam would have consisted of the tuning of the laser to maximum output in the axial mode, the converging of the overall beam onto a spatial filter (a pinhole of a few μm diameter), the tuning of the filter so as to block the off-axis modes, and the recollimation of the clean output. This procedure was clearly omitted by Voutsinos and Judd; no mention of it appears in their text, and no modification of the laser output

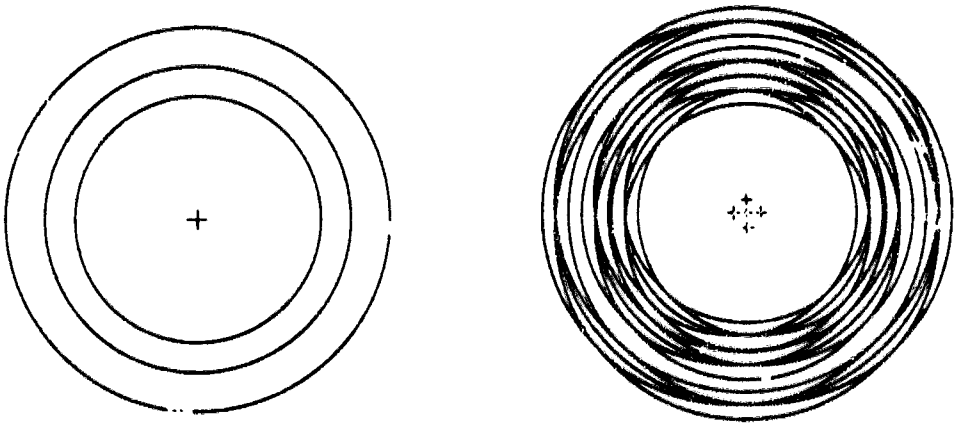

SINGLE - MODE FRINGE PATTERN

EQUIVALENT MULTIMODE PATTERN (4 off-axis modes)

FIG. 9.14 EFFECT OF MULTIMODE LASER OPERATION

(other than beam expansion) is shown in the apparatus sketch. The strength of the consequent multimode effects would have been dependent on laser tuning. If, for example, the laser had been tuned for maximum power, then four off-axis modes of equal strength (and a weaker axial mode) would have been present and the multimode fringes would have been strong.

These remarks are not intended to suggest that the work of Voutsinos and Judd is invalid, but rather that it is not sufficiently above criticism to invalidate the present work.

9.6 CLOSURE

The opening sections of this chapter presented a numerical analysis of the rate of evaporation of thin microlayers (as observed in this study), but with the microlayer assumed stagnant. The analysis suggested the presence of liquid replenishment, independently of the optical evidence of Chapter 8, and further, showed that the evaporation of the replenished microlayers might well have been a significant contributor to the total vapour flow into bubbles. Thus the optical measurements of the present study were reconciled with the microthermometry findings of Cooper and Lloyd [99, 100].

Next, the overall forces acting on the observed bubbles were analysed. Buoyancy forces, tending to lift the bubbles off their microlayers were found to be predominant. The pattern of bubble forces was thus demonstrated as being compatible with a microlayer inflow or replenishment mechanism.

The microlayer thickness measurements of the present study were then compared with those of Judd [150] and of Voutsinos and Judd [151]. The work of Judd was shown to have been founded on the early publication of portions of the present work [152] and to have given essentially the same results. The study of Voutsinos and Judd, however, deriving from laser

rather than conventional interferometry, was found to give radically different results, with microlayer thicknesses exceeding by an order of magnitude those here reported. The rejection (on the grounds of a monochromaticity error) of Judd's earlier work was shown to have been unsatisfactorily argued and the allegation that a similar error might have occurred in the author's published work [152] (and thus in this thesis) was answered. No monochromaticity error, nor other optical defects that could have resulted in the suggested low fringe count could be found. The examination of Voutsinos and Judd's work, however, revealed imperfections of laser technique which could have led to extraneous fringes and thus to erroneously high microlayer thicknesses. It was noted, on the other hand, that the measurements of Voutsinos and Judd were in more direct agreement (without the invocation of microlayer replenishment) with the findings of surface microthermometry studies.

It would appear that the conflict between the two sets of interference measurements can only be resolved by further, similar work employing a correctly operated laser. The author is, for reasons already stated, in no position to conduct such work. Should such work be forthcoming and Voutsinos and Judd be proved correct, then the present study could be seen as having initiated an ultimately successful experimental approach.

CHAPTER 10

SUMMARY AND CONCLUSIONS

Interim summaries and concluding comments have been given at various points throughout this work. It would now be well, even at the risk of some repetition, to gather the most important of these together and to emphasise the contributions made.

Part 1 of this thesis provided a broad overview of the mechanism of nucleate pool boiling and applied the findings to the problem of correlating and predicting such heat transfer.

An interpretive review of the literature was presented in which the chief transfer processes constituting the boiling mechanism were identified and, where possible, assessed quantitatively. The treatment was largely confined to saturated pool boiling in the presence of isolated bubbles and, because of the nature of the published material, to terrestrial gravity and to atmospheric and lower pressures.

It was shown that in the region of isolated bubbles each bubble has associated with it an 'area of bubble influence' and that, as an approximation, the boiling process may be considered as entirely limited to such areas. The remaining surface may thus be considered as supporting undisturbed natural convection.

Each area of bubble influence was shown to support a complex pattern of primary transfer processes at the heating surface and subsequent redistributions of energy in the fluid phases. Mean rates of heat transfer, q^i, were defined for

each transfer process or for related groups of such processes. The chief features of their breakdown and interrelation were:

(a) q_T^i, the total area-of-influence heat transfer rate, is resolved into q_{ML}^i, the heat flow into the liquid microlayer (there causing microlayer evaporation) and into further primary surface-to-liquid heat flows which build up the thermal layer.

(b) These latter heat flows are redistributed into q_{BWE}^i, the heat transferred due to evaporation at the walls of attached bubbles, and q_{BC}^i, the heat transferred from the thermal layer into the liquid bulk by bubble-induced convection.

(c) q_{ML}^i and q_{BWL}^i together constitute the latent heat transport q_{LH}^i, that is, the heat transfer due to evaporation at all surfaces of the attached bubble.

(d) The primary surface-to-liquid heat transfer processes in the area of bubble influence thus manifest themselves partly as latent heat transport and partly as bubble-induced convection:

$$q_T^i = q_{LH}^i + q_{BC}^i \qquad (10.1)$$

(e) In subcooled boiling q_{LH}^i is redistributed into $q_{CONDENS}^i$, that portion of q_{LH}^i which recondenses from attached bubbles, and q_{LHvis}^i, the remaining portion of q_{LH}^i which visibly detaches from the surface as vapour.

The review showed that the concept of negligible latent heat transport ($q_{LH}^i << q_T^i$) derives from early boiling studies in which not q_{LH}^i, but quantities obscurely related to it were measured. In particular it derives from subcooled boiling

studies in which q^i_{LHvis} was found to be negligible. Neglect of the term $q^i_{CONDENS}$, loose semantics and arbitrary extrapolation led to the widespread application of the concept to all conditions of nucleate boiling.

It was shown that with q^i_{LH} considered negligible, bubble-induced convection became generally accepted as the predominant thermal-layer-to-bulk heat flow ($q^i_{BC} \sim q^i_T$). Some of the many resulting heat transfer models and correlations were reviewed and their limitations and (when present) valid features noted.

A review of experimental studies on the thermal boundary layer was given. This indicated (at least for saturated and near-saturated boiling) that q^i_{BC}, while significant, does not constitute the predominant fraction of q^i_T. The primary heat transfer processes building up the thermal layer in the area of bubble influence were found to be convective and dependent (in a complex manner) on bubble movement.

Determinations of the latent heat transport in the area of bubble influence were reviewed. For saturated boiling both indirect arguments and bubble measurements indicate that the previously discredited latent heat transport is in fact the major mode of heat transfer from the thermal layer into the bulk. The measurements cover a wide range of test conditions, heating surfaces and fluids. Those conducted at terrestrial and reduced gravities generally indicate a latent heat transport contribution of at least 70 per cent:

$$q^i_{LH} \geq 0,7\ q^i_T \qquad (10.2)$$

At multi-g accelerations, however, the contribution falls off.

For the case of subcooled boiling indirect estimates of the term $q^i_{CONDENS}$ were shown to suggest strongly, if not

conclusively, that q^i_{LH} ($= q^i_{LHvis} + q^i_{CONDENS}$) is of comparable magnitude to q^i_T.

In saturated boiling at terrestrial gravity the total boiling heat flux was shown to be approximated closely by the sum of the latent heat flux and of the undisturbed natural convection heat flux:

$$(q/A)_T = (q/A)_{LH} + (q/A)_{NC} \qquad (10.3)$$

Thus the mean heat flow q^i_{BC}, due to intermittent bubble-convection, is of approximately the same magnitude as the natural convection heat flow were it to operate undisturbed over the entire area of bubble influence.

The correlation of nucleate boiling heat transfer should ideally be based on the primary surface-to-liquid heat transfer processes in the area of bubble influence. These processes were shown to be of such intricacy that their models have become analysable only when simplified to the point where they no longer relate to reality. An examination of the 'bulk convection' correlations illustrated this difficulty.

An alternative approach was suggested. Its basis was the predominance of latent heat transport in the area of bubble influence and the approximation of bubble-induced convection by natural convection (equations 10.2 and 10.3).

The resulting model was analysed without recourse to further mechanistic assumptions. Coupled with a method of surface characterisation similar to that of Mikic and Rohsenow [47], this led to a new and realistic heat transfer correlation for saturated pool boiling. Comparisons with experimental data were presented. These indicated that the correlation allows the prediction of boiling curves q/A versus ΔT_{sat}

at any pressure, provided that at least one boiling curve for the same surface, or preferably the same surface-liquid combination, is available as a reference. Although derived in terms of isolated bubbles, that is, low heat flux, the correlation continues to hold throughout the linear range of log-log boiling curves. Its validity is probably restricted to terrestrial gravity and to non-metallic liquids.

With the importance of latent heat transport thus established, Part 2 of the thesis took a detailed view of one of the component processes of latent heat transport, namely micro-layer evaporation.

A review of previous microlayer work was given. This revealed the existence of only one set of direct measurements of microlayer geometry, by Sharp [104], but these had been conducted on artificially flattened bubbles of unknown growth rate. The review thus pointed to a need for synchronised optical records, at various conditions of normal boiling, of: (a) microlayer shape and thickness versus time, and (b) overall bubble growth and detachment. Such measurements, it was argued, would lead to an assessment of the microlayer contribution q^i_{ML}/q^i_T.

The apparatus built up to permit such measurements was described. Its main, and largely novel, features were: a transparent electrically heated surface which formed the floor of a boiling tank, high-speed ciné interference photography from below which provided details of microlayer geometry, and an image reflection system which caused the bubble profile view and the microlayer view to appear side by side and on the same frame of film. Some unusual techniques in the preparation of the heating surface were described in detail.

An analysis of the optics of the interference system was

given. It's most important findings were that only a limited range of liquid refractive indices, and thus test liquids, gave acceptable fringe contrast (methanol and ethanol were suitable), and that the maximum measurable microlayer thickness was approximately 4 μm.

The experimental techniques, data processing and interpretation were described.

Results for seven bubble cycles were presented. These covered the liquids methanol and ethanol, pressures of 24 to 43 kN/m^2, overall heat fluxes of 30 to 70 kW/m^2 and bulk subcooling of 0 to 20 K. The bubbles displayed involution upon departure and the emission of secondary vapour columns and bursts of secondary bubbles. Explanations of these all but unknown phenomena were furnished.

The main results consisted of histories of microlayer geometry, of bubble volume and of dimensions characterising bubble shape. In all cases microlayers were found to be of submicron thickness; microlayer thinning (visible evaporation) was restricted to the inner layer edge with the thickness elsewhere remaining constant or increasing with time, and the contribution of this visible evaporation to the total vapour flow into bubbles (that is, to latent heat transport) was found to be negligible. These findings are in apparent conflict with the deductions of surface-thermometry studies and in particular with those of Cooper and Lloyd [99, 100]. The microlayer thickening, however, demonstrated that liquid in-flow or replenishment occurred simultaneously with the evaporation process.

This replenishment was investigated further by means of a numerical analysis of the rate of evaporation of stagnant microlayers having thicknesses as observed in this study. Extensions to the Crank-Nicolson technique to cover moving-boundary evaporation problems were described. The analysis,

firstly, suggested the presence of liquid replenishment independently of the optical evidence, and secondly, showed that the evaporation of continuously replenished microlayers (q^i_{ML}) might well have been a significant contributor to the total vapour flow into bubbles (q^i_{LH}). The optical measurements of the present study were thus reconciled with the surface thermometry findings of Cooper and Lloyd [99, 100].

The mechanism of liquid flow within the microlayer was not examined. Photographic results were, however, presented which indicate that the forces causing microlayer in-flow are of the same order of magnitude as those associated with bubble deformation and departure.

The overall forces of inertia, surface tension, viscosity and buoyancy were thus evaluated for the bubbles observed in this study. Except in the very early stages of bubble growth the buoyancy forces, tending to lift bubbles continuously off their microlayers, were found to predominate. The pattern of bubble forces was thus shown to be compatible with microlayer replenishment.

Finally, the microlayer measurements of this study were compared with those of Judd [150] and of Voutsinos and Judd [151]. The studies were found to have derived from published portions of the present work [152] and when employing conventional interferometry [150] to have given essentially the same result. With laser interferometry [151], however, very much thicker microlayers had resulted. The question of a possible optics error either in the present study or in the laser study of Voutsinos and Judd was analysed in some detail, but could not be finally resolved.

10.1 SUGGESTIONS FOR FUTURE WORK

This study has of necessity touched upon numerous topics requiring attention. Only those considered most urgent and linked most closely with the main conclusions are here mentioned:

It is suggested that the assessment of latent heat transport by direct bubble measurements be extended to pressures higher than atmospheric.

The heat transfer correlation of Chapter 3 should be further tested and the effect of various heater materials and of fouling on the surface-characterisation constants K and m should be investigated.

The dynamics of replenishment flow into and within the microlayer should be analysed.

The numerical analysis of microlayer conduction and evaporation should be extended to take replenishment flow into account.

Most important, the conflict between the microlayer measurements of the present study and those of Voutsinos and Judd [151] should be resolved by similar work employing a correctly operated laser.

With the interference technique then firmly established it should, in combination with the bubble profile reflection technique, be applied to a wider range of fluids, pressures and flow conditions.

APPENDIX 1

VAPOUR CAVITY COLLAPSE WITH LIQUID JET FORMATION

In highly subcooled nucleate boiling the collapse of bubbles on or near the heating surface is followed by the ejection of a hot liquid slug into the pool bulk. It is of interest to speculate on the mechanism of slug ejection, by drawing upon the results of cavitation studies.

An excellent review of cavitation hydrodynamics as well as experimental work relevant to the present problem is provided by Benjamin and Ellis [60]. They show that cavitation bubbles imploding spherically in an infinite field (Rayleigh implosion), typically produce pressure pulses of the order of $10^6 kN/m^2$. The amplitude of such pressure waves, however, falls off very rapidly with radial distance. If now a wall is present at such a distance that the pressure is still appreciable, the collapse is no longer spherical and powerful effects, additional to normal Rayleigh implosion, can arise: For imploding vapour cavities in contact with or close proximity to a wall, the liquid inflow can become distorted such that a liquid jet, directed towards the wall, is formed on the cavity surface. Such jets can be clearly seen in the high-speed photographs of Benjamin and Ellis [60].

Plesset and Chapman [212] have presented a theoretical analysis of such collapse. Figure A1.1, taken from their work, shows the outline in section of successive stages of collapse for (a) a bubble in contact with a wall, and (b) a bubble initially half its radius from the wall at the closest point. Plesset and Chapman provided theoretical maximum jet tip velocities as a function of time (and hence cavity shape) for a particular value of $\Delta P/\rho_L$. (ΔP is the constant pressure difference between the liquid outside and the vapour inside the bubble). Further they showed that

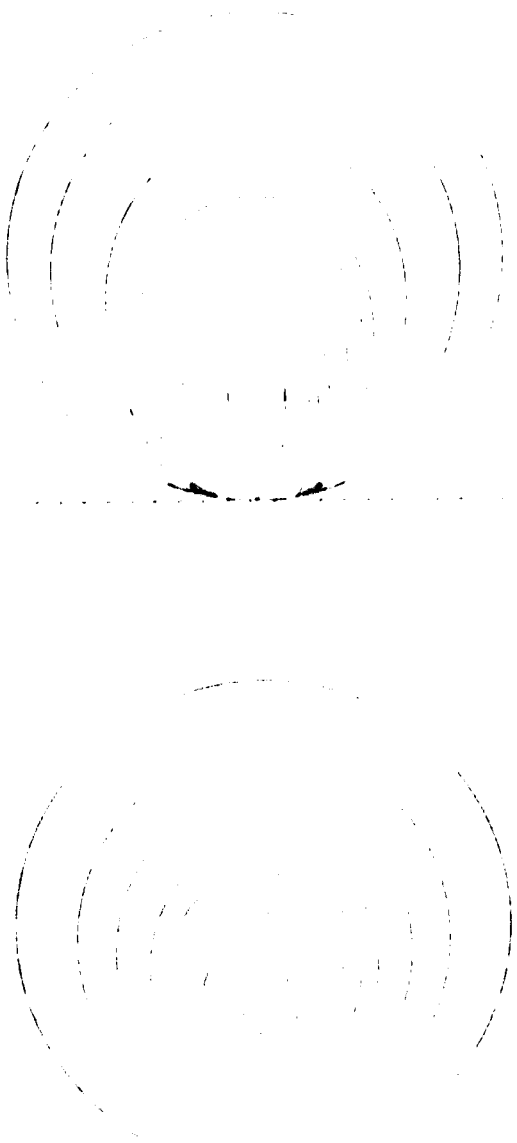

(a)

(b)

FIG. A1.1 SUCCESSIVE STAGES OF COLLAPSE OF CAVITATION BUBBLE
(a) in contact with wall
(b) in close proximity to wall
(Theory of Plesset and Chapman [212])

the jet velocities scale with $(\Delta P/\rho_L)^{\frac{1}{2}}$, thus allowing the calculation of velocities for other pressures.

Assuming for the moment that the above collapse mechanism operates in highly subcooled nucleate boiling, we now estimate the order of magnitude of the jet velocities under the conditions of Gunther's forced convection boiling study of water [74]. The required ΔP values are obtainable from Bankoff and Mikesell's analysis [69] of Gunther's data. The analysis shows that ΔP is essentially constant throughout each bubble life, and that in the subcooling range of 45 to 100 K its value for all bubbles lies between 2,9 and 4,5 kN/m^2. The jet velocity is here determined for the intermediate value of 3,7 kN/m^2. Plesset and Chapman's data [212] show that for an attached bubble the jet velocity at the instant it strikes the surface, is 128 m/s for a value of $\Delta P/\rho_L$ of (100 kN/m^2)/(1 g/cm^3). With an assumed ρ_L of 1 g/cm^3 for Gunther's work, the jet velocity is $128 \times (0,037)^{0,5}$, that is 24,6 m/s. Thus bubbles collapsing during the highly subcooled boiling of water could possibly direct liquid jets of roughly this magnitude towards the surface. The observed slugs of liquid ejected from the surface might then arise from the reflection of the collapse jets.

It is not possible, even from the detailed photographs of Bähr [57], to ascertain whether or not jet-type collapse does occur in subcooled boiling. The elongation of the bubble prior to involution (stage 3, Figure A1.1a) certainly does not take place. Jet formation is, however, not ruled out. Figure 5 in Benjamin and Ellis' paper [60] shows severe departure from the theoretical collapse geometry, yet an involution jet is definitely present.

Strictly speaking, the collapse jet analysis is valid only for bubbles initially at rest and in the absence of extraneous asymmetric effects (e.g. gravity, tangential liquid velocity). It is not known whether real boiling departs

sufficiently from the ideal conditions to invalidate the analysis. Even if it does, there exist further possibilities, reviewed by Benjamin and Ellis, whereby effects additional to pure Rayleigh collapse might arise.

Jet-type bubble collapse in subcooled boiling is here suggested merely as a possibility, with the further suggestion that a closer look at cavitation collapse might prove profitable.

APPENDIX 2

SATURATED-BOILING STUDY OF RALLIS AND JAWUREK

This appendix reproduces the published saturated-boiling study of Rallis and Jawurek [2]. It provides, firstly, the experimental details of the latent heat transport measurements discussed in Section 2.6.5, secondly, a study on the interrelation of bubble frequency and departure volume, and thirdly, the beginnings of the nucleation correlation given in Section 3.2.1.

Figure 6 contains a minor plotting error which has been corrected in Figure 2.19, Chapter 2.

The notation and references are separate from those of the remainder of the thesis.

333.

Int. J. Heat Mass Transfer. Vol. 7, pp. 1051–1068. Pergamon Press 1964. Printed in Great Britain

LATENT HEAT TRANSPORT IN SATURATED NUCLEATE BOILING

C. J. RALLIS* and H. H. JAWUREK†

Department of Mechanical Engineering,
University of the Witwatersrand, Johannesburg, South Africa

(*Received* 4 *December* 1963 *and in revised form* 15 *April* 1964)

Abstract—Experimental work on the nucleate pool boiling of water at saturation is reported. This indicates that latent heat transport, $(q/A)_{LH}$, is at all stages significant. The ratio $(q/A)_{LH}/(q/A)_{TOT}$ increases steadily with increasing heat flux and appears to tend to unity as $(q/A)_{TOT}$ tends towards burnout. Latent heat transport and convection together account for the total flux in saturated boiling.

The basic parameters entering into the formulation of $(q/A)_{LH}$, that is, the product of bubble frequency and bubble volume at departure, fV_d, and the bubble source concentration, N, are further investigated.

It is shown that most published findings on the parameter fV_d are inapplicable to heat-transfer correlations due to the incorrect definition of means. Experimental results show that (i) the (arithmetic) mean product $\overline{fV_d}$ increases with flux, and (ii) at a particular flux the product fV_d is approximately the same for each bubble source.

The data for N on water and on organics boiling at various pressures indicate that the relation

$$(q/A) = \text{constant}\ N^{n}$$

where $n \simeq 0.5$ appears to hold only in the region of isolated bubbles.

A hypothesis is evolved and confirmed experimentally according to which the curve of N vs ΔT_{sat} takes the form of a cumulative frequency distribution.

Analysis and confirmatory experiments show that nucleation and nucleate boiling cannot be made to proceed indefinitely at lower and lower pressures, for a particular surface–liquid combination a pressure exists which marks the threshold of a hitherto unrecognized regime of unstable nucleate boiling. At lower pressures the nucleate regime is altogether absent.

NOMENCLATURE

a,	constant;
A,	heat-transfer area [ft^2];
b,	constant;
c, C,	constants;
D_d,	equivalent spherical bubble diameter at departure [ft];
f,	bubble frequency [s^{-1} or h^{-1}];
f_i,	bubble frequency of individual source [s^{-1} or h^{-1}];
f,	mean (arithmetic, unless otherwise stated) of f_i;
$\overline{fV_d}$,	arithmetic mean of products $f_i V_{di}$;
g,	gravitation acceleration [ft h^{-2}];
G_d,	mass velocity of vapour in departing bubbles [lb$_m$ h ft^{-2}];
m,	constant;
n,	constant;
n_s,	number of bubble sources on heat-transfer surface;
$N = n_s/A$,	bubble source concentration [ft^{-2}];
N_s,	nucleation site concentration [ft^{-2}];
Nu,	Nusselt number;
P_L,	liquid pressure [atm];
Pr,	Prandtl number;
Q_{fv},	enthalpy of formation of bubble [Btu];
(q/A), $(q/A)_{TOT}$,	total heat flux [Btu h ft^2];
$(q/A)_{LH}$,	latent heat transport, defined by equation (2) [Btu h ft^{-2}];
$(q/A)_{NC}$,	natural convection flux [Btu h ft^{-2}];
r,	nucleation cavity mouth radius [ft];
r_{max},	mouth radius of largest potentially active cavity [ft];

† Professor of Fluid Mechanics.
‡ South African Atomic Energy Board Bursar.

r^*_{max}, mouth radius of largest active cavity [ft];
r^*_{min}, mouth radius of smallest active cavity [ft];
Re, Reynolds number;
T_{sat}, saturation temperature of liquid [°R];
T_w, heater wall temperature [°R];
ΔT_{sat}, $(T_w - T_{sat})$ [degR];
V_b, bubble volume [ft³];
V_d, bubble volume at departure [ft³];
V_{dt}, bubble volume at departure for a particular source [ft³];
$\bar{V}_d$, mean (arithmetic, unless otherwise stated) of V_d;
v_v, specific volume of vapour [ft³/lb$_m$].

Greek symbols

δ, limiting thermal boundary layer thickness [ft];
λ_v, latent heat of vaporization [Btu/lb$_m$];
ρ_v, ρ_L, vapour and liquid density [lb$_m$/ft³];
σ, surface tension [lb$_f$/ft].

1. INTRODUCTION

1.1 *Definition of latent heat transport*

This paper deals primarily with the transport of energy away from a heating surface associated with the formation of bubbles thereon during saturated nucleate pool boiling.

It has been shown [1, 2] that the energy Q_b required to form a bubble of volume V_b and of radius larger than about 10^{-3} ft, is given, to a good approximation, by

$$Q_b = V_b \rho_v \lambda_v \tag{1}$$

with properties evaluated at the saturated state corresponding to the liquid pressure.

Since the diameter of bubbles at the instant of departure from a heated surface exceeds 10^{-3} ft by several orders of magnitude, the energy carried away from such a surface by bubbles may be formulated as

$$(q/A)_{LH} = \rho_v \lambda_v \sum_{i=1}^{n} f_i \bar{V}_{di} A \tag{2}$$

Evidently equation (1) only represents the latent heat of formation of a bubble, other terms being negligible. Thus the flux contribution given by equation (2) is termed *latent heat transport*.

Inasmuch as our ultimate aim is the correlation of nucleate boiling heat fluxes, the choice of V_d, the bubble volume at the instant of departure from the heating surface, is the only logical one. It has been shown by Jakob [3], and is verified in the present study (at least for the case of low-flux boiling), that bubbles in saturated boiling continue to grow after departure until they reach the free liquid surface. The heat required for this growth must originally have left the heating surface by some convection mechanism, and must be correlated on that basis.

It is further accepted that the bulk of the heat required for *attached* bubble growth must also be transferred from the heating surface, via the liquid sub-layer, by some conduction convection process. Evidently the ebullition mechanism is invoked and becomes rate controlling, when the normal convection processes tend to "saturation" and are no longer able to cope with the rate of heat supply. The exact distribution of heat flow between these two possible paths, that is convection and ebullition, clearly will be flux-dependent. It therefore appears preferable to correlate the flux contribution of the heat of formation of attached bubbles separately and in terms of equation (2).

To sum up therefore: The latent heat transport defined by equation (2) accounts for the heat that leaves the surface by conduction and convection to form bubbles up to the point of their departure; the difference between the total flux and the latent heat transport represents the heat that leaves the surface by convection, thereafter to manifest itself partly in the further growth of rising bubbles and partly in evaporation without ebullition at the free liquid surface.

1.2 *Previous work on latent heat transport*

It has until recently been generally held that in nucleate boiling, whether sub-cooled or saturated, latent heat transport as defined above contributes insignificantly to the total heat flux. This notion appears to have been based on the sub-cooled boiling studies of Gunther and Kreith [4] and Rohsenow and Clark [1].

As a result the high heat-transfer rates typical

of nucleate boiling have, in the main, been attributed to bubble-induced agitation near the heating surface. This has lead to correlation equations of the general form:

$$Nu = \text{const.}\ Re^{m}.Pr^{n} \qquad (3)$$

where the dimensionless parameters are evaluated in terms of bubble characteristics. The better known of these have recently been reviewed by Zuber and Fried [5].

At a particular pressure and for a given surface liquid combination these reduce approximately to:

$$(q/A) = \text{const.}\ (\Delta T_{sa})^{n} \qquad (4)$$

Clearly since the nucleation characteristics of the heating surface are ignored, such equations cannot adequately correlate nucleate boiling data. Attempts to accommodate nucleation effects by the inclusion of active site concentration terms have lead to equations of the form [6–9]

$$(q/A) = \text{const.}\ N^{r}(\Delta T_{sa})^{s} \qquad (5)$$

Inasmuch as these relations do not take account of latent heat transport, N represents the number of liquid flow-inducing sources.

Recent indirect evidence [10–12], however, suggests that latent heat transport cannot be ignored in saturated boiling. Irrespective of the heat-transfer mechanism operating in nucleate boiling, a study of the parameters entering into equation (2), as well as their inter-relation, would appear to be necessary.

In our reports of 1960 [13, 14] attempts at the photographic determination of N, f and V_b and at the evaluation of latent heat transport in saturated boiling were reported. It was shown that for water and ethyl alcohol boiling at atmospheric pressure latent heat transport increases steadily with increasing flux, until in the vicinity of the peak flux it alone accounts for the total flux. At no stage was its contribution negligible. Due to shortcomings of the photographic technique the bubble volume at departure could not be accurately determined. Also, bubble frequencies could only be measured at relatively low fluxes, high-flux values being obtained by extrapolation using an empirical equation fitted to the low-flux data. Thus there was some doubt as to the accuracy of the latent heat transport determination. The main conclusions reached are, however, still considered valid.

1.3 *Purpose and outline of this study*

Summarizing then: One is faced with a situation in which every better known heat-transfer correlation for saturated nucleate boiling is based on the experimentally unverified assumption that the contribution to the total flux by latent heat transport is negligible. Recent work indicates that this concept is almost certainly incorrect.

In this paper determinations of latent heat transport in saturated boiling of water at atmospheric pressure are reported. Further investigations into the basic parameters entering into the latent heat transport equation, that is equation (2), are presented.

In Section 2 experimental work on latent heat transport is described. Section 3 deals with bubble frequencies and bubble volumes at departure and their inter-relation. Section 4 provides data on the concentration of bubble producing sites and is a study of nucleation.

2. CONTRIBUTION TO THE TOTAL FLUX BY LATENT HEAT TRANSPORT

2.1 *Apparatus and measuring technique*

The apparatus used permitted determination of the heat flux and temperature difference between the heating surface and the liquid bulk; a means of measuring N, f and V_b was also provided.

Boiling vessel (*Fig.* 1). This contained a horizontal, electrically heated nickel wire, 0·02 in dia., which acted both as a heating element and as a resistance thermometer. (A wire rather than a flat plate was used because of the greater ease in interpreting the resultant photographs. Also edge effects were thereby avoided.) An auxiliary heater maintained the liquid bulk at the saturation temperature corresponding to ambient atmospheric pressure (~12 psia). A mercury-in-glass thermometer measured the liquid bulk temperature. The test wire was placed in an inner tank. This has been shown to be necessary if stagnant pool conditions are to be maintained in the test

of nucleate boiling have, in the main, been attributed to bubble-induced agitation near the heating surface. This has lead to correlation equations of the general form:

$$Nu = \text{const.}\ Re^{m}.Pr^{n} \qquad (3)$$

where the dimensionless parameters are evaluated in terms of bubble characteristics. The better known of these have recently been reviewed by Zuber and Fried [5].

At a particular pressure and for a given surface liquid combination these reduce approximately to:

$$(q/l) = \text{const.}\ (\Delta T_{sa})^{n} \qquad (4)$$

Clearly since the nucleation characteristics of the heating surface are ignored, such equations cannot adequately correlate nucleate boiling data. Attempts to accommodate nucleation effects by the inclusion of active site concentration terms have lead to equations of the form [6–9]:

$$(q/l) = \text{const.}\ N^{s}(\Delta T_{sa})^{n} \qquad (5)$$

Inasmuch as these relations do not take account of latent heat transport, N represents the number of liquid flow-inducing sources.

Recent indirect evidence [10–12], however, suggests that latent heat transport cannot be ignored in saturated boiling. Irrespective of the heat-transfer mechanism operating in nucleate boiling, a study of the parameters entering into equation (2), as well as their inter-relation, would appear to be necessary.

In our reports of 1960 [13, 14] attempts at the photographic determination of N, f and V_d and at the evaluation of latent heat transport in saturated boiling were reported. It was shown that for water and ethyl alcohol boiling at atmospheric pressure latent heat transport increases steadily with increasing flux, until in the vicinity of the peak flux it alone accounts for the total flux. At no stage was its contribution negligible. Due to shortcomings of the photographic technique the bubble volume at departure could not be accurately determined. Also, bubble frequencies could only be measured at relatively low fluxes, high-flux values being obtained by extrapolation using an empirical equation fitted to the low-flux data. Thus there was some doubt as to the accuracy of the latent heat transport determination. The main conclusions reached are, however, still considered valid.

1.3 *Purpose and outline of this study*

Summarizing then: One is faced with a situation in which every better known heat-transfer correlation for saturated nucleate boiling is based on the experimentally unverified assumption that the contribution to the total flux by latent heat transport is negligible. Recent work indicates that this concept is almost certainly incorrect.

In this paper determinations of latent heat transport in saturated boiling of water at atmospheric pressure are reported. Further investigations into the basic parameters entering into the latent heat transport equation, that is equation (2), are presented.

In Section 2 experimental work on latent heat transport is described. Section 3 deals with bubble frequencies and bubble volumes at departure and their inter-relation. Section 4 provides data on the concentration of bubble producing sites and is a study of nucleation.

2. CONTRIBUTION TO THE TOTAL FLUX BY LATENT HEAT TRANSPORT

2.1 *Apparatus and measuring technique*

The apparatus used permitted determination of the heat flux and temperature difference between the heating surface and the liquid bulk; a means of measuring N, f and V_d was also provided.

Boiling vessel (*Fig.* 1). This contained a horizontal, electrically heated nickel wire, 0·02 in dia., which acted both as a heating element and as a resistance thermometer. (A wire rather than a flat plate was used because of the greater ease in interpreting the resultant photographs. Also edge effects were thereby avoided.) An auxiliary heater maintained the liquid bulk at the saturation temperature corresponding to ambient atmospheric pressure (~12 psia). A mercury-in-glass thermometer measured the liquid bulk temperature. The test wire was placed in an inner tank. This has been shown to be necessary if stagnant pool conditions are to be maintained in the test

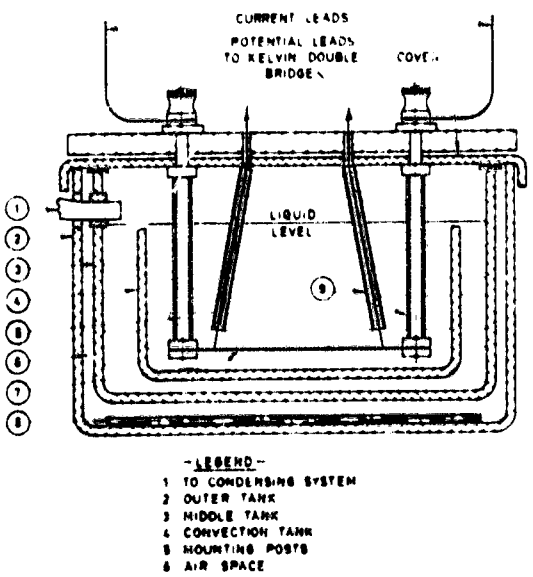

FIG. 1. Boiling vessel.

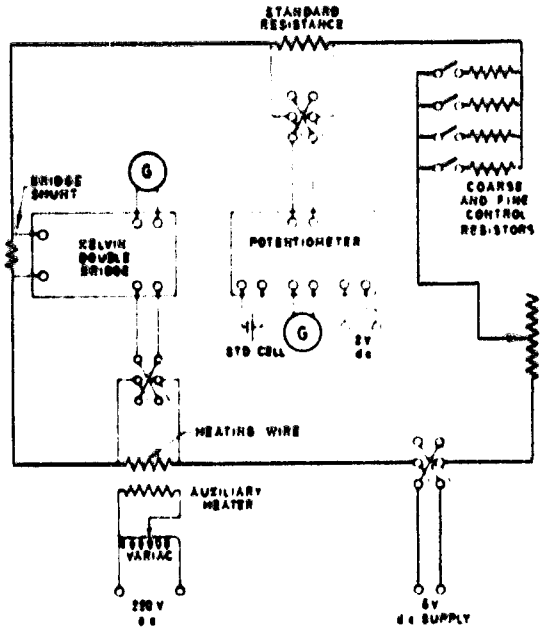

FIG. 2. Heating and measuring circuit diagram.

liquid [15]; its omission results in variation of the heat transfer from the wire with the power level of the auxiliary heater.

The whole system was completely sealed off from the atmosphere thus ensuring utmost cleanliness during testing.

Electrical system (*Fig.* 2). The wire resistance was measured by means of a Kelvin double bridge, whereas the heating current was determined from the volt-drop across a standard resistance in series with the heating wire.

Photographic technique. This consisted of taking a fixed number of successive photographs of the test section and bubble field. A variable-speed drum camera, provided with a commutator for triggering a flashing light source, was used. Timing marks were provided by a neon-lamp. The control circuit used is shown diagrammatically in Fig. 3. With this system 16 successive frames could be obtained, a

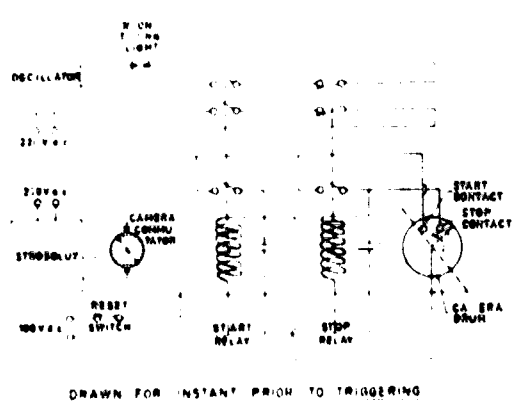

FIG. 3. Photography control circuit.

taking speed of about 85 frames/s being generally used. This allowed at least one cycle of the low frequency bubbles to appear on each loop. Specimen photographs are shown in Fig. 4.

2.2 *Test procedure*

After thorough cleaning the boiling tank was filled with the test liquid de-ionized water. De-aeration of the liquid and the heating surface was effected by high-flux boiling for approximately 6 h.

The test proper was then commenced. Measurement of the wire resistance and the potential drop over the standard resistor were

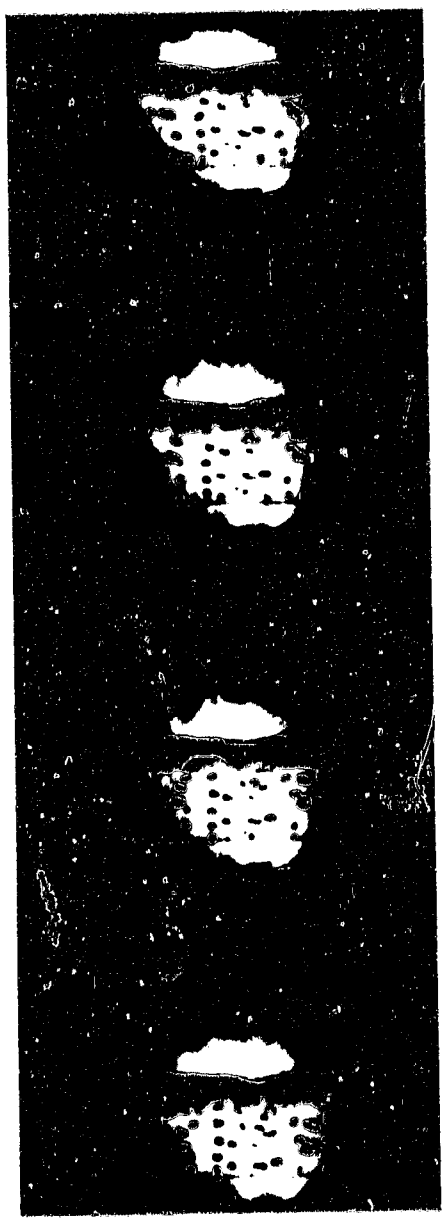

FIG. 4(a). Specimen photograph. Film loop 3 (q/A) = 38·6 × 10^3 Btu h ft^2.

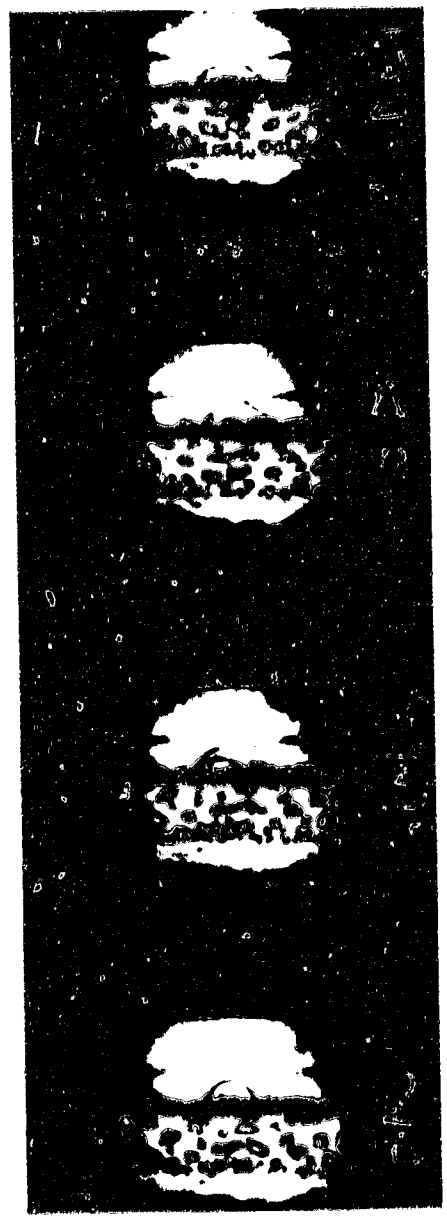

FIG. 4(b). Specimen photograph. Film loop 0 (q/A) = 157 × 10^3 Btu h ft^2.

(facing p. 1054)

taken. A loop of film was exposed in the manner described above. This procedure was repeated at progressively lower fluxes, some four to five minutes being allowed for conditions to settle after each change in heating current. Determination of the boiling curve with flux progressively decreasing has been shown by several workers to give the most reproducible results. Measurements were extended into the region of natural convection.

2.3 *Computations, errors and interpretation of photographs*

Heat fluxes and temperature differences (wire surface to liquid bulk) were calculated from electrical and thermometric measurements. Kok [15] using this apparatus, estimated the maximum error in heat flux determinations as ± 1 per cent and the error in the temperature difference as ± 5 per cent under worst conditions.

The negatives of the film loops obtained were examined under magnification by projecting them onto a screen. Bubble sources, frequencies and volumes at departure were determined.

At low fluxes the number of bubble sources could be counted with ease [see Fig. 4(a)]. At higher fluxes adjacent growing bubbles coalesced to form larger vapour globules [see Fig. 4(b)].†

The photographs of Séméria [16, 17] and Gaertner [11] clearly show large vapour globules attached to the heating surface by several stems. Such large globules are made up of vapour emanating from several nucleation sites. Bubble volume at departure can only be defined as the volume of a vapour globule leaving the surface, irrespective of whether the globule arises from one or more nucleation sites. Thus to maintain the meaning of equation (2), N, the number of bubble sources per unit area, must be defined as the number of regions per unit area from which vapour globules emanate, irrespective of whether such regions contain one or more nucleation sites. At low flux in the region of isolated bubbles the bubble source concentration equals the nucleation site concentration; after bubble coalescence this relation ceases to hold. The error in determining N is roughly the same as that in the measurement of the heating surface area, that is ± 1 per cent.

Preliminary tests conducted at various camera speeds showed that, with the optimum speed of approximately 85 frames/s used, the maximum error in determining the bubble frequency is about ± 2 per cent.

Because of the relatively low camera speed it was rarely possible to obtain a photograph of a bubble at the instant of departure. Jakob [3], however, has found that at about the time of departure a bubble grows relatively slowly. Figure 5 shows three bubble-volume vs time

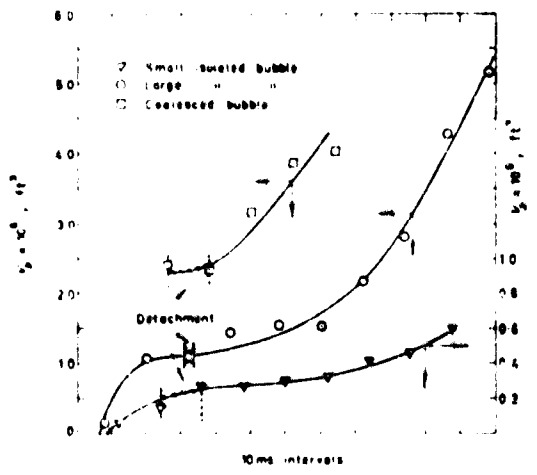

FIG. 5. Bubble growth curves.

curves determined with the apparatus described above. For all three types of bubble considered the growth curves flatten out in the vicinity of departure. The instant of departure was caught only for the large isolated bubble. Thus the first picture showing a bubble detached can be satisfactorily used for the determination of bubble volume at departure, whenever departure is not photographed; this procedure was adopted throughout.

Bubble volumes were calculated on the assumption that bubbles are spheroids. At low flux this assumption holds well; at high flux its validity is dubious. For this and other reasons measurements were not extended to very high fluxes.

† Evidently the flux at which discrete bubbles or globules occur is much higher with thin wires than with flat plates [11, 18, 19]. Continuous vapour columns or jets were not observed even at the highest heat flux investigated, 157 000 Btu/h ft².

When bubble dimensions were measured under magnification some error was introduced due to blurring of the outlines. The resulting error in bubble volume is estimated at ± 20 per cent for the smallest bubbles observed and less than ± 5 per cent for the largest. Taking bubble size distribution into account, this leads to an error in latent heat transport of ± 8 per cent at both the highest and the lowest heat fluxes measured.

The overall error in the determination of latent heat transport may thus be taken as ± 12 per cent.

2.4 *Results and discussion*

The boiling curve, log (q/A) vs ΔT_{sat}, and the latent heat transport, as calculated from equation (2), are plotted in Fig. 6. The natural convection data are correlated and extrapolated by an equation of the form $(q/A)_{NC} = C\Delta T_{sat}^{4}$

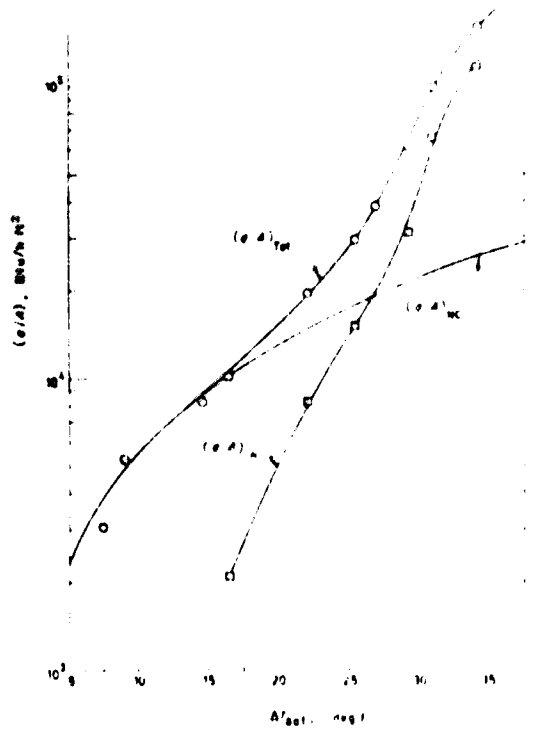

FIG. 6. Boiling curve for water also showing latent heat transport and extrapolated natural convection curve.

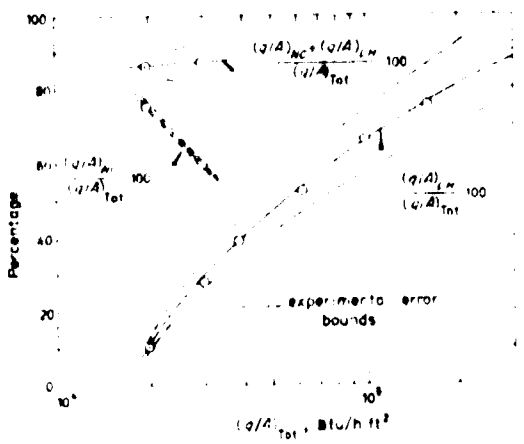

FIG. 7. Latent heat transport and convection as percentages of total heat flux.

[13, 14]. The percentage contribution of latent heat transport to the total flux is plotted against $(q/A)_{Tot}$ in Fig. 7. Clearly this contribution is nowhere insignificant.

The error-bounds on Fig. 7 are based on values of ± 12 per cent in latent heat transport and ± 1 per cent in total flux. Evidently the latent heat transport contribution increases smoothly with flux; at the peak flux (not determined in this study but generally in the vicinity of 4 to 6 × 10^5 Btu/h ft²) it alone might represent the total flux. It is also noteworthy that the relation

$$(q/A)_{LH} = \text{const.}\,(q/A)_{Tot} \qquad (6)$$

stated or implied in several studies does not hold.

It was stated earlier that latent heat transport and convection (natural and bubble-induced) are the predominant mechanisms operative during saturated boiling. Other possible mechanisms, e.g. mass transfer through bubbles, were considered negligible. The following substantiates this view: Hsu and Graham [20] have shown that, with respect to thermal boundary layer disturbance, the area of influence of one bubble source is small and corresponds to about two bubble diameters. It seems reasonable to assume therefore that in the region of very low bubble-source concentration the *convection* mechanism from a heating surface may be

approximated by one of undisturbed *natural convection*. Thus for the first two determinations at low flux the percentage convection contribution (obtained from extrapolated natural convection data) is plotted in Fig. 7. The sum of the percentage latent heat contribution and the percentage convection contribution is very nearly 100 per cent within the estimated error bounds. It is felt that the small discrepancy shown is due to the neglect of bubble-induced flow.

3. RELATION BETWEEN BUBBLE FREQUENCY AND BUBBLE VOLUME AT DEPARTURE

3.1 *Review of previous work*

The product of bubble frequency, f, and bubble diameter† (or bubble volume) at departure, D_d, enters into many analyses of nucleate boiling and also into the expression for latent heat transport, equation (2). As such the interrelation between frequency and diameter at departure has been the subject of several investigations, both analytical and experimental. A brief survey of these is given here.

Jakob and Linke [21] and Fritz and Ende [22] presented the first experimental studies of bubble detachment. In the limited flux range investigated mean frequencies and bubble diameters at departure were found to be independent of flux. Thus the product of mean diameter, D_d and mean frequency, f, was a constant, that is, at a particular pressure

$$D_d \cdot f = \text{const.} \tag{7}$$

More recently Perkins and Westwater [23] presented a similar study for the medium and high flux boiling of methanol. They found that for fluxes up to 80 per cent of the peak flux the mean frequencies and mean departure diameters remained constant; hence their product was also a constant.

The same result was obtained by Yamagata *et al.* [18] for the boiling of water in the region of isolated bubbles. After the onset of coalescence the data showed a larger scatter.

In the region of the peak heat flux an analysis by Deissler [24] suggests the relation between mean departure diameter and frequency as

$$D_d^{0.5} f = \text{const.} \tag{8}$$

Cole [25] was able to obtain some experimental substantiation of Deissler's analysis.

A recent analysis by McFadden and Grassmann [26] also leads to equation (8) and is supported by limited data on the boiling of liquid nitrogen.

Zuber [27] has proposed an equation yielding the product of mean bubble frequency and mean departure diameter in terms of physical properties of liquid and vapour.

$$D_d f = 0{\cdot}59 \left[\sigma g(\rho_L - \rho_v)\, \rho_L^2\right]^{0.25} \tag{9}$$

At constant pressure this relation reduces to Jakob's equation (7).

The following section considers the significance of these results.

3.2 *Definition of mean bubble frequency and mean bubble volume (or diameter) at departure*

The purpose of studying bubble frequencies and volumes at departure, as well as their product, is the obtention of the mass velocity of bubbles leaving the heating surface.

Consider a heating surface of area A having n bubble producing sites of individual frequencies f_i and individual bubble volumes at departure V_{di}, where $i = 1, 2, \ldots, n$. The fundamental definition of the mass velocity of departing bubbles, G_d, is

$$G_d = \sum_{i=1}^{n} (f_i V_{di})\, \rho_v / A \tag{10}$$

G_d can also be expressed in terms of mean frequencies and volumes such that

$$G_d = (n \cdot 1) f \cdot \overline{V}_d \rho_v = \sum_{i=1}^{n} (f_i V_{di})\, \rho_v / A \tag{11}$$

The left-hand side of equation (11) is the generally used, though not fundamental, definition of the mass velocity of departing bubbles.

It is the general practice to substitute into the left-hand side of equation (11) the *arithmetic* means of bubble frequencies and departure volumes in an attempt to obtain G_d. This procedure is clearly invalid [28].

† For non-spherical bubbles defined as equivalent spherical diameter.

Evidently equation (11) permits any definition of one of the parameters f or Γ_d; the definition of the other is then fixed. Thus, for example, if we define mean bubble volume at departure as the arithmetic mean of bubble volumes over all sources, that is,

$$\Gamma_d = \sum_{i=1}^{n} V_{di}/n \tag{12a}$$

then the necessary definition of mean frequency follows from equation (11) as

$$f = \sum_{i=1}^{n} (f_i V_{di}) \Big/ \sum_{i=1}^{n} V_{di} \tag{12b}$$

For purposes of obtaining the mass velocity it is unnecessary to separate the product $f V_d$ into f and Γ_d. We therefore define the mean of the product of frequency and departure volume as

$$\overline{fV_d} = \sum_{i=1}^{n} (f_i V_{di})/n \tag{13}$$

and G_d as,

$$G_d = (n/A)\overline{fV_d}\,\rho_v = \sum_{i=1}^{n} (f_i V_{di})\,\rho_v/A \tag{14}$$

Equation (13) is consistent with the two expressions for G_d in equation (14).

3.3 *Expected behaviour of $f_i V_{di}$ and $\overline{fV_d}$*

For a constant flux from a heating surface, it is possible to produce various arguments which suggest that at any particular surface temperature the product $f_i V_{di}$ should be the same for all sources. Consider, for example, the following: A bubble in growing extracts heat from the thermal boundary layer and in departing leaves behind an area of destroyed boundary layer [20, 29]. Bubbles of large departure volumes will cause large areas of destruction. Now bubble frequency is determined by the waiting period (the time required for the recovery of the boundary layer) and by the bubble growth period. The waiting period and the growth period are generally of comparable magnitude. A large area of destruction will have a long waiting period and a large departure volume will require a long growth period. Thus a large departure volume is associated with a low frequency and vice-versa. This description is oversimplified—see for example [20]; however it does suggest the possibility of an interrelation of the type

$$f_i V_{di} = \text{const.} \tag{15}$$

where $i = 1, 2, \ldots, n$, and n is the number of bubble sources. Some statistical scatter is to be expected.

Dealing now with the variation of the mean product $\overline{fV_d}$ with flux (or temperature difference) the definition of latent heat transport is recalled

$$(q/A)_{LH} = N\overline{fV_d}\,\lambda_v\,\rho_v \tag{16}$$

N and $\overline{fV_d}$ are the only terms that vary with flux. If $(q/A)_{LH}$ and N are plotted against $(q/A)_{Tot}$ an idea of the variation of $\overline{fV_d}$ can be obtained from the slopes. In Fig. 8 the data of the present study are represented in this fashion. The N vs $(q/A)_{Tot}$ curve will be discussed in Section 4. It is immediately clear that $\overline{fV_d}$ cannot be independent of flux since the slopes of these curves are not equal; also that $\overline{fV_d}$ should increase slowly at first and more rapidly

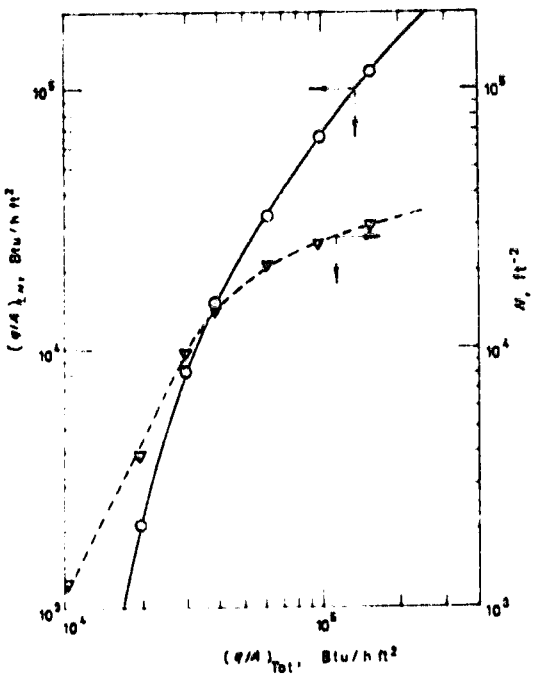

FIG. 8. Latent heat transport and bubble source concentration versus total heat flux, showing difference in slopes.

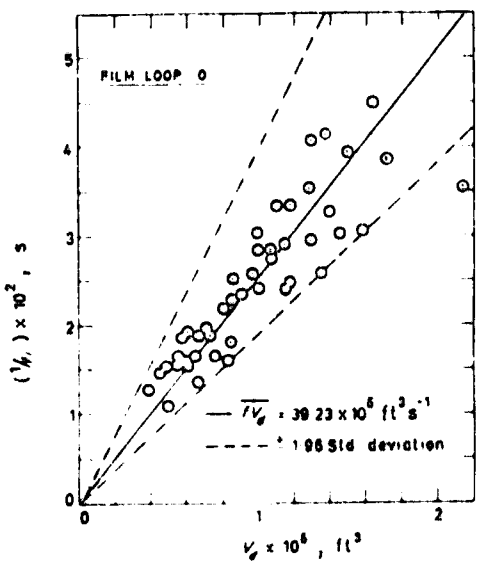

FIG. 9. Relationship between bubble frequency and volume at departure. *Note:* In (c) two bubbles of large volume and unmeasured frequency are not shown. For latent heat transport purposes their contribution was included by estimating their frequency from $\overline{fV_d}$.

as the flux (or the temperature difference) increases.

3.4. *Experimental results and discussion*

The product $f_i V_{di}$. For purposes of testing the hypothesis that at a particular flux $f_i V_{di}$ const. it is convenient to write this relation as

$$V_{di} = \text{const.}\,(1/f_i) \qquad (17)$$

Thus when plotting V_{di} against $(1/f_i)$ a straight line through the origin is obtained if the hypothesis holds. In Fig. 9 three sets of data, two at high flux and one at low flux, are shown. The full line on each represents the arithmetic mean of the products $f_i V_{di}$, that is $\overline{fV_d}$, at that flux. Similar plots were obtained for all six film loops exposed, with the data of loop 5 (at the lowest flux) showing a much higher scatter. Thus the proposed relation, equation (15) or (17) holds within certain scatter limits.

It is of interest to determine the correlation coefficient for V_{di} and $(1/f_i)$ for the six tests. A correlation coefficient, r, may be computed for any two-dimensional set of observations, but unless the underlying population is two-dimensionally normally distributed the interpretation of r is uncertain. Thus only if both V_{di} and $(1/f_i)$ are normally distributed for a set of observations can the correlation coefficient be regarded as a measure of their interrelation, with $|r| = 1$ indicating linear dependence [30].

For the observations here reported the distributions of V_d and $(1/f)$ were generally not normal. However, the departure from normality was not large, especially for the data at higher fluxes. As an example, Fig. 10 shows the

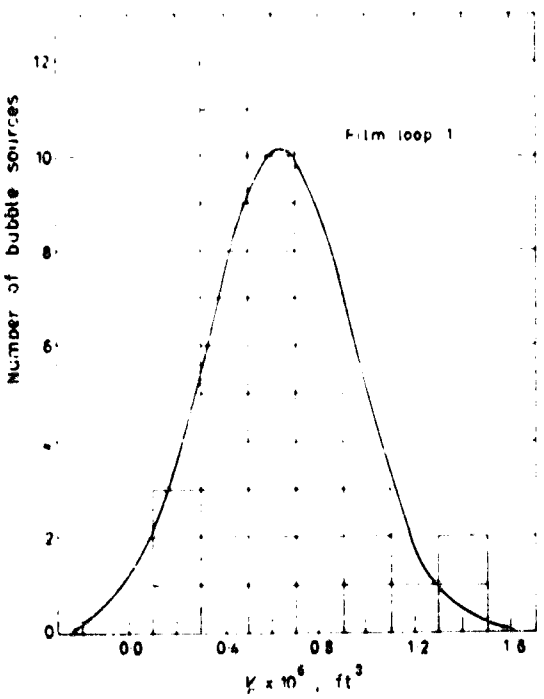

FIG. 10. Histogram of departure volumes (film loop 1) with superimposed normal distribution.

histogram of V_d for film loop 1 compared with the normal distribution of mean and variance equal to that of the histogram. Thus some significance may be attached to the correlation coefficients for the tests here reported.

The coefficients obtained ranged from 0·83 to 0·92 for film loops 0 to 4, with loop 5 at the lowest flux yielding 0·67. This represents significant support for the hypothesis that at a particular flux (which is not too low) the volumetric vapour flow rate is the same from each source.

Consider the scatter in the values of the product $f_i V_{di}$ at a particular flux. At low fluxes where bubble formation frequently occurs in bursts this scatter is to be expected. Difficulties in measuring bubble volumes, especially after the onset of coalescence, have also been mentioned. In addition, because of the limited number of frames in each loop, it was necessary to assume that at any flux successive bubble periods and departure volumes from a particular source were equal. Hsu and Graham [20], when studying the ebullition cycle from a single source during steady boiling, found large variations in both waiting and growth periods. The variation of their sum, the bubble period $(1/f_i)$ was less but still significant. Unfortunately the film loops of the tests reported here were not sufficiently long to allow a reasonable determination of f_i and V_{di} values where each is an average over a period of time from a particular source. This is probably responsible for most of the observed scatter.

The product $\overline{fV_d}$. The variation of the product $\overline{fV_d}$ with both flux and ΔT_{sat} is shown in Fig. 11.

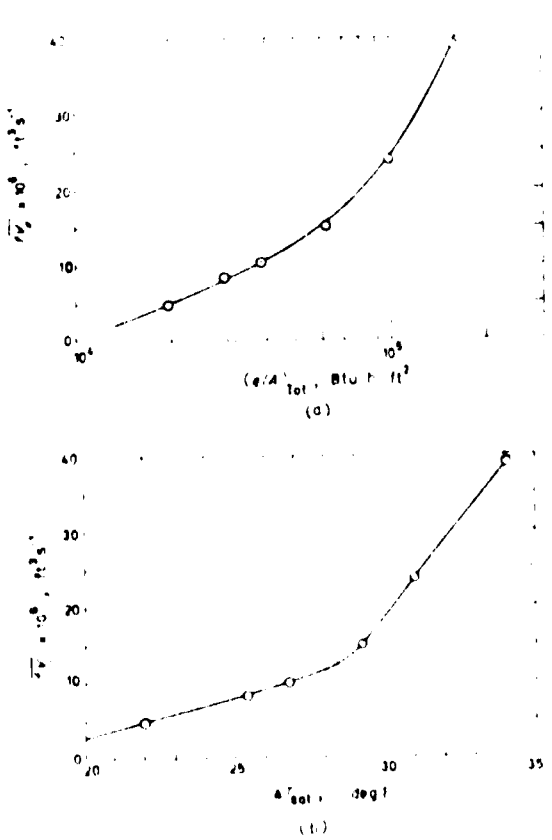

FIG. 11. Variation of mean product of bubble frequency and departure volume with (a) heat flux and (b) wall superheat.

As anticipated from Fig. 8 this product is not constant. The "knee" in Fig. 11(b) is associated with the onset of coalescence.

4. NUCLEATION SITES AND BUBBLE SOURCES

4.1 *Preliminary consideration and predictions*

Effect of temperature difference. Nucleation proceeds from surface cavities of certain geometry [31, 32, 33, 34]. The mean mouth size of these cavities will in general be distributed in some way – for argument's sake as in Fig. 12.

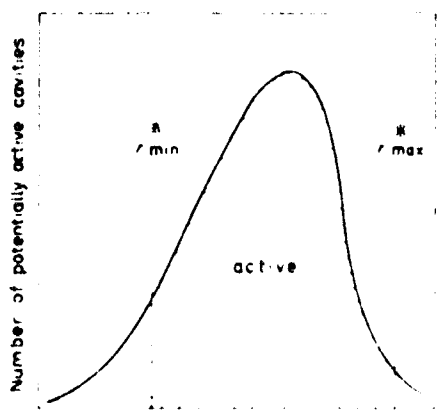

FIG. 12. Hypothetical size-distribution of nucleation cavities.

Under given conditions a particular size range of these cavities will be active. The size of the largest active cavity, r^*_{max}, may be boundary-layer controlled; the size of the smallest active cavity, r^*_{min}, is thermodynamically controlled.

For the time being consideration is limited to "smooth" surfaces, that is, to conditions such that the largest cavity present on the surface (of mouth radius r_{mcs}) is always active that is,

$$r_{max} = r_{mcs} = \text{const.} \tag{18a}$$

This is equivalent to saying that the limiting thermal boundary-layer thicknesses, δ, which is flux and pressure dependent, must at all stages be great enough to contain the vapour nucleus from the largest cavity, that is,

$$\delta = r_{max} \tag{18b}$$

Nucleation may be then characterized to a reasonable approximation [11, 57] by

$$r^*_{min} = 2\sigma T_{sat}\, v_f/\lambda_l\, \Delta T_{sat} \tag{19}$$

Now it is recalled that in the study of Griffith and Wallis [33] it was shown that an equation virtually identical to equation (19) did not hold for artificial cavities punched into a surface from which boiling took place. It appears, however, that with the relatively large cavity size employed ($r = 2{\cdot}7 \times 10^{-3}$ in) the situation arose where $r > \delta$. Thus the punched cavities were not active at all and smaller natural cavities led to superheats higher than those predicted. In a constant temperature field [33] and under conditions where the limitation of equation (18) was satisfied [35] equation (19) did hold.

At constant pressure and with physical properties evaluated at the saturation temperature equation (19) reduces to

$$r^*_{min} = \text{const.}/\Delta T_{sat} \tag{20}$$

Thus the rate of change of the active cavity (nucleation site) concentration with ΔT_{sat}, $-\mathrm{d}f/\mathrm{d}(\Delta T_{sat})$, may be drawn against ΔT_{sat} as in Fig. 13(a), that is, approximately as the lateral inversion of the cavity size distribution of Fig. 12.

Consider now a liquid at saturation temperature and events accompanying a gradual raising of the wall superheat, ΔT_{sat}. At a temperature difference $(\Delta T_{sat})_{min}$ the first cavity of radius r_{max} is activated. As ΔT_{sat} is raised, smaller cavities become active and the nucleation site concentration, f', on the surface increases. Figure 13(b) shows the variation of f' with ΔT_{sat}, that is, the cumulative distribution corresponding to that of Fig. 13(a). At some point, say A, bubble coalescence on the surface will commence. It now becomes necessary to distinguish between the nucleation site concentration f' and the bubble source concentration, N. In the interval $\Delta(\Delta T_{sat})$, $\Delta f'$ cavities are activated. If bubbles growing from these were all to coalesce with already existing bubbles then the N versus ΔT_{sat} curve would branch out horizontally to point B in Fig. 13(b). This is an extreme case. In actual fact only a fraction, say x, of $\Delta f'$ will be lost as bubble sources. At the onset of coalescence x is expected to be small; thus the N vs ΔT_{sat} curve moves to point A'. x will be higher in each interval of progressively greater ΔT_{sat}. Thus the N vs ΔT_{sat} curve will take the shape shown in Fig.

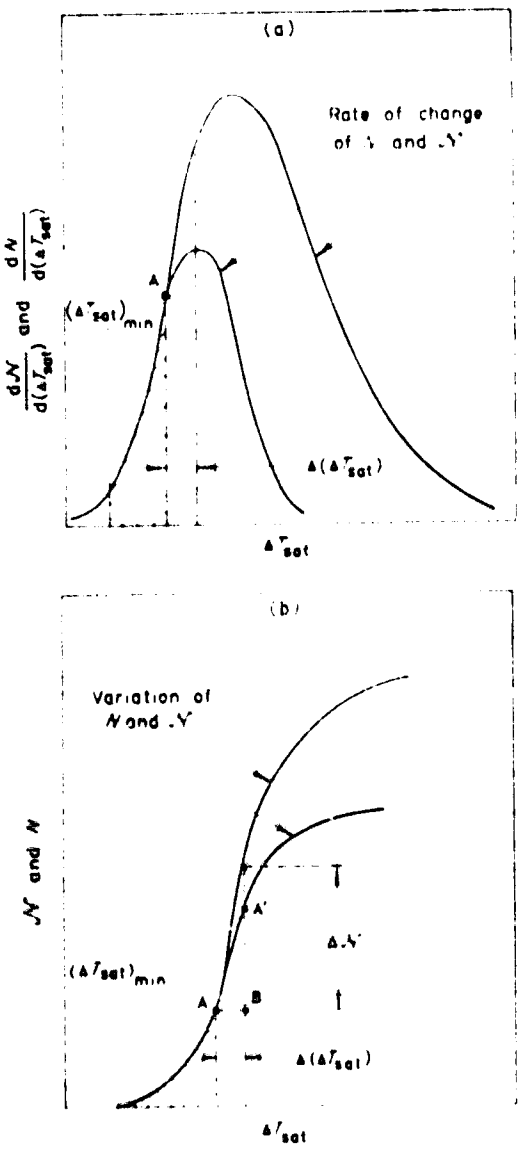

FIG. 13. Hypothetical bubble population: (a) Rate of change of nucleation site ($\dot{N}$) and bubble source ($\Delta\dot{N}$) concentrations with wall superheat (ΔT_{sat}) (b) $\dot{N}$ and N vs ΔT_{sat}.

13(b). This curve represents the integration of the distribution $dN/d(\Delta T_{sat})$ versus ΔT_{sat} shown in Fig. 13(a).

Consideration was originally limited to systems where r^*_{max} is independent of flux and ΔT_{sat}. This imposed the condition that the relation $\delta \geq r_{max}$ must hold at all stages. Depending on the micro-roughness of a surface this condition may or may not be satisfied. If it is not then r^*_{max} is boundary-layer controlled. The limiting boundary-layer thickness is expected to decrease with increasing flux and ΔT_{sat} [16]. Thus with sufficiently rough surfaces r^*_{max} will decrease with increasing ΔT_{sat}. This would cause a lowering of the N versus ΔT_{sat} curve. In the coalescence regime the decrease in N due to this effect might well be compensated by a corresponding reduction in coalescence. Unfortunately no quantitative information on δ and its variation with flux, in the vicinity of a bubble source, is available.

Whatever the surface, the experimentally obtainable N versus ΔT_{sat} curve is expected to assume the shape of some cumulative frequency distribution. This might not be readily recognizable, especially if available data cover a limited range only. Differentiation and plotting of the $dN/d(\Delta T_{sat})$ versus ΔT_{sat} distribution should yield more information.

In Section 4.2 experimental data will be examined in the light of these predictions.

The effect of pressure. Séméria [16] has pointed out that the effect of pressure on equation (19) is such as to permit the use of

$$r^*_{max} \propto \text{const.}/\Delta T_{sat} \cdot P_L \qquad (21)$$

for water in the pressure range 1 to 50 atm. This correlation is also applicable, to a rougher approximation, to several other substances if P_L is substantially below their critical pressure (see Fig. 14).

Thus if the pressure is reduced on a boiling system r^*_{min} increases. During operation at some low pressure the situation will arise where $r^*_{min} = r^*_{max}$, that is, where the size range of active cavities is zero. Nucleation, and hence nucleate boiling, must then be expected to cease, or otherwise to proceed by some mechanism other than the normal. It is seen from equation (21) that this critical situation may be reached (at some low pressure) in the middle of a boiling curve as ΔT_{sat} is progressively lowered. At some even lower pressure the ΔT_{sat} required for normal nucleation is greater than that associated with the peak flux; below

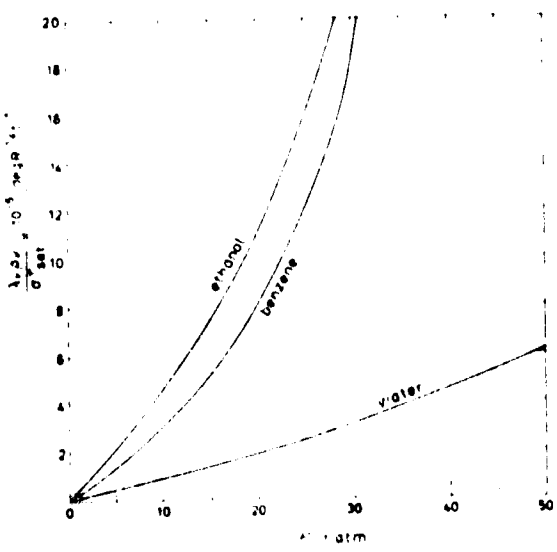

FIG. 14. Variation of $\lambda_l \rho_l \sigma T_{sat}$ with pressure [see equations (19) and (21)].

this pressure the normal nucleate regime is altogether absent.

In Section 4.2 experimental work aimed at the verification of these predictions is reported.

4.2 *Experimental work and discussion*

Effect of temperature difference and flux. In Fig. 15 the data of the present study are handled in the manner suggested in Section 4.1. These results appear to support the proposed hypothesis surprisingly well. The fact that the distributions N vs ΔT_{sat} and $dN/d(\Delta T_{sat})$ vs ΔT_{sat} roughly approximate to normal is of no particular significance and arises from the micro-structure of the heating surface employed. In fact, other data [15] which were analysed in this fashion showed these trends less clearly. However, the approach appears to be potentially valuable. Before significant advances can be made along these lines more quantitative information on coalescence must be obtained. Séméria [16, 17] has recognized this necessity.

Bubble sources and flux. It is more common to present data on bubble source concentration as log (q/A) vs log N plots. In Fig. 16 data of the present study are plotted in this manner. In addition, data on low pressure boiling of ethanol and benzene [35] are also given. These data were obtained by visual counting with an apparatus very similar to the one described earlier, but allowing pressure variations. The heating wire diameter was 0·0076 in.

In the low and intermediate flux range the relationship

$$(q/A)_{tot} \quad \text{const.} \, N^{0.5} \tag{22}$$

proposed by several workers evidently holds. At higher fluxes however, N increases more slowly with flux, with the index reaching 2·6 for for the water data. The visual data on organics could not be extended to sufficiently high fluxes. The "knees" of the curves correspond to the onset of coalescence.

Effect of pressure. The predictions of Section 4.1 suggest the necessity of conducting boiling runs [(q/A) decreasing] at various low pressures with a particular surface liquid combination. Such tests were performed [35] at saturation temperature, great care being taken to avoid the well-known "hysteresis" effect and to maintain

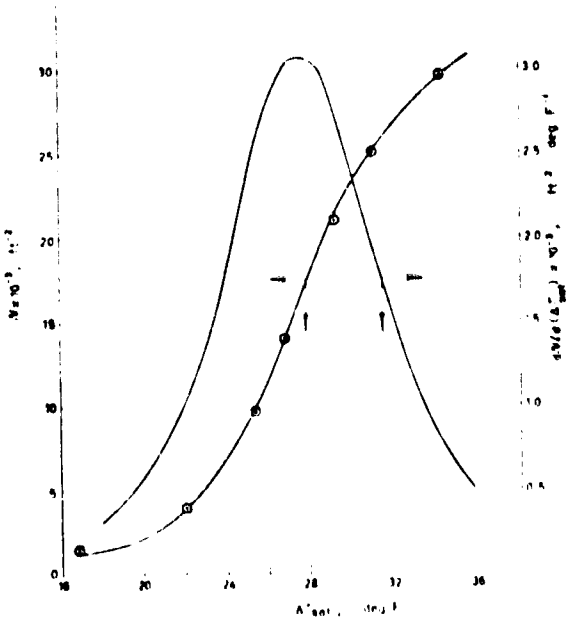

FIG. 15. Observed variation of bubble source concentration and its rate of change with wall superheat.

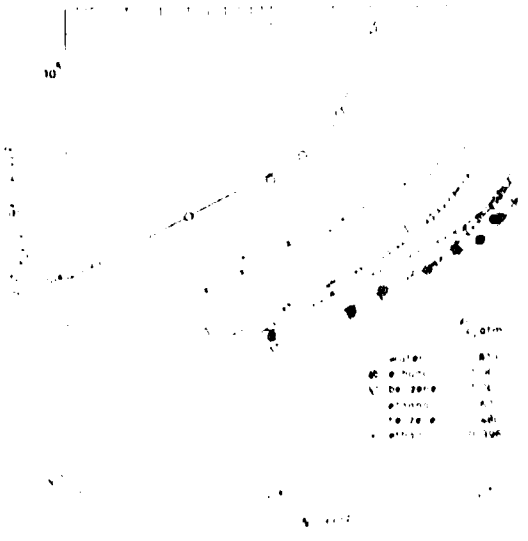

FIG. 16. Variation of bubble source concentration with heat flux.

reproducibility. Results obtained for ethanol are presented in Fig. 17.

During run E.1 (1·0 atm) and run E.2 (0·677 atm) the well-known boiling curves were traced. This also applies to run E.3 (0·396 atm) in the high flux range.

At low flux, run E.3 exhibits a highly unusual change in direction. This behaviour appears to be associated with the cessation of operation of the normal mechanism of nucleation. Inspection of Fig. 16 in which the N vs (q/A) data for this run are reported shows that no dramatic change in the bubble source concentration occurred at this point. However, nucleation seemed to become unstable; bubbles no longer emanated from fixed sources in column-formation, but appeared to be formed at points shifting on the surface. This effect was particularly noticeable in run E.4 (0·294 atm) where bubble-producing sources jumped around on

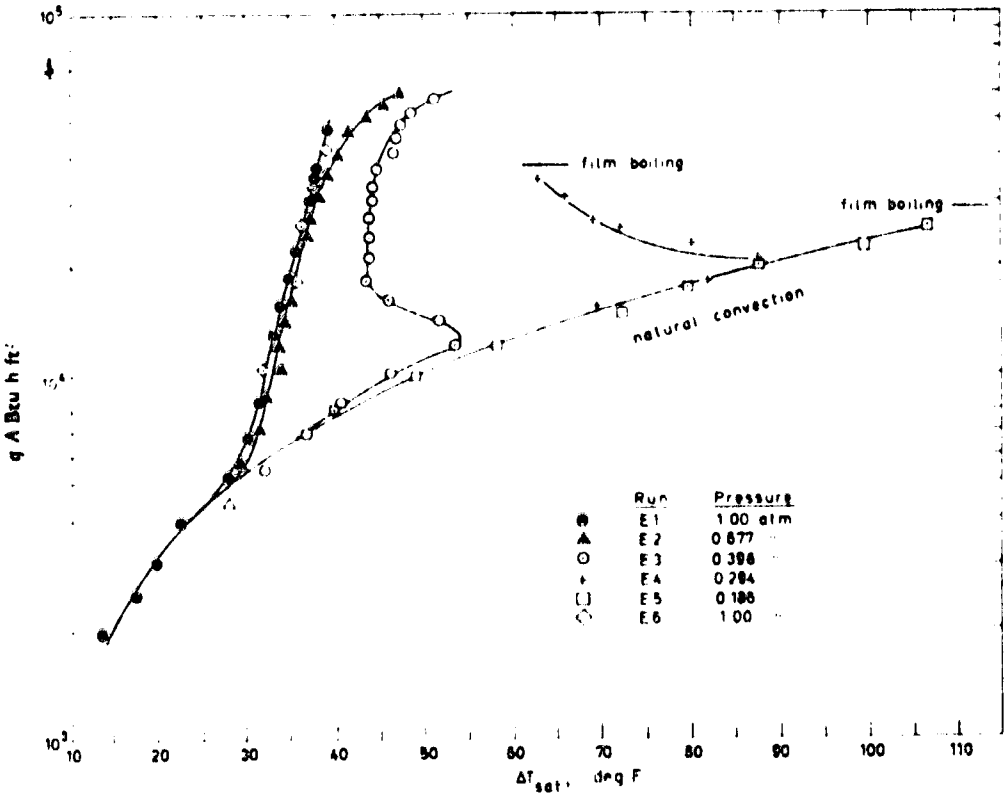

FIG. 17. Boiling curves for ethanol showing unstable nucleate boiling and absence of the nucleate regime at low pressure.

the surface in a rapid and apparently random manner. A curve of the shape of run E.3 has been obtained by van Stralen [36] for the boiling of a solution of whey in water at 0·132 atm pressure. Boiling as in run E.4 does not appear to have been hitherto reported.

The phenomena of runs E.3 and E.4 cannot be attributed to "hysteresis effects" or "temperature overshoot" since: (i) runs were performed at decreasing flux, (ii) the test procedure in obtaining runs E.3 and E.4 was identical to that adopted for the stable runs E.1 and E.2, and (iii) the behaviour did not die away with time; in fact on one occasion during operation in the unstable region the flux was maintained at the same setting for over an hour, but the bubble pattern remained irregular; in the same run at higher flux no irregularity was observed.

Run E.5 (0·136 atm) illustrates the complete cessation of nucleation. At a flux slightly higher than that of the last point recorded the surface burst into film boiling. The nucleate regime was entirely absent. Van Stralen [37] and Lienhard and Schrock [38] have observed the same phenomenon.

Run E.6 (1·0 atm) is a satisfactory check on reproducibility.

Similar results to the above were obtained for benzene, bromobenzene, *n*-hexanol and both mixed and pure isomers of xylene.

The predictions of Section 4.1 thus appear to be verified. At some low pressure the cessation of nucleation by the normal mechanism occurs. This can take place in the middle of a boiling curve. A hitherto unrecognized regime of unstable nucleate boiling exists at low pressure. At even lower pressure the nucleate regime is altogether absent.

For the case where the limitation of equation (18) is obeyed it appears possible to predict the onset of the unstable boiling region [57]. This will be fully dealt with elsewhere.

The cessation-of-nucleation phenomenon has been known for many years in the guise of "bumping". Generations of organic chemists performing "vacuum-distillations" in glass apparatus have added anything from chunks of coal to talcum powder [39] in an effort to prevent these minor explosions. Sometimes these devices were helpful, sometimes not, depending upon whether they did or did not provide the nucleation sites previously absent.

It is felt that low pressure work of the type described above is potentially an extremely powerful tool in the general study of nucleation.

5. CONCLUSIONS

(1) Latent heat transport and convection together account for the total flux in saturated nucleate boiling.

(2) Latent heat transport is at stages significant; it is probable that at burnout it alone represents the total flux.

(3) The mean product of bubble frequency and departure volume, $\overline{fV_d}$, *if correctly defined*, increases throughout the flux range.

(4) At fixed flux and pressure the product fV_d is the same for each bubble source within reasonable statistical scatter.

(5) The relationship between heat flux (q A) and number of bubble sources per unit area, N,

$$(q\ A) \quad \text{const.}\ N^n$$

where $n \simeq 0{\cdot}5$ holds only in the absence of coalescence.

(6) It appears possible to determine the *size distribution* of potential nucleation cavities on a surface if the following are available:

(a) The distribution of $\mathrm{d}N/\mathrm{d}(\Delta T_{\mathrm{sat}})$ vs ΔT_{sat} together with data on coalescence, thus allowing the determination of the $\mathrm{d}A'/\mathrm{d}(\Delta T_{\mathrm{sat}})$ vs ΔT_{sat} distribution.

(b) A criterion of nucleation in non-uniform fields.

(7) The approximate equation

$$r'_{\mathrm{min}} \quad 2\sigma T_{\mathrm{sat}} r_f / \lambda_f \Delta T_{\mathrm{sat}}$$

being a necessary but not sufficient criterion of nucleation under boiling conditions can, however, yield predictions on the size range of nucleation cavities. These have been verified by experiments and lead to the following general conclusions:

(a) The effect of lowering the pressure on a boiling system is such as to decrease the size range of active cavities.

(b) For a particular surface liquid combination a particular low pressure exists below which the boiling curve exhibits instability.

(c) This threshold is reached when the size range of cavities active in the normal sense becomes zero. Beyond this threshold there exists a hitherto unrecognized regime of unstable nucleate boiling. In this unstable regime nucleation and boiling proceed by mechanisms other than the normal. At even lower pressures the nucleate regime is altogether absent.

ACKNOWLEDGEMENTS

Messrs S. Hyman and D. J. Carhell assisted in obtaining data on water

Thanks are extended to the South African Council for Scientific and Industrial Research for their faith in financially supporting this programme over the years.

H. H. Jawurek at present holds a bursary from the South African Atomic Energy Board. He was formerly supported by a junior lectureship at the University of Cape Town, Department of Chemical Engineering, to whose Head, Dr. A. D. Carr, sincere thanks are offered.

REFERENCES

1. W. M. Rohsenow and J. A. Clark, A study of the mechanism of boiling heat transfer, *Trans. Amer. Soc. Mech. Engrs* 73, 609–620 (1951).
2. R. F. Larson, contribution to ref. 1.
3. M. Jakob, *Heat Transfer*, Vol. 1, p. 634. John Wiley, New York (1949).
4. F. C. Gunther and F. Kreith, Photographic study of bubble formation in heat transfer to subcooled water, *Heat Transfer and Fluid Mechanics Institute*, p. 113–138. ASME (1949).
5. N. Zuber and F. Fried, Two phase flow and boiling heat transfer to cryogenic liquids, *J. Amer. Rocket Soc.* 32, 1332–1341 (1962).
6. H. M. Kurihara and J. E. Myers, The effects of superheat and surface roughness on boiling coefficients, *J. Amer. Inst. Chem. Engrs* 6, 83–91 (1960).
7. N. Zuber, Hydrodynamic aspects of nucleate pool boiling, Ramo-Wooldridge Research Laboratory Report, *RW-RL*-164 (1960).
8. C. L. Tien, A hydrodynamic model for nucleate pool boiling, *Int. J. Heat Mass Transfer* 5, 533–540 (1962).
9. J. H. Lienhard, A semi-rational nucleate boiling heat flux correlation, *Int. J. Heat Mass Transfer* 6, 216–219 (1963).
10. F. D. Moore and R. B. Mesler, The measurement of rapid surface temperature fluctuations during nucleate boiling of water, *J. Amer. Inst. Chem. Engrs* 7, 620–624 (1961).
11. R. F. Gaertner, Photographic study of nucleate pool boiling on a horizontal surface. General Electric Co. Research Laboratory Report 63-*RL*-3357*C*, Schenectady, N.Y. (1963).
12. S. G. Bankoff, A note on latent heat transport in nucleate boiling, *J. Amer. Inst. Chem. Engrs* 8, 63–65 (1962).
13. C. J. Rallis, R. V. Greenland and A. Kok, Stagnant pool boiling from horizontal wires under saturated and sub-cooled conditions, *S. Afr. Mech. Engr* 10, 171–186 (1961).
14. R. V. Greenland, An investigation into stagnant pool nucleate boiling from horizontal wires for saturated and sub-cooled conditions, *M.Sc. Thesis* in Mech. Engng, Univ. of the Witwatersrand, Johannesburg, S. Africa (1960).
15. A. Kok, An experimental investigation of nucleate boiling heat transfer under stagnant pool conditions, *M.Sc. Thesis* in Mech. Engng, Univ. of the Witwatersrand, Johannesburg, S. Africa (1960).
16. R. I. Semeria, Quelques résultats sur le méchanisme de l'ebullition. *VHemes Journees de l'Hydraulique, Soc. Hydrotechnique de France*, Question II, Rapport No. 3, Paris (1962).
17. R. I. Semeria, An experimental study of the characteristics of vapour bubbles, Paper 7, *Symposium of Two-phase Fluid Flow*, Inst. Mech. Engrs, London (1962).
18. K. Yamagata, F. Hirano, K. Nishikawa and H. Matsuoka, Nucleate boiling of water on the horizontal heating surface, *Mem. Fac. Engng, Kyushu* 15, No. 1, 99–163 (1955).
19. B. J. Stock, Observations on transition boiling heat transfer phenomena. Argonne National Lab. Report *ANL*-6175, Argonne, Ill. (1960).
20. Y. Y. Hsu and R. W. Graham, An analytical and experimental study of the thermal boundary layer and ebullition cycle in nucleate boiling, *NASA TN-D*-594, Lewis Research Centre, Cleveland, Ohio (1961).
21. M. Jakob and W. Linke, Der Wärmeubergang von einer waagerechten Platte an siedendes Wasser, *Forsch. Geb. Ing.* 4, 75 (1933).
22. W. Fritz and W. Ende, Über den Verdampfungsvorgang nach kinematographischen Aufnahmen an Dampfblasen, *Phys. Z.* 37, 391–401 (1936).
23. H. S. Perkins and J. W. Westwater, Measurements of bubbles formed in boiling methanol, *J. Amer. Inst. Chem. Engrs* 2, 471–476 (1956).
24. R. G. Deissler, *Columbia Heat Transfer Symp.*, New York (1954). Cited in ref. 49.
25. R. Cole, A photographic study of pool boiling in the region of the critical heat flux, *J. Amer. Inst. Chem. Engrs* 6, 533–538 (1960).
26. P. W. McFadden and P. Grassmann, The relation between bubble frequency and diameter during nucleate pool boiling, *Int. J. Heat Mass Transfer* 5, 169–173 (1962).
27. N. Zuber, Hydrodynamic aspects of boiling heat transfer. U.S. Atomic Energy Commission Rep. *AECU*-4439, AEC Tech. Inf. Serv., Oak Ridge, Tenn. (1959).

28. H. H. JAWUREK, The definition of mean bubble frequency and mean bubble volume at departure in nucleate boiling, *S. Afr. Mech. Engrs* 13, 47–48 (1963).
29. Y. Y. HSU, On the size range of active nucleation cavities on a heating surface, *J. Heat Transfer* C84, 207–219 (1962).
30. A. HALD, *Statistical Theory with Engineering Applications*, Chapter 19, section 13. John Wiley, New York (1952).
31. S. G. BANKOFF, Ebullition from solid surfaces in the absence of a pre-existing gaseous phase, *Trans. Amer. Soc. Mech. Engrs* 79, 735–740 (1957).
32. H. B. CLARK, P. S. STRENGE and J. W. WESTWATER, Active sites for nucleate boiling, *Chem. Engng Progr. Symp. Ser.* 55, No. 29, 103–110 (1959).
33. P. GRIFFITH and J. D. WALLIS, The role of surface conditions in nucleate boiling, *Chem. Engng Progr. Symp. Ser.* 56, No. 30, 49–65 (1960).
34. S. G. BANKOFF, Entrapment of gas in the spreading of a liquid over a rough surface, *J. Amer. Inst. Chem. Engrs* 4, 24–26 (1958).
35. H. H. JAWUREK, Nucleation during boiling with special reference to its cessation at low pressure. *M.Sc. Thesis* in Chem. Engng, University of Cape Town, Rondebosch, S. Africa (1962).
36. S. J. D. VAN STRALEN, Heat transfer to boiling binary liquid mixtures, Part III, *Brit. Chem. Engng* 6, 834 (1961).
37. S. J. D. VAN STRALEN, Heat transfer to boiling binary liquid mixtures at atmospheric and sub-atmospheric pressures, *Chem. Engng Sci.* 5, 290–296 (1956).
38. J. H. LIENHARD and V. I. SCHROCK, The effect of pressure, geometry and the equation of state upon the peak and minimum boiling heat flux, *J. Heat Transfer* C85, 261–272 (1963).
39. J. W. WESTWATER, *Advances in Chemical Engineering*, Vol. 2 (Edited by T. B. DREW and J. W. HOOPER), pp. 27–29. Academic Press, New York (1953).

APPENDIX 3

DETERMINATION OF q^i_{LH}/q^i_T FROM $(q/A)_{LH}/(q/A)'_{NB}$

DATA OF JUDD AND MERTE

Judd and Merte [95] determined the following heat flux ratio:

$$(q/A)_{LH}/(q/A)'_{NB} = (q/A)_{LH}/\left[(q/A)_T - (q/A)_{NC}\,(A_{NC}/A_T)_{inst}\right] \qquad (A3.1)$$

where

$$(A_{NC}/A_T)_{inst} = 1 - A_i N_{inst} \qquad (A3.2)$$

The area-of-influence ratio here required is

$$q^i_{LH}/q^i_T = (q/A)_{LH}/(q/A)_{NB} = (q/A)_{LH}/\left[(q/A)_T - (q/A)_{NC}(A_{NC}/A_T)\right] \qquad (A3.3)$$

where

$$(A_{NC}/A_T) = 1 - A_i N$$

For both cases the area of influence is given by

$$A_i = 3\,(\pi/4)\,D^2_{max} \qquad (A3.5)$$

Terrestrial gravity values of $(q/A)_{LH}/(q/A)'_{NB}$ and the additional data necessary to convert this ratio to q^i_{LH}/q^i_T are shown in Table A3.1. The data are approximate and derive from figures in Judd and Merte's paper.

TABLE A3.1

DATA OF JUDD AND MERTE

(At terrestrial gravity, $g/g_c = 1$)

$(q/A)_T$ kW/m²	ΔT_{sat} K	$\bar{D}_{max}$ m	N_{inst} m^{-2}	N m^{-2}	$\frac{(q/A)_{LH}}{(q/A)_{NB}}$
11,5	15,6	5×10^{-4}	$6,5 \times 10^{5}$	$1,2 \times 10^{6}$	0,78
21,1	16,6	5×10^{-4}	$1,1 \times 10^{6}$	$2,2 \times 10^{6}$	0,78
41,6	17,8	5×10^{-4}	$1,8 \times 10^{6}$	$3,3 \times 10^{6}$	0,78
Source in [95]	Fig.7	Fig.6	Fig.4	Fig.4	Fig.10

Steps in the calculation of q^i_{LH}/q^i_T, via equations A3.1 to A3.5, are summarised in Table A3.2.

TABLE A3.2

CALCULATION OF q^i_{LH}/q^i_T

$(q/A)_T$ kW/m²	$(q/A)_{NC}$ kW/m²	$\left(\frac{A_{NC}}{A_T}\right)_{inst}$	$(q/A)'_{NB}$ kW/m²	$(q/A)'_{LH}$ kW/m²	$\left(\frac{A_{NC}}{A_T}\right)$	$(q/A)_{NB}$ kW/m²	$\frac{q^i_{LH}}{q^i_T}$
11,5	4,31	0,617	8,81	6,90	0,293	10,24	0,67
21,1	4,68	0,352	19,45	15,21	0	21,1	0,72
41,6	5,14	0	41,6	32,45	0	41,6	0,78

APPENDIX 4

CHOICE OF ACTIVATION CRITERION FOR NUCLEATION CAVITIES

The mouth radii, r, of potentially active cavities, that is, cavities capable of entrapping vapour, will, for any surface-liquid combination, have some frequency distribution. For given conditions a range of these cavities will be active.

The mouth radius of the smallest active cavity is, according to a slight modification of the treatment of Griffith and Wallis [48] given as follows:

$$r^*_{min} = 2\sigma T_{sat} \Big/ \rho_v \lambda \Delta T_{sat} \qquad (A4.1)$$

Thus as ΔT_{sat} is raised from zero, the largest potentially active cavity on the surface is the first to become active ($r^*_{max} = r_{max}$). Further increase of ΔT_{sat} causes activation of progressively smaller cavities while all larger cavities remain active.

Equation A4.1 gives the equilibrium condition of a vapour nucleus sitting cap-wise on a cavity with the cap radius equal to the cavity mouth radius. The equation was originally derived for a constant-temperature field, with the ΔT term signifying the wall-and-liquid superheat at a particular pressure. Under such conditions the equation was tested on artificial cavities and was found to hold [48]. In the presence of a temperature gradient, with boiling from artificial cavities, the agreement ceased [48, 118-120]. For boiling from natural cavities, however, indirect tests [3, 18] indicated that r^*_{min} is at least proportional to the terms on the right-hand side of equation A4.1.

Direct size measurements of natural active sites were provided by Shoukri and Judd [121]. The heater was a copper block having surface finishes varying from a machined finish of

$0,4 \times 10^{-6}$ m centre-line-average roughness to a mirror polish of $0,1 \times 10^{-6}$ m centre-line-average. The test liquid was water boiling at atmoshperic pressure at heat fluxes ranging from 60 to 200 kW/m². In all cases the measured value of r^*_{min} was in good agreement with equation A4.1.

Hsu [122] and Han and Griffith [42] have proposed nucleation criteria which, in addition to the equilibrium condition of equation A4.1, take account of the time-varying liquid temperature gradient above a nucleation cavity. Both analyses are based on the assumption that a vapour nucleus (cap over cavity mouth) can only grow if the temperature in the liquid at the nucleus apex reaches that of the vapour in the nucleus. The liquid temperature gradients were obtained by solution of the transient conduction equation according to the dubious bulk convection model (see Section 2.3.2). Both a minimum and a maximum active cavity mouth radius are thus predicted.

For artificial cavities the agreement between the measured and the predicted mouth radius size range appeared, on casual examination, to be satisfactory [118-120]. Active cavities larger than the largest predicted size were, however, found, thus casting doubt upon the existence of the upper size limit [118, 119]. For natural cavities occurring on heaters of various surface finishes Shoukri and Judd [121] found the active sizes to lie within the predicted range, but grouped towards the lower size limit. The largest active (and thus vapour-entrapping) cavity was, in all tests, smaller than the maximum size predicted by the Hsu model.

The more elaborate nucleation criteria of Hsu [122] and of Han and Griffith [42] thus appear to offer no advantage over equation A4.1. Furthermore the assumption governing the existence of an upper active cavity size limit may be questioned: Surely a nucleus with condensation at the apex can grow if the vapour addition near its base exceeds the loss by condensation? Howell and Siegel [119] have in fact derived a

nucleus activation criterion based on such net vapour addition. Their equation, however, predicts nucleation behaviour not significantly different from that of equation A4.1.

Equation A4.1, without an additional upper cavity size limit, is thus adopted in the present treatment. Tests of its validity are presented in Section 3.2.1.

APPENDIX 5

PHYSICAL PROPERTIES REQUIRED FOR TESTING NUCLEATION CRITERION AGAINST DATA OF ANDERSON

The nucleation criterion required to be tested against the data of Anderson [123] was:

$$r^*_{min} = 2T_{sat}\sigma/\lambda\rho_v\Delta T_{sat} \qquad (A5.1)$$

Surface tension, σ, latent heat of vaporisation, λ, and vapour density, ρ_v, all at saturation, were thus required for the compounds and conditions shown in Table A5.1.

TABLE A5.1

CONDITIONS OF ANDERSON'S STUDY

Test Liquid		P kN/m²	T_{sat} °C	Remarks
Freon 113	$CF_2Cl.CFCl_2$	102	47,7	atm. B.P.
Freon 113	$CF_2Cl.CFCl_2$	157	61,1	-
Carbon tetrachloride	CCl_4	100	76,8	atm. B.P.
Chloroform	$CHCl_3$	102	60,6	atm. B.P.
1,2 Dichloroethane	$CH_2Cl.CH_2Cl$	101	82,3	atm. B.P.
1,1,2 Trichloroethane	$CHCl_2.CH_2Cl$	100	114	atm. B.P.

A5.1 PRIMARY DATA

The following physical properties were available directly from the literature:

Surface tension: at the atmospheric boiling point for carbon tetrachloride [51], chloroform and trichloroethane [210].

Latent heat of vaporisation: in nomograph form (difficult to read accurately) for Freon 113 and carbon tetrachloride [51] and in tables for chloroform [213].

Surface tension: at room temperature for Freon 113 [214] and dichloroethane [210].

The remaining required properties were calculated as outlined below.

A5.2 CALCULATED DATA

Vapour density

This was calculated from the Ideal Gas Law with compressibility factor corrections as given for saturated vapours by Hougen et al [215]. The necessary critical constants were available from the literature [214, 216, 217] for all compounds except trichloroethane. In this case critical temperature and pressure were calculated by Lyderson's method [213] and critical volume by the Schuster-Lyderson method [213]. The whole procedure, including critical constant estimates, was checked for Freon 113; the calculated density differed from an experimental value [214] by less than 3 per cent.

Latent heat of vaporisation

This was calculated from the critical properties by the method of Giacolone [213] and again from critical properties and the atmospheric boiling point by the method of Riedel [213]. The latter method applies only at atmospheric pressure. Values obtained by the two theoretical methods and (where available) from the literature differed by less than 4 per cent. For dichloroethane and trichloroethane the means of the two theoretical values were finally used. For the remaining compounds the means of all three values were used.

Surface tension

For Freon 113 and dichloroethane surface tension at the boiling point were calculated from published [214] room temperature values. McLeod's equation [218] was used. This states that the ratio $\sigma^{0,25}/(\rho_L-\rho_V)$ is equal to a constant, C', independent of temperature for each substance. For example, in the temperature range 20 to 200 ^{o}C, C' varies by less than 1 per cent for benzene and by 3 per cent for ethanol. The method called for liquid densities at the boiling points. These densities were obtained from published room temperature values by the method of Benson [213]. Benson's method itself was checked against a published value of the liquid density of Freon 113 at -15 ^{o}C [217] and found to be in error by less than 1,5 per cent.

A5.3 SUMMARY OF REQUIRED PROPERTIES

All physical properties (literature values and calculated values) required in equation A5.1 for the conditions of Anderson's runs are summarised in Table A5.2.

TABLE A5.2

SUMMARY OF PHYSICAL PROPERTIES; EQUATION A5.1, ANDERSON'S RUNS

Test Liquid	T_{sat} K	σ J/m^2	ρ_v kg/m^3	λ kJ/kg	$\frac{2T_{sat}\sigma}{\lambda\rho_v}$ m K
Freon 113	320,8	0,0164	7,465	145	$9,721 \times 10^{-6}$
Freon 113	334,3	0,0150	11,36	143	$6,174 \times 10^{-6}$
Carbon tetrachloride	349,9	0,0198	5,446	188	$1,353 \times 10^{-5}$
Chloroform	333,7	0,0194	4,550	240	$1,186 \times 10^{-5}$
1,2 Dichloroethane	355,1	0,0182	3,146	322	$1,166 \times 10^{-5}$
1,1,2 Trichloroethane	387,5	0,0220	4,109	260	$1,487 \times 10^{-5}$

APPENDIX 6

TEST FOR OPTICAL THICKNESS OF 'ELECTROPANE' COATINGS

'Electropane' sheets were supplied with stannic oxide coatings of slightly uneven optical thickness. This could be judged from variations in interference colour when the sheets were viewed in white light. It was required to establish which interference colour corresponded to an optical thickness of $\lambda/2$ for λ = 437 nm.

The following approximate test was used: A number of small pieces, each of recognisably different interference colour, were cut from the 'Electropane' sheets. On one half of each piece the coating was removed chemically (see Section 5.2.5), while on the other half the coating remained intact. These pieces were now viewed under normal incidence in collimated monochromatic light of wavelength 437 nm. Since glass carrying a thin film of optical thickness $\lambda/2$ has the same reflectance as bare glass [173], the required coating was the one that was invisible. The surface satisfying this condition was kept as an interference colour reference.

APPENDIX 7

DETERMINATION OF MEAN HEAT FLUX FROM BOILING SURFACE

In order to calculate the mean boiling heat flux from measurements of the electrical input it was necessary to consider the convective losses from the bottom of the heating disc, the leads resistance between the wattmeter and the boiling film, and the geometry of the heating film. These are dealt with in turn below and are followed by an estimate of the accuracy of the final heat flux values.

A7.1 CONVECTIVE LOSSES FROM BOTTOM OF HEATING DISC

With the disc treated as a heated plate facing downwards, the heat transfer coefficient for losses by laminar natural convection from the bottom of the disc to the surrounding air is given [51] as follows:

$$hL/k = 0{,}27\ [(L^3\rho^2\beta\Delta T/\mu^2)(C\mu/k)]^{0{,}25} \qquad (A7.1)$$

where the characteristic length L is the exposed diameter of the disc, ΔT is the temperature difference between the bottom face of the disc and the bulk air, and all physical properties refer to air at the mean film temperature.

To check on laminarity the term in square brackets, that is, the product Gr. Pr, was evaluated for a ΔT of 50 K (an overestimate), an air temperature of 45 ^{o}C and an L of 30 mm. The resulting product Gr. Pr was 9×10^4, that is, well below 2×10^7, the value marking the onset of turbulence. The corresponding heat transfer coefficient was 3,7 W/m^{2}K.

By retaining the overestimated ΔT of 50 K the heat loss, $h\Delta T$, was 185 W/m^2.

The lowest boiling fluxes studied were of the order of 3×10^4 W/m^2. The estimated losses from the bottom of the disc were thus some 0,5 per cent of the surface flux.

Equation A7.1 refers to a plate free at the edges. With the heating disc enclosed as shown in Figure 5.5, a thermal boundary layer very much thicker than that implicit in equation A7.1 must have built up beneath it. Losses were thus very much smaller than the 0,5 per cent estimated from equation A7.1 and may be neglected altogether.

A7.2 CORRECTION FOR LEADS RESISTANCE

The wattmeter measured the power dissipated in the heating film and in the intermediate connecting leads.

The leads resistance was measured (on a Wheatstone bridge) with the heating surface removed and a thick copper wire (of negligible resistance) soldered in its place. The leads resistance, ΔR, was 0,397 Ω. The resistance of the heating surfaces themselves, R, was approximately 60 Ω.

At a current flow of I the measured power dissipation, W_M, was $I^2(R + \Delta R)$ and the required power dissipation over the boiling surface, W_B, was I^2R. Thus

$$W_B/W_M = 60/60,397 = 0,993 \qquad (A7.2)$$

A correction factor of 0,99 was thus applied to all wattmeter readings.

A7.3 GEOMETRY OF HEATING FILM

The geometry of the heating film is shown in Figure A7.1.

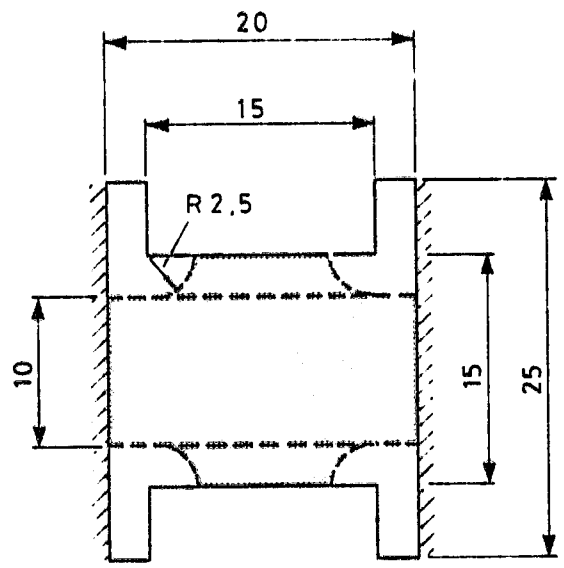

FIG. A7.1 HEATING FILM

Over the central (speckled) portion of the film the power dissipation was uniform within ± 3 per cent (see Section 5.2.5 and Figure 5.2). The heat flux over this central uniformly heated area was the same as would have been obtained had the film been a simple rectangle of 15 mm width and 20 mm length between contacts.

Accurate measurements, using a Nikon profile projector, showed the length between contacts to be 20,15 mm. The rectangular section thus had an area of 302,2 mm^2 and the mean uniform heat flux, in W/m^2, was given by

$$(q/A) = W_B/(302{,}3 \times 10^{-6}) = 3308\ W_B \qquad (A7.3)$$

where W_B was the total wattage dissipated in the heating film.

An alternative method of calculating the mean uniform heat flux involved the search for the outermost undistorted equipotential lines on the Teledeltos plot. In Figure 5.2 these were the lines corresponding to 30 and 70 per cent of the total potential drop. The distance between these lines multiplied by the width of the film (15 mm) thus gave the area over which 40 per cent of the total power input was dissipated. This method resulted in a flux conversion factor essentially identical to that of equation A7.3. The length measurement between the equipotential lines is, however, less reliable than that between the contacts.

A7.4 OVERALL CONVERSION FACTOR

From the foregoing the overall conversion factor from the wattmeter readings, W_M, to mean heat flux, in W/m^2, follows as

$$q/A = 0{,}99 \times 3308\ W_M = 3275\ W_M \qquad (A7.4)$$

A7.5 ACCURACY OF HEAT FLUX DETERMINATIONS

With a guaranteed wattmeter accuracy of 0,2 per cent of full scale deflection, and with negligible heat losses from the bottom of the disc, the main sources of error were the uncertainty in the area of the heating film, the unevenness of flux distribution over the film and radial heat losses from the edge of the film.

The distance between the contacts of the heating film (20,15 mm) was known accurately and was fixed by the width of the steel mask used in vacuum evaporation of the contacts. The width of the film (15 mm) was, however, determined during the chemical film removal (see Section 5.2.5) and was uncertain within ± 0,5 mm. The film area was thus accurate to ± 3 per cent.

Over the central portion of the heating film (the speckled area in Figure A7.1) the distribution of the heat flux, as determined from the Teledeltos conducting sheet analogue, was even within ± 5 per cent. This estimate neglected variations in the thickness of the film and radial heat losses towards the uncoated portions of the disc. Thickness variations in the film could be judged from its interference colour and appeared to be negligible. Radial losses could not readily be estimated, but might have been significant near the edge of the film.

The overall accuracy of the reported heat flux values was thus estimated as ± 7 per cent for the central rectangular area of 10 x 20 mm, shown speckled in Figure A7.1. Beyond this area, nearer the edge of the film, the heat flux was lower than the reported value, possibly by as much as 10 per cent.

APPENDIX 8

MEAN TEMPERATURE OF BOILING SURFACE

The mean surface temperature of the boiling surface was determined from thermocouple temperature measurements of the bottom of the boiling disc. The thermocouple was attached as shown in Figure [illegible] and Figure A8.. The following sections show that the thermal contact resistance, the fin losses and the axial conduction losses of the thermocouple were all negligible. An experimental verification of the temperature measuring technique and an assessment of accuracy follow.

A8.1 THERMAL CONTACT

The thermal contact between the thermocouple and the glass surface was checked by temperature measurements during which the tip of the thermocouple sheath (apart from being attached by adhesive tape as usual) was indium-soldered to the glass. With methanol boiling under typical test conditions from the upper disc surface ($q/A \approx$ [illegible] kW/m^2, $P \approx 25\ kN/m^2$) the same temperatures were recorded with and without the soldered attachment.

A8.2 FIN LOSSES FROM THERMOCOUPLE

Appendix 7 showed the convective heat losses from the flat bottom of the boiling disc to have been negligible. The axially attached thermocouple, however, could be regarded as constituting an extended surface, or fin, which might have increased the losses and thus itself recorded an erroneously low temperature. To check this error the thermocouple was treated as equivalent to two rectangular fins, formed by splitting the thermocouple sheath along its

FIG. A8.1 THERMOCOUPLES TREATED AS FINS.

length and folding the two halves straight, see Figure A8.1.

The steady-state temperature distribution in a rectangular fin, insulated at the tip, is given as follows [209]:

$$(T - T_L) = (T_o - T_b) \cosh\{m(L - x)\}/\cosh(mL) \qquad (A8.1)$$

where T is the temperature of the fin as a function of length x, T_o is the fin root temperature (x = 0), L is the root-to-tip length of the fin and m is given by

$$m = (h/2k\ y_o)^{\frac{1}{2}} \qquad (A8.2)$$

where h is the convection coefficient from the fin surface, k is the thermal conductivity of the fin material, y_o is half the fin thickness, and the factor 2 accounts for convection from only one face of the fin (Figure A8.1).

With a thermocouple sheath thickness of 0,06 mm, y_o was 3×10^{-5} m; k, for stainless steel, was 16,3 W/m K; and h, from Appendix 7, was 3,7 W/m^2 K. Thus m was 61,5 m^{-1}.

The length L was taken as half the thermocouple sheath diameter, that is, as 0,785 mm. The temperature was required at the position of the thermocouple junction; this was taken as midway along the length of the fin, or at x = 0,393 mm. With these values equation A8.1 gave

$$(T - T_b) = 0,9991\ (T_o - T_b) \qquad (A8.3)$$

that is, the temperature T, sensed by the thermocouple, was identical with T_o, the temperature of the glass surface, and extended surface losses were totally negligible.

A8.3 AXIAL CONDUCTION LOSSES IN THERMOCOUPLE

Axial conduction losses in the thermocouple were checked by

length and folding the two halves straight, see Figure A8.1.

The steady-state temperature distribution in a rectangular fin, insulated at the tip, is given as follows [209]:

$$(T - T_b) = (T_o - T_b) \cosh\{m(L - x)\}/\cosh(mL) \qquad (A8.1)$$

where T is the temperature of the fin as a function of length x, T_o is the fin root temperature (x = 0), L is the root-to-tip length of the fin and m is given by

$$m = (h/2k\ y_o)^{\frac{1}{2}} \qquad (A8.2)$$

where h is the convection coefficient from the fin surface, k is the thermal conductivity of the fin material, y_o is half the fin thickness, and the factor 2 accounts for convection from only one face of the fin (Figure A8.1).

With a thermocouple sheath thickness of 0,06 mm, y_o was 3×10^{-5} m; k, for stainless steel, was 16,3 W/m K; and h, from Appendix 7, was 3,7 W/m^2 K. Thus m was 61,5 m^{-1}.

The length L was taken as half the thermocouple sheath diameter, that is, as 0,785 mm. The temperature was required at the position of the thermocouple junction; this was taken as midway along the length of the fin, or at x = 0,393 mm. With these values equation A8.1 gave

$$(T - T_b) = 0,9991\ (T_o - T_b) \qquad (A8.3)$$

that is, the temperature T, sensed by the thermocouple, was identical with T_o, the temperature of the glass surface, and extended surface losses were totally negligible.

A8.3 AXIAL CONDUCTION LOSSES IN THERMOCOUPLE

Axial conduction losses in the thermocouple were checked by

temperature measurements in which the length of thermocouple in contact with the surface was varied from 5 to 20 mm (the standard length was about 10 mm). Identical boiling conditions prevailed in all tests. The recorded temperatures varied by some 3 ^{o}C and showed no trend with the attachment length. Axial conduction losses thus appeared to have been negligible.

A8.4 EXPERIMENTAL VERIFICATION

From the foregoing it would appear that the temperature measured at the lower disc surface corresponded closely to the mean temperature of the upper (boiling) disc surface. An experimental verification was, however, considered desirable.

To this end the temperature of the boiling surface was measured by a similar thermocouple, bent into an L-shape and lowered onto the surface. Under boiling conditions the thermocouple was periodically enveloped in vapour and recorded a temperature considerably lower than that attached to the bottom of the heater. With the upper disc surface in natural convection, however, the two temperatures agreed more closely. The top thermocouple, however, continued to read 2 to 3 ^{o}C lower than that attached to the bottom.

Fin losses from the upper thermocouple were thus checked. Equation A8.1 and A8.2 were again applied, but the fin convection coefficient, h, was approximated, by regarding the thermocouple sheath as a horizontal cylinder in laminar convection, as follows [51]:

$$hD/k = 0{,}53\left[(D^3\rho^2\beta\Delta T/\mu^2)(C\mu/k)\right]^{0{,}25} \qquad (A8.4)$$

With D taken as 0,5 mm (the sheath diameter), ΔT as 30 K and physical properties evaluated for methanol at 50 ^{o}C, a

coefficient h of 689 W/m^2 K resulted. Equation A8.1 then reduced to

$$(T - T_b) = 0{,}861\ (T_o - T_b) \qquad \text{(A8.5)}$$

For a surface temperature of 65 ^oC and a bulk liquid temperature of 35 ^oC (typical test conditions) the predicted thermocouple temperature was 61 ^oC, or in error by -4 ^oC.

The temperature discrepancy between the upper and lower thermocouples thus appeared to be explainable in terms of fin losses. The thermocouple attached to the lower surface of the disc would thus appear to have closely approximated to the true mean temperature of the boiling surface.

A8.5 ACCURACY OF REPORTED SURFACE TEMPERATURES

In view of the random temperature variations of 3 ^oC in tests with various thermocouple attachment methods, and the slight uncertainty in the experimental verification just discussed, it was felt that the accuracy of the reported mean boiling surface temperatures was of the order of ± 5 ^oC.

APPENDIX 9

MAXIMUM MEASURABLE MICROLAYER THICKNESS AND BEAM MONOCHROMATICITY

In Chapter 6, Section 6.3.4, an analysis was given of the interrelation of fringe visibility and beam monochromaticity. It was shown that with the illumination employed, namely a beam of Gaussian spectral distribution of bandwidth 18 nm and peak wavelength 437 nm, fringes would be visible up to a microlayer thickness of 3,8 μm. For purposes of checking this result an alternative simple relation, due to Gates [179], is examined below.

Gates states, without specifying the type of spectral distribution, that easily recognisable fringes will be obtained for an optical path difference of $\bar{x}$ if the spectral width of the source is considerably less than $\lambda^2/\bar{x}$. In other words, for an incident beam of peak wavelength λ_o and bandwidth $d\lambda$, the maximum optical path difference in a film for which fringes will be visible is given by

$$\bar{x} = \lambda_o^2/d\lambda \qquad (A9.1)$$

For the case considered (λ_o = 437 nm, $d\lambda$ = 18 nm)

$$\bar{x} = 24,3\ \lambda_o \qquad (A9.2)$$

Fringes will thus be visible up to an optical thickness, nd, of 12,15λ, or, for methanol (n = 1,33), up to a microlayer thickness of 4,0 μm. The two estimates are thus in agreement.

The comparison of equation A9.1 with equations 6.27 and 6.28

of Chapter 6 shows that for a beam of Gaussian distribution Gates' rule implies a limiting contrast for fringe visibility of 0,15. This is in approximate agreement with Françon's value of 0,2 (see [172] p 79).

APPENDIX 10

CINÉ FILM AND PROCESSING

The simultaneous photography of the bubble profiles, of the blue interference fringes and the red timing marks necessitated a panchromatic film capable of high contrast and at least moderate resolution. The high framing rate and the levels of the available illuminations called for an emulsion of reasonable sensitivity (that is, speed). Speed, contrast and resolving power are all to some extent dependent on development. In this study development, fixing and washing were carried out somewhat unconventionally in an automatic rapid film processor.

The rapid processor, a machine manufactured by John Hadland Photographic Instrumentation, transported the film at a rate of approximately 0,6 metres per minute through four heated tanks, each of 2,5 litres capacity, the first containing developer and the remainder fixer and rinsing water, and from there through a hot-air heating tunnel onto the take-up spool. The film resided some 50 seconds in each tank. Processing in such short times was possible only with solutions at high concentrations and temperatures, and with high-energy or X-ray developers. This forced development gave increased contrast and film speed, both desirable features, but tended to increase the graininess of the image. Thus, to maintain the required moderate resolution, an emulsion giving extremely fine grain under normal development was required. Further, the emulsion was required to withstand the high solution temperatures without undue softening.

After many trials with various emulsions and processing solutions the following combination was found satisfactory:

Film : Gevaert Scientia 45C62, a scientific emulsion normally giving an ASA speed of 12 to 25, a gamma of 2 to 3 and a resolution of 180 lines per mm;

Development : 50 seconds at 35 ^{o}C in May and Baker 'Exprol' X-ray developer, diluted in the ratio of 1 part to 1 part of water;

Fixing : Twice for 50 seconds at 35 ^{o}C in May and Baker 'Amfix', diluted in the ratio 1 part to 1,5 parts of water, no hardner added;

Washing : 50 seconds at 35 ^{o}C in water containing 6 drops of Kodak 'Photoflo' wetting agent per 2,5 litre tank.

The resulting negative film was suitable for preliminary viewing, but was incompletely washed. Thus at the end of a day's work all successful films were rewashed, with all four tanks containing water at 25 ^{o}C, and the last having wetting agent added as detailed above.

The rapid film processing led to an image quality slightly inferior to that obtainable by normal methods. It did, however, permit the rapid execution of successive runs, while yet allowing the results of each to be judged before the start of the next. This was essential since failures and repeat runs were frequent.

APPENDIX 11

ENLARGEMENT AND PRINT PROCESSING

The microlayer interferograms and the bubble profile views were transcribed frame-by-frame onto prints at an enlargement of approximately 30 times. A standard enlarger was used, fitted with a high-quality wide-angle lens, the Schneider Componon 28 mm f4. The prints were made up and rapid-processed using the Ilford 'Ilfoprint' system.

'Ilfoprint' relies on special paper in which a hydroquinone developer is incorporated into the emulsion during manufacture. Upon wetting with an activator solution the exposed silver halides in the emulsion are reduced to the visible silver within two seconds. Contact with a stabilizer solution converts the unexposed halides to a non-light-sensitive salt. Activation and stabilisation takes place in an automatic 'Ilfoprint' processor. The machine incorporates a series of rollers which apply the activator, then feed the print through the stabilizer bath, squeegee it and deliver it sufficiently dry for handling. The entire processing of a 20 x 25 cm print occupies 15 seconds. The prints are stable for at least five years, but can be rendered permanent by subsequent normal fixing and washing.

Ilfoprint Grade R2 paper and the standard proprietary chemicals were used. The results were of a quality indistinguishable from that obtained by normal methods. The required several hundred prints were made up rapidly and consistently, without operator fatigue.

APPENDIX 12

MICROLAYER REFRACTIVE INDICES. METHANOL AND ETHANOL

Light and dark interference fringes corresponded to increments of microlayer thickness of $\lambda/4n_1$, where λ is the wavelength of the incident beam (0,437 μm) and n_1 is the microlayer refractive index. Refractive indices were thus required for methanol and ethanol at a wavelength of 0,437 μm and at representative microlayer temperatures.

Refractive indices at 20 ^{o}C and at various wavelengths are given in Table A12.1. The first three rows show published values [210]. The last row shows the value at λ = 0,437 μm, as obtained by graphical interpolation accurate to the third decimal figure.

TABLE A12.1

REFRACTIVE INDICES AT 20 ^{o}C versus WAVELENGTH

Wavelength, λ μm	Refractive index, n_1, for: methanol	ethanol	Source
0,589	1,329	1,361	[210]
0,486	1,333	1,365	[210]
0,434	1,336	1,369	[210]
0,437	1,336	1,369	graphical interpolation

The variation of refractive index with temperature is available [210] over the ranges 18 to 35 ^{o}C for methanol and 0 to 40 ^{o}C

for ethanol. At λ = 0,437 μm the resulting overall refractive index data then become:

Methanol: $n_l = 1{,}336 - 3{,}6 \times 10^{-4} (T - 20)$ (A12.1)

Ethanol : $n_l = 1{,}369 - 4{,}0 \times 10^{-4} (T - 20)$ (A12.2)

The temperature within the microlayer varies with its thickness, its radius and with time. Chapter 4 indicates that extremes of microlayer temperatures may be taken as T_w, the measured mean heater wall temperature, and as T_{sat}. Table A12.2 shows refractive indices at these temperatures and at the mean temperature $(T_w + T_{sat})/2$ for all runs reported in this work.

TABLE A12.2

REFRACTIVE INDICES AT 0,437 μm versus TEMPERATURE

Run *	T_w °C	T_{sat} † °C	$(T_w+T_{sat})/2$ °C	Refractive index at: T_w	T_{sat}	$(T_w+T_{sat})/2$
M10	72	35,2	53,6	1,317	1,331	1,324
M13	68	33,9	51,0	1,319	1,331	1,325
M14	68,5	40,4	54,5	1,319	1,329	1,324
M19	72,5	40,4	56,5	1,317	1,329	1,323
M20	77	45,5	61,3	1,315	1,327	1,321
E 8	79	47,6	63,3	1,345	1,358	1,352
E12	85	53,2	69,1	1,343	1,356	1,349

*M denotes methanol, E denotes ethanol.

†Calculated from system pressure, see Appendix 13.

It is seen that the choice of microlayer temperature is not of critical importance. The refractive indices at $(T_w + T_{sat})/2$ differ from those at the extreme temperatures by a mere 0,5 per cent and were accepted for the evaluation of the microlayer thickness.

Since the mean temperatures $(T_w + T_{sat})/2$ in all cases lie somewhat outside the temperature ranges for which equations A12.1 and A12.2 were derived, the overall accuracy of the refractive indices may be taken as ± 1 per cent. Within these error bounds, however, the values for all methanol runs and all ethanol runs may be taken as identical. Thus for purposes of evaluating microlayer thicknesses we have for all runs:

methanol: $n_1 = 1,32$
ethanol : $n_1 = 1,35$

APPENDIX 13

SATURATION TEMPERATURE AS A FUNCTION OF PRESSURE

Expressions for the saturation temperature as a function of pressure were obtained by fitting a re-arranged form of the Clausius-Clapeyron equation to published vapour pressure data. For both methanol and ethanol the regressions covered eight data points [216] in the pressure range 1,33 to 101,3 kN/m^2. The final equations are:

methanol: $T_{sat} = 2109,4/(8,2481 - \log P) - 273,2$ (A13.1)

ethanol : $T_{sat} = 2200,4/(8,2639 - \log P) - 273,2$ (A13.2)

where T_{sat} is in ^{o}C and P is in kN/m^2.

In the temperature range covered in this study the maximum deviation of equation A13.1 is 1 ^{o}C and that of equation A13.2, 0,2 ^{o}C.

APPENDIX 14

TABLES OF EXPERIMENTAL RESULTS

Tables A14.1 to A14.14 give the complete listing of data points on microlayer geometry, bubble volume and characteristic bubble dimensions, all versus time, for the seven runs presented in Chapter 8. Blanks in the tables indicate that no data point was obtainable for one of the following reasons:

(1) The microlayer had not yet, or no longer, extended to a particular thickness (the corresponding fringe was absent),

(2) the microlayer profile had become vertical (fringes had merged),

(3) a fringe had been too indistinct, irregular or fragmented to permit a meaningful measurement,

(4) the outermost edge of the microlayer had not been detectable.

TABLE A14.1

MICROLAYER GEOMETRY. RUN M10

Frame No.	Time ms	Bubble base radius, r (mm), for: Microlayer thickness d (μm) of: 0,0	0,083	0,166	0,249	0,332	0,415	0,498	0,581	0,664	M'layer periphery
826	0,0										
827	1,0	0,22									
828	2,0	0,38									
829	3,0	0,44	1,16	1,90							
830	4,0	0,57	1,25	1,90							
831	5,0	0,62	1,28	1,87	2,29	2,78					2,95
832	6,0	0,71	1,25	1,85	2,29	2,73					
833	7,0	0,71	1,28	1,85	2,25	2,73					
834	8,0	0,79	1,30	1,85	2,27	2,73	3,26	3,70			3,97
835	9,0	0,88	1,30	1,82	2,29	2,75	3,27	3,70			3,97
836	10,0	0,93	1,25	1,78	2,27	2,73	3,28	3,70			4,01
837	11,0	0,97	1,30	1,78	2,27	2,73	3,28	3,75			4,14
838	12,0	1,01	1,32	1,76	2,22	2,73	3,28	3,75			4,23
839	13,0	1,06	1,34	1,76	2,22	2,75	3,31	3,70			4,41
840	14,0	1,10	1,34	1,74	2,25	2,69	3,31	3,66			1,50
841	15,0	1,15	1,41	1,74	2,27	2,69	3,26	3,66			4,58
842	16,0	1,19	1,38	1,72	2,29	2,64	3,26	3,66	4,05	4,32	4,58
843	0	1,25	1,41	1,74	2,27	2,69	3,26	3,61	4,05	4,32	4,67
844	18,0	1,28	1,43	1,76	2,25	2,73	3,26	3,61	4,05	4,32	4,63
845	19,0	1,32	1,45	1,76	2,29	2,69	3,28	3,61	4,05	4,32	4,58
846	20,0	1,37	1,45	1,74	2,29	2,66	3,26	3,66	4,05	4,28	4,54
847	21,0	1,43		1,81	2,29	2,69	3,22	3,61	4,05	4,28	4,54
848	22,0	1,45		1,81	2,29	2,64	3,17	3,57	4,01	4,28	4,54
849	23,0	1,50		1,76	2,29	2,64	3,17	3,53	3,97	4,23	4,50
850	24,0	1,59		1,76	2,29	2,66		3,53	3,97	4,23	4,45
851	25,0	1,63			2,29	2,69			3,88	4,14	4,50
852	26,0	1,67			2,29	2,69	3,17			4,14	4,45
853	27,0	1,67			2,25	2,69				4,05	4,36
854	28,0	1,72			2,29	2,69	3,17			3,97	4,32
855	29,0	1,72			2,29	2,64	3,17			3,88	4,23
856	30,0	1,76			2,29	2,64	3,09			3,70	4,14
857	31,0	1,76			2,29	2,60	3,09			3,61	4,10
858	32,0	1,76				2,60				3,53	3,75
859	33,0	1,85				2,57	3,10			3,44	3,66
860	34,0	1,85				2,57	3,13			3,17	3,44
861	35,0	1,94									3,17
862	36,0	1,94									3,09
863	37,0	1,94									2,82
864	38,0	1,85									2,56
865	39,0	1,85									2,20
866	40,0	1,59									1,76
867	41,0	1,34									
868	42,0	1,19									1,19
869	43,0	0,79									0,79
870	44,0	0,0									0,0

TABLE A14.2

BUBBLE VOLUME AND CHARACTERISTIC DIMENSIONS. RUN M10

Frame No.	Time ms	V mm^3	D_w mm	H mm	D_c mm	D_s mm
826	0,0	0,0	0,0	0,00		0,00
827	1,0	1,4	1,67	0,83		1,40
828	2,0	25,8	3,70	2,29		3,67
829	3,0	57,0	6,17	3,00		4,78
830	4,0	104,8	7,32	3,60		5,85
831	5,0	164,0	8,46	4,27	5,90	6,79
832	6,0	212,4	9,03	4,71		7,40
833	7,0	271,6	9,91	5,06		8,03
834	8,0	341,9	10,75	5,47	7,94	8,68
835	9,0	391,6	11,25	5,82	7,94	9,08
836	10,0	472,7	11,99	6,17	8,02	9,67
837	11,0	548,3	12,52	6,52	8,28	10,16
838	12,0	604,6	12,96	6,79	8,46	10,49
839	13,0	685,3	13,31	7,14	8,82	10,94
840	14,0	713,5	13,75	7,58	9,00	11,09
841	15,0	795,1	14,02	7,76	9,16	11,49
842	16,0	933,8	14,53	8,14	9,16	12,13
843	17,0	986,1	14,72	8,23	9,34	12,35
844	18,0	1069	15,07	8,64	9,26	12,69
845	19,0	1129	15,25	8,99	9,16	12,92
846	20,0	1208	15,60	9,17	9,08	13,21
847	21,0	1235	15,69	9,43	9,08	13,31
848	22,0	1304	15,95	9,70	9,08	13,56
849	23,0	1363	16,04	9,87	9,00	13,76
850	24,0	1405	16,48	10,05	8,90	13,90
851	25,0	1425	16,40	10,17	9,00	13,96
852	26,0	1456	16,40	10,31	8,90	14,06
853	27,0	1547	16,57	10,67	8,72	14,35
854	28,0	1595	16,78	10,89	8,64	14,50
855	29,0	1597	16,66	10,97	8,46	14,50
856	30,0	1646	16,84	11,19	8,28	14,65
857	31,0	1638	16,66	11,37	8,20	14,63
858	32,0	1614	16,78	11,46	7,50	14,55
859	33,0	1633	16,75	11,76	7,32	14,61
860	34,0	1679	16,84	11,99	6,88	14,75
861	35,0	1602	16,66	11,99	6,34	14,52
862	36,0	1634	16,75	12,16	6,18	14,61
863	37,0	1586	16,66	12,08	5,64	14,50
864	38,0	1550	16,54	12,16	5,12	14,36
865	39,0	1549	16,31	12,34	4,40	14,35
866	40,0	1489	16,25	12,34	3,52	14,17
867	41,0	1426	16,13	12,43		13,97
868	42,0	1431	16,04	12,73	2,38	13,98
869	43,0	1361	15,95	12,87	1,58	13,75
870	44,0	1321	15,95	12,73	0,00	13,61

TABLE A14.3

MICROLAYER GEOMETRY. RUN M13

Frame No.	Time ms	Bubble base radius, r (mm), for: microlayer thickness, d (μm) of: 0,0	0,083	0,166	0,249	0,332	0,415	0,498	M'layer periphery
1053	0,00								
1054	1,67	0,31							2,33
1055	3,34	0,63							2,96
1056	5,01	0,85	2,42	3,41					3,59
1057	6,68	0,99	2,42	3,41					3,85
1058	8,35	1,17	2,53	3,41	3,93	4,44			4,62
1059	10,02	1,25	2,55	3,36	3,91	4,39			5,05
1060	11,69	1,39	2,60	3,[illegible]	3,90	4,39			5,29
1061	13,36	1,54	2,71	3,[illegible]	3,90	4,37			5,20
1062	15,03	1,60	2,75	3,27	3,89	4,33			5,29
1063	16,70	1,70	2,78	3,32	3,89	4,35	4,87	5,34	5,42
1064	18,37	1,86	2,84	3,32	3,85	4,33	4,75	5,10	5,29
1065	20,04	1,95	2,82	3,27	3,87	4,31	4,72	5,06	5,20
1066	21,71	2,12	2,82	3,30	3,85	4,33	4,66	4,92	5,06
1067	23,38	2,13	2,89	3,29	3,86	4,31	4,54	4,74	4,78
1068	25,05	2,29	2,87	3,27	3,85	4,35			4,75
1069	26,72	2,45	2,80	3,25	3,84	4,27			4,48
1070	28,39	2,45	2,82	3,27	3,69	4,03			4,12
1071	30,06	2,58	2,87	3,27					3,68
1072	31,73	2,73	2,87	3,27					3,57
1073	33,40	2,82	2,87	3,14					
1074	35,07	2,76							2,76
1075	36,74	2,24							2,24
1076	38,41	1,66							1,66
1077	40,08	0,81							0,81
1078	41,75	0,00							0,00

TABLE A14.4

BUBBLE VOLUME AND CHARACTERISTIC DIMENSIONS. RUN M13

Frame No.	Time ms	V mm^3	D_w mm	H mm	D_c mm	D_s mm
1053	0,00	0,0	0,00	0,00	0,00	0,00
1054	1,67	21,0	4,30	2,24	4,66	3,43
1055	3,34	146,7	8,25	4,12	5,92	6,54
1056	5,01	284,8	10,22	5,29	7,18	8,16
1057	6,78	445,5	11,38	6,01	7,70	9,26
1058	8,35	546,2	12,37	6,63	9,24	10,14
1059	10,02	683,0	13,18	7,17	10,10	10,93
1060	11,69	787,1	13,93	7,89	10,58	11,46
1061	13,36	883,6	14,25	8,34	10,40	11,91
1062	15,03	976,3	14,61	8,61	10,58	12,31
1063	16,70	1063	14,79	9,02	10,84	12,66
1064	18,37	1169	15,15	9,50	10,58	13,07
1065	20,04	1298	15,42	9,90	10,40	13,53
1066	21,71	1361	15,63	10,40	10,12	13,75
1067	23,38	1376	15,60	10,67	19,56	13,80
1068	25,05	1393	15,51	10,94	9,50	13,86
1069	26,72	1418	15,69	11,21	8,96	13,94
1070	28,39	1432	15,60	11,47	8,24	13,98
1071	30,06	1398	15,42	11,65	7,36	13,87
1072	31,73	1399	15,42	11,89	7,14	13,88
1073	33,40	1354	15,24	12,01	6,28*	13,73
1074	35,07	1269	14,84	12,19	5,52	13,43
1075	36,74	1219	14,61	12,37	4,48	13,25
1076	38,41	1151	14,43	12,59	3,32	13,00
1077	40,08	1102	14,25	12,82	1,62	12,81
1078†	41,75	1045	(14,16)	(9,77)	0,00	12,59

* estimated from Figure 8.9

† bubble already departed

TABLE A14.5

MICROLAYER GEOMETRY. RUN M14

Frame No.	Time ms	Bubble base radius, r (mm), for: microlayer thickness, d (μm), of: 0,00	0,083	0,166	0,249	0,332	,415	0,498	M'layer periphery
775	0,00								
776	1,21	0,38							1,36
777	2,42	0,61							,25
778	3,63	0,80	1,78	2,90					,01
779	4,84	0,91	1,88	2,91					3,01
780	6,05	0,97	1,94	2,89					3,52
781	7,26	1,11	2,01	2,83	3,25	3,67			3,67
782	8,47	1,20	2,07	2,82	3,20	3,66			3,80
783	9,68	1,27	2,07	2,79	3,19	3,68			3,99
784	10,89	1,35	2,07	2,78	3,21	3,64			4,09
785	12,10	1,44	2,11	2,78	3,21	3,66			4,13
786	13,31	1,50	2,11	2,76	3,21	3,64			4,13
787	14,52	1,64	2,16	2,72	3,17	3,62			4,16
788	15,73	1,73	2,21	2,75	3,15	3,62	3,81	4,02	4,23
789	16,94	1,80	2,24	2,72	3,17	3,62	3,82	4,04	4,23
790	18,15	1,84	2,21	2,72	3,15	3,57	3,76	3,99	4,27
791	19,36	1,88	2,25	2,72	3,19	3,61	3,79	3,99	4,23
792	20,57	1,97	2,29	2,68	3,19	3,59	3,76	3,94	4,04
793	21,78	2,09	2,35	2,68	3,17	3,57	3,71	3,90	3,94
794	22,99	2,07	2,40	2,68	3,15	3,44	3,57	3,76	3,85
795	24,20	2,09	2,35	2,72					3,66
796	25,41	2,16	2,44	2,72					3,52
797	26,62	2 25	2,44	2,63					3,38
798	27,83	2,23							3,19
799	29,04	2,13							2,96
800	30,25	2,02							2,72
801	31,46	1,94							2,49
802	32,67	1,78							2,07
803	33,88	1,64							1,88
804	35,09	1,46							1,69
805	36,30	1,13							1,13
806	37,51	0,47							0,47
807	38,72	0,00							0,00

TABLE A14.6

BUBBLE VOLUME AND CHARACTERISTIC DIMENSIONS. RUN M14

Frame No	Time ms	V mm^3	D_w mm	H mm	D_c mm	D_s mm
775	0,00	0,0	0,00	0,00	0,00	0,00
776	1,21	6,1	3,83	1,88	2,72	2,26
777	2,42	82,7	6,89	3,34	4,50	5,40
778	3,63	135,6	8,17	3,94	6,02	6,37
779	4,84	203,9	9,13	4,56	6,02	7,30
780	6,05	253,4	9,90	4,83	7,04	7,85
781	7,26	304,6	10,52	5,35	7,34	8,35
782	8,47	382,8	11,18	5,69	7,60	9,01
783	9,68	433,1	11,65	6,20	7,98	9,39
784	10,89	494,7	12,08	6,48	8,18	9,81
785	12,10	581,4	12,40	6,88	8,26	10,36
786	13,31	622,0	12,83	7,14	8,26	10, 9
787	14,52	682,7	13,15	7,51	8,32	10,92
788	15,73	734,5	13,34	7,85	8,46	11,19
789	16,94	759,0	13,62	8,08	8,46	11,32
790	18,15	823,3	13,71	8,27	8,54	11,63
791	19,36	922,0	13,90	8,73	8,46	12,08
792	20,57	955,2	14,05	8,88	8,08	12,22
793	21,78	981,3	14,20	9,20	7,88	12,33
794	22,99	1000	14,33	9,35	7,70	12,41
795	24,20	1018	14,33	9,62	7,32	12,48
796	25,41	1093	14,46	9,92	7,04	12,78
797	26,62	1132	14,65	10,14	6,76	12,93
798	27,83	1137	14,56	10,39	6,38	12,95
799	29,04	1163	14,69	10,71	5,92	13,05
800	30,25	1162	14,69	10,86	5,44	13,04
801	31,46	1176	14,69	11,06	4,98	13,09
802	32,67	1181	14,60	11,08	4,14	13,11
803	33,88	1202	14,84	11,61	3,76	13,19
804	35,09	1164	14,78	11,68	3,38	13,05
805	36,30	1199	14,71	12,02	2,26	13,18
806	37,51	1183	14,65	12,12	0,94	13,12
807	38,72	1165	14,71	12,47	0,00	13,05

TABLE A14.7

MICROLAYER GEOMETRY. RUN M19

Frame No.	Time ms	Bubble base radius, r (mm), for: microlayer thickness, i (μm), of:				
		0,0	0,083	0,166	0,249	0,332
1797	0					
1798	1,01					
1799	2,02	0,57	1,18	1,82		
1800	3,03	0,74	1,23	1,77		
1801	4,04	0,89	1,30	1,73	2,02	2,32
1802	5,05	0,95	30	1,71	2,00	2,30
1803	6,06	1,04	,,35	1,71	1,99	2,28
1804	7,07	1,07	1,36	1,66	1,97	2,22
1805	8,08	1,13	1,39	1,65	1,96	2,24
1806	9,09	1,20	1,44	1,65	1,92	2,24
1807	10,10	1,25	1,44	1,67	1,94	2,19
1808	11,11	1,33	1,50	1,67	1,96	2,22
1809	12,12	1,37	1,48	1,63	1,98	2,23
1810	13,13	1,47	1,55	1,67		
1811	14,14	1,46	1,55	1,65		
1812	15,15	1,50		1,62		
1813	16,16	1,51		1,60		
1814	17,17	1,44				
1815	18,18	1,34				
1816	19,19	1,15				
1817	20,20	0,83				
1818	21,21	0,30				
1819	22,22	0,0				

TABLE A14.8

BUBBLE VOLUME AND CHARACTERISTIC DIMENSIONS. RUN M19

Frame No.	Time ms	V mm^3	D_W mm	H mm	D_C * mm	D_S mm
1797	0,00	0,0	0,00	0,00	0,00	0,00
1798	1,01	0,5	0,96	0,70		0,95
1799	2,02	27,0	4,81	2,35	3,65	3,72
1800	3,03	57,1	6,10	2,93	4,24	4,78
1801	4,04	73,7	6,72	3,27	4,64	5,20
1802	5,05	94,6	7,16	3,51	4,87	5,65
1803	6,06	116,8	7,5.	3,91	5,00	6,06
1804	7,07	134,9	7,8.	4,05	5,02	6,36
1805	8,08	146,6	7,92	4,27	4,99	6,54
1806	9,09	155,3	7,98	4,35	4,92	6,67
1807	10,10	165,6	8,06	4,61	4,82	6,81
1808	11,11	166,3	8,06	4,61	4,68	6,82
1809	12,12	169,0	8,10	4,81	4,50	6,86
1810	13,13	167,8	7,98	4,77	4,30	6,84
1811	14,14	163,2	7,82	4,93	4,08	6,7.
1812	15,15	159,0	7,66	4,93	3,82	6,7.
1813	16,16	151,0	7,46	5,15	3,54	6,61
1814	17,17	136,3	7,38	5,1.	3,16	6,39
1815	18,18	128,6	7,16	5,35	2,76	6,26
1816	19,19	113,8	7,02	5,35	2,30	6,01
1817	20,20	108,4	6,98	5,41	1,66	5,92
1818	21,21	9. ,5	6,82	5,41	0,50	5,71

* estimated from Figure 8.15

TABLE A14.9

MICROLAYER GEOMETRY. RUN M20

Frame No.	Time ms	Bubble base radius, r (mm), for: microlayer thickness, d (μm), of: 0,0	0,83	0,166	0,249	0,332	0,415	0,498	M'layer periphery
1160	0,00								
1161	1,25								
1162	2,50	0,56							2,14
1163	3,75	0,70	1,37	2,12					
1164	5,00	0,86	1,46	2,03	2,34	2,66			
1165	6,25	0,98	1,48	2,00	2,25	2,57			2,82
1166	7,50	1,11		,00	2,26	2,55			2,83
1167	8,75	,22		1,97	2,24	2,58			3,05
1168	10,00	1,29	1	1,97	2,29	2,59			3,20
1169	11,25	1,38	1,65	1,97	2,30	2,59	2,88	3,15	3,25
1170	12,50	1,46	1,72	1,92	2,26	2,59	2,87	3,23	3,45
1171	13,75	1,58	1,72	1,87	2,21	2,55	2,90	3,22	3,45
1172	15,00	1,60	1,7	1,90	2,20	2,59	2,89	3,20	3,37
1173	16,25	1,70	1,7	1,89	2,26	2,56	2,85	3,20	3,37
1174	17,50	1,82			2,26	2,56	2,88	3,15	3,30
1175	18,75	1,87			2,28	2,58	2,91	3,17	3,28
1176	20,00	1,97			2,31	2,58			3,20
1177	21,25	2,02			2,31	2,59			2,97
1178	22,50	2,09			2,32	2,58			2,83
1179	23,75	2,12			2,31	2,56			2,66
1180	25,00	2,12							2,48
1181	26,25	2,07							
1182	27,50	2,07							
1183	28,75	1,87							1,87
1184	30,00	1,67							1,67
1185	31,25	1,38							1,38
1186	32,50	1,05							1,05
1187	33,75	0,62							0,62
1188	35,00	0,00							0,00

TABLE A14.10

BUBBLE VOLUME AND CHARACTERISTIC DIMENSIONS. RUN M20

Frame No.	Time ms	V mm^3	D_w mm	H mm	D_c mm	D_s mm
1160	0,00	0,0	0,00	0,00	0,00	0,00
1161	1,25	1,0	1,57	0,79		1,25
1162	2,50	35,1	5,12	2,60	4,28	4,06
1163	3,75	75,1	6,60	3,35		5,23
1164	5,00	113,8	7,48	3,90		6,01
1165	6,25	153,2	8,01	4,23	5,64	6,64
1166	7,50	193,2	8,60	4,72	5.-	7,17
1167	8,75	224,4	9,11	5,12	,10	7,54
1168	10,00	283,4	9,45	5,57	6,4-	8,15
1169	11,25	307,6	9,76	5,71	6,50	8,38
1170	12,50	348,7	10,14	6,24	6,90	8,73
1171	13,75	369,4	10,47	6,63	6,90	8,90
1172	15,00	423,0	10,71	6,89	6,74	9,31
1173	16,25	445,9	10,83	7,22	6,74	9,48
1174	17,50	477,7	10,93	7,62	6,60	9,70
1175	18,75	495,8	11,02	7,72	6,56	9,82
1176	20,00	509,5	11,22	8,21	6,40	9,91
1177	21,25	548,3	11,22	8,27	5,94	10,15
1178	22,50	565,4	11,32	8,66	5,66	10,26
1179	23,75	583,7	11,34	8,82	5,32	10,37
1180	25,00	579,3	11,22	9,19	4,96	10,34
1181	26,25	609,0	11,18	9,35		10,52
1182	27,50	599,5	11,12	9,69		10,46
1183	28,75	603,2	11,18	9,78	3,74	10,48
1184	30,00	621,7	11,32	10,14	3,34	10,59
1185	31,25	623,2	11,28	10,24	2,76	10,60
1186	32,50	624,8	11,42	10,63	2,10	10,61
1187	33,75	625,9	11,42	10,87	1,24	10,61

TABLE A14.11

MICROLAYER GEOMETRY. RUN E8

Frame No.	Time ms	Bubble base radius, r (mm). for: microlayer thickness, d (μm), of: 0,0	0,081	0,162	0,243	0,324	M'layer periphery
1304	0,00	0,00					
1305	1,12	0,20					
1306	2,24	0,27	1,04				2,09
1307	3,36	0,41	1,00	1,68			2,31
1308	4,48	0,47	1,04	1,[illegible]			2,45
1309	5,60	0,50	1,04	1,7[illegible]	2,22	2,63	
1310	6,72	0,[illegible]	1,09	1,63	2,18	2,49	2,68
1311	7,84	0,68	1,16	1,74	2,13	2,48	2,68
1312	8,96	0,73	1,18	1,68	2,05	2,43	2,63
1313	10,08	0,78	1,18	1,72	1,99	2,36	2,51
1314	11,20	0,86	1,22	1,68	2,04	2,40	2,58
1315	12,32	0,89	1,27	1,74	1,99	2,40	2,58
1316	13,44	0,92	1,31	1,79	2,04	2,38	2,54
1317	14,56	0,98	1,31	1,[illegible]	2,01	2,36	2,49
1318	15,68	1,02	1,36	1,[illegible]	2,07	2,36	2,54
1319	16,80	1,07	1,38	1,74	2,07	2,38	2,45
1320	17,92	1,13	1,41	1,[illegible]	1,99	2,30	2,36
1321	19,04	1,18	1,45	1,[illegible]			2,27
1322	20,16	1,18	1,41	1,68			2,18
1323	21,28	1,22	1,45	1,[illegible]			2,09
1324	22,40	1,22	1,45	1,72			1,90
1325	23,52	1,27	1,45	1,70			
1326	24,64	1,31	1,50	1,68			
1327	25,76	1,41					
1328	26,88	1,18					1,18
1329	28,00	0,86					0,86
1330	29,12	0,54					0,54
1331	30,24	0,18					0,18

TABLE A14.12

BUBBLE VOLUME AND CHARACTERISTIC DIMENSIONS. RUN E8

Frame No.	Time ms	V mm^3	D_w mm	H mm	D_c mm	D_s mm
1304	0,00	0,0	0,00	0,00	0,00	0,00
1305	1,12	11,7	3,36	2,18		2,82
1306	2,24	34,7	4,90	2,65	4,18	4,05
1307	3,36	60,5	5,89	3,26	4,62	4,87
1308	4,48	81,4	6,67	3,54	4,90	5,38
1309	5,60	102,4	7,07	3,74		5,80
1310	6,72	121,9	7,51	3,99	5,36	6,15
1311	7,84	146,1	7,74	4,43	5,36	6,53
1312	8,96	154,3	7,98	4,57	5,26	6,65
1313	10,08	186,7	8,22	4,79	5,22	7,09
1314	11,20	191,8	8,49	4,93	5,16	7,16
1315	12,32	211,6	8,74	5,30	5,16	7,39
1316	13,44	212,1	8,86	5,44	5,08	7,40
1317	14,56	233,7	8,89	5,69	4,98	7,64
1318	15,68	246,7	9,19	5,84	5,08	7,78
1319	16,80	259,3	9,19	6,08	4,90	7,91
1320	17,92	261,3	9,21	6,20	4,72	7,93
1321	19,04	280,5	9,39	6,49	4,54	8,12
1322	20,16	289,3	9,29	6,53	4,36	8,21
1323	21,28	293,9	9,43	6,75	4,18	8,25
1324	22,40	301,6	9,29	6,89	3,80	8,32
1325	23,52	292,9	9,47	7,04		8,24
1326	24,64	280,1	9,25	7,11		8,12
1327	25,76	294,4	9,38	7,40		8,25
1328	26,88	275,4	9,25	7,44	2,36	8,07
1329	28,00	268,4	9,29	7,62	1,72	8,00
1330	29,12	264,0	9,25	7,76	1,08	7,96
1331	30,24	245,9	9,25	7,93	0,36	7,77

TABLE A14.13

MICROLAYER GEOMETRY. RUN E12

Frame No	Time ms	Bubble base radius, r (mm), for: microlayer thickness, d (μm), of: 0,0	0,081	0,162	0,243	0,324	0,405	0,486	M'layer periphery
494	0,00								
495	1,14	0,00							
496	2,28	0,43							
497	3,42	0,58	1,29	2,02					2,13
498	4,56	0,64	1,30	1,93					
499	5,70	0,73	1,33	1,91	2,25	2,59			
500	6,84	0,85	1,30	1,85	2,16	2,56			2,74
501	7,98	0,85	1,30	1,86	2,16	2,57			2,80
502	9,12	0,92	1,33	1,78	2,10	2,53			2,78
503	10,26	0,94	1,36	1,79	2,14	2,54			2,80
504	11,40	0,96	1,35	1,81	2,10	2,52			2,85
505	12,54	1,01	1,39	1,81	2,16	2,54			2,89
506	13,68	1,08	1,42	1,84	2,13	2,53			2,94
507	14,82	1,10	1,47	1,84	2,20	2,57			2,94
508	15,96	1,15	1,45	1,80	2,16	2,50			2,94
509	17,10	1,20	1,44	1,81	2,20	2,53			2,99
510	18,24	1,24	1,49	1,82	2,20	2,48	2,65	2,85	2,99
511	19,38	1,29	1,50	1,79	2,16	2,50	2,63	2,80	2,94
512	20,52	1,31	1,56	1,86	2,13	2,43	2,57	2,76	2,89
513	21,66	1,38	1,56	1,84	2,11	2,43	2,62	2,76	2,85
514	22,80	1,42	1,56	1,87	2,16	2,42			2,71
515	23,94	1,49	1,61	1,84	2,16	2,39			2,57
516	25,08	1,48		1,79	2,16	2,39			2,18
517	26,22	1,53		1,75					2,39
518	27,36	1,61							2,11
519	28,50	1,67							2,16
520	29,64	1,66							1,98
521	30,78	1,63							1,91
522	31,92	1,57							
523	33,06	1,41							
524	34,20	1,29							1,39
525	35,34	1,01							1,01
526	36,48	0,52							0,52
527	37,62	0,00							0,00

TABLE A14.14

BUBBLE VOLUME AND CHARACTERISTIC DIMENSIONS. RUN E12

Frame No.	Time ms	V mm^3	D_w mm	H mm	D_c mm	D_s mm
494	0,00	0,0	0,00	0,00	0,00	0,00
495	1,14	0,8	1,38	0,77		1,17
496	2,28	28,4	3,85	2,38		3,78
497	3,42	60,7	6,05	2,93	4,26	4,88
498	4,56	92,3	6,75	3,43		5,61
499	5,70	134,7	7,43	3,70		6,36
500	6,84	142,4	8,00	4,00	5,48	6,48
501	7,98	173,6	8,62	4,36	5,60	6,92
502	9,12	203,3	9,08	4,62	5,56	7,30
503	10,26	238,2	9,57	4,95	5,60	7,69
504	11,40	270,3	9,96	5,13	5,70	8,02
505	12,54	305,8	10,40	5,50	5,78	8,36
506	13,68	336,2	10,64	5,79	5,88	8,63
507	14,82	367,3	11,00	6,05	5,88	8,89
508	15,96	400,3	11,33	6,05	5,88	9,14
509	17,10	423,1	11,55	6,42	5,98	9,32
510	18,24	441,7	11,70	6,42	5,98	9,45
511	19,38	484,7	12,01	6,78	5,88	9,75
512	20,52	501,2	12,01	6,97	5,78	9,86
513	21,66	537,2	12,38	7,19	5,70	10,09
514	22,80	545,5	12,45	7,24	5,42	10,14
515	23,94	567,3	12,65	7,52	5,14	10,27
516	25,08	563,7	12,74	7,61	4,96	10,25
517	26,22	612,6	13,02	7,88	4,78	10,54
518	27,36	621,3	13,07	8,33	4,22	10,59
519	28,50	604,3	13,02	8,03	4,32	10,49
520	29,64	612,9	13,20	8,36	3,96	10,54
521	30,78	619,3	13,11	8,53	3,82	10,58
522	31,92	601,2	13,15	8,75		10,47
523	33,06	625,8	13,33	8,80		10,61
524	34,20	605,9	13,29	8,99	2,58	10,50
525	35,34	610,5	13,48	9,30	2,02	10,53
526	36,48	618,9	13,53	9,39	1,04	10,57
527	37,62	606,5	13,61	9,57	0,00	10,50

APPENDIX 15

LIQUID AND VAPOUR DENSITIES. METHANOL AND ETHANOL

Liquid densities (g/cm^3) were calculated as a function of temperature (^oC) from equations A15.1 and A15.2 below. The equations hold up to 60 ^oC and 80 ^oC, with accuracies of 0,003 per cent and 0,03 per cent, respectively [210].

Methanol:

$$\rho_L = 0{,}80999 - 9{,}253 \times 10^{-4}T - 4{,}1 \times 10^{-7}T^2 \qquad \text{(A15.1)}$$

Ethanol:

$$\rho_L = 0{,}80625 - 8{,}461 \times 10^{-4}T + 1{,}6 \times 10^{-7}T^2 - 8{,}5 \times 10^{-9}T^3 \qquad \text{(A15.2)}$$

Vapour densities were calculated from the Ideal Gas Law with compressibility factor corrections as given for saturated vapours by Hougen et al [215].

Resulting densities are shown in Table A15.1. For purposes of establishing the density ratio (column i) required in Section 8.5, the microlayer liquid was assumed to be at the mean temperature $(T_w + T_{sat})/2$ and the vapour temperature was taken as T_{sat}.

TABLE A15.1

LIQUID AND VAPOUR DENSITIES

a	b	c	d	e	f	g	h	i
Run *	T_w	T_{sat}	$\frac{T_w+T_{sat}}{2}$	ρ_L (T_w)	ρ_L (T_{sat})	ρ_L $\left(\frac{T_w+T_{sat}}{2}\right)$	ρ_V (T_{sat})	ρ_L/ρ_V (g/h)
	^oC	^oC	^oC	kg/m^3	kg/m^3	kg/m^3	kg/m^3	
M10	72,0	35,2	53,6	741	777	759	0,326	2328
M13	68,0	33,9	51,0	745	778	762	0,307	2482
M14	68,5	40,4	54,5	745	772	758	0,418	1813
M19	72,5	40,4	56,5	741	772	756	0,418	1809
M20	77,0	45,5	61,3	736	767	752	0,526	1430
E 8	79,0	47,6	63,3	736	765	751	0,443	1695
E12	85,0	53,2	69,1	730	760	746	0,577	1293

*M denotes methanol

E denotes ethanol

APPENDIX 16

LIQUID VISCOSITIES. METHANOL AND ETHANOL

Dynamic liquid viscosities (centipoise) at various temperatures (K) were obtained from equations A16.1 and A16.2 below. The equations resulted from regressions on three reference data points each, given by Reid and Sherwood [219] in the temperature range 5 to 60 °C for methanol, and 0 to 75 °C for ethanol. When tested against additional data [214] in the same temperature range, the maximum error was found to be +2,4 per cent for equation A16.1 and -1,3 per cent for equation A15.2.

Methanol:

$$\mu_L = -5,3559 + 156,8/T - 4,4319 \times 10^4/T^2 \qquad \text{(A16.1)}$$

Ethanol:

$$\mu_L = -7,7672 + 3020,4/T - 2,0284 \times 10^5/T^2 \qquad \text{(A16.2)}$$

Table A16.1 gives dynamic viscosities for all runs at temperatures T_{sat} and $(T_w + T_{sat})/2$, as well as liquid densities (obtained from Appendix 15) and kinematic viscotics at the mean microlayer temperature $(T_w + T_{sat})/2$.

TABLE A16.1

DYNAMIC AND KINEMATIC LIQUID VISCOSITIES

Run *	T_{sat}	$\frac{T_w+T_{sat}}{2}$	$\mu (T_{sat})$	$\mu \left(\frac{T_w+T_{sat}}{2}\right)$	$\rho_L \left(\frac{T_w+T_{sat}}{2}\right)$	$\nu = \frac{\mu}{\rho_L} \left(\frac{T_w+T_{sat}}{2}\right)$
	^oC	^oC	c poise	c poise	g/cm^3	m^2/s
M10	35,2	53,6	0,478	0,378	0,759	$0,498 \times 10^{-6}$
M13	33,9	51,0	0,486	0,390	0,762	$0,512 \times 10^{-6}$
M14	40,4	54,5	0,446	0,374	0,758	$0,493 \times 10^{-6}$
M19	40,4	56,5	0,446	0,365	0,756	$0,483 \times 10^{-6}$
M20	45,5	61,3	0,418	0,345	0,752	$0,459 \times 10^{-6}$
E 8	47,6	63,3	0,724	0,558	0,751	$0,743 \times 10^{-6}$
E12	53,2	69,1	0,659	0,509	0,746	$0,682 \times 10^{-6}$

*M denotes methanol
E denotes ethanol

APPENDIX 17

SURFACE TENSION. METHANOL AND ETHANOL

The variation of surface tension with temperature is given by equation A17.1 below [219], where T is the required temperature, T_r the corresponding reduced temperature, and the subscript 'o' refers to a reference temperature for which a data point is available.

$$\sigma_T = \sigma_o\{(1 - T_r)/(1 - T_{r_o})\}^{1,2} \qquad (A17.1)$$

Reference data [219] give σ_o as 0,0217 J/m² at 30 °C for methanol, and as 0,0194 J/m² at 50 °C for ethanol. The critical temperatures are 513,2 K for methanol and 516,3 K for ethanol. Substitution into equation A17.1 gives:

Methanol:

$$\sigma_T = 0,0634[1 - \{(T + 273,2)/513,2\}]^{1,2} \qquad (A17.2)$$

Ethanol:

$$\sigma_T = 0,0633[1 - \{(T + 273,2)/516,3\}]^{1,2} \qquad (A17.3)$$

Within the temperature ranges covered in this work, equations A17.2 and A17.3 appear to have accuracies of better than 0,5 per cent.

Table A17.1 gives the required surface tension data at saturation temperature.

TABLE A17.1

SURFACE TENSION

Run *	T_{sat} ^{o}C	σ J/m^2
M10	35,2	0,0211
M13	33,9	0,0212
M14	40,4	0,0204
M19	40,4	0,0204
M20	45,5	0,0198
E 8	47,6	0,0197
E12	53,2	0,0190

*M denotes methanol

E denotes ethanol

APPENDIX 18

NUMERICAL SOLUTION OF TRANSIENT CONDUCTION - EVAPORATION PROBLEM

The problem to be solved was formally defined in Figure 9.2 and equations 9.3 to 9.13 in Chapter 9. For ease of reference Figure 9.2 is reproduced as Figure A18.1; the equations will be recalled below as required.

A18.1 CRANK-NICOLSON METHOD

The general method of solution adopted is illustrated for the case of a region with internal heat generation (e.g. region 2 in Figure A18.1), for which the conduction equation (cf equation 9.4) is

$$\partial T/\partial t = \alpha \partial^2 T/\partial x^2 + G \qquad \text{(A18.1)}$$

where

$$G = q^*/\rho c \qquad \text{(A18/2)}$$

With the x region subdivided into increments h (= Δx) and the t region into increments ℓ (= Δt), see Figure A18.2, such that

$$x_i = ih \,, \quad i = 0, 1, 2 \ldots \qquad \text{(A18.3)}$$

$$t_k = k\ell \,, \quad k = 0, 1, 2 \ldots \qquad \text{(A18.4)}$$

the Crank-Nicolson finite difference approximation [201, 202, 205] to equation A18.1 is

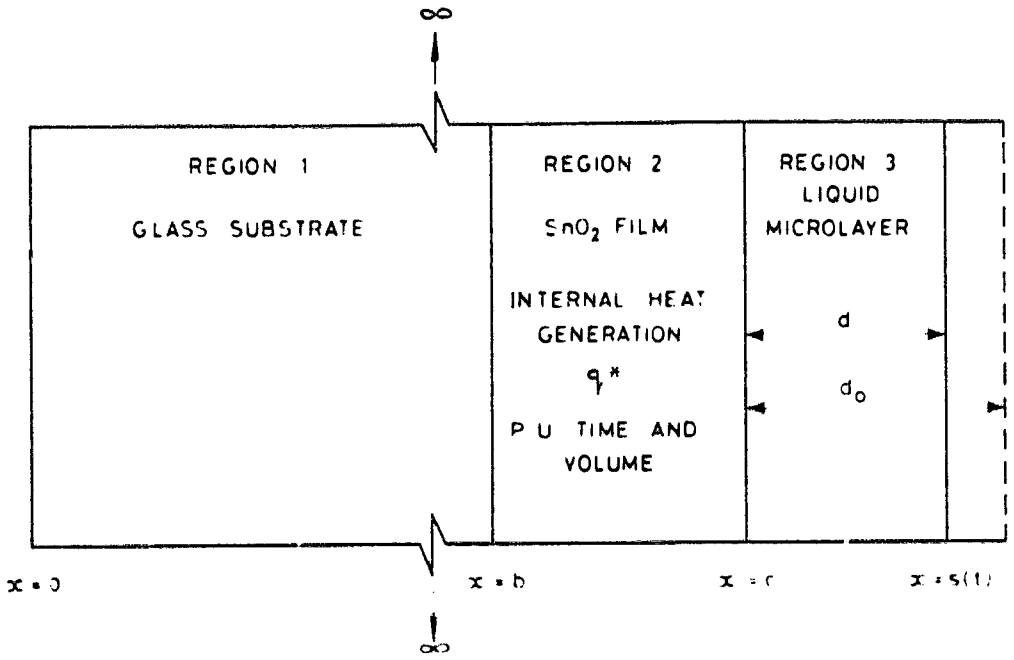

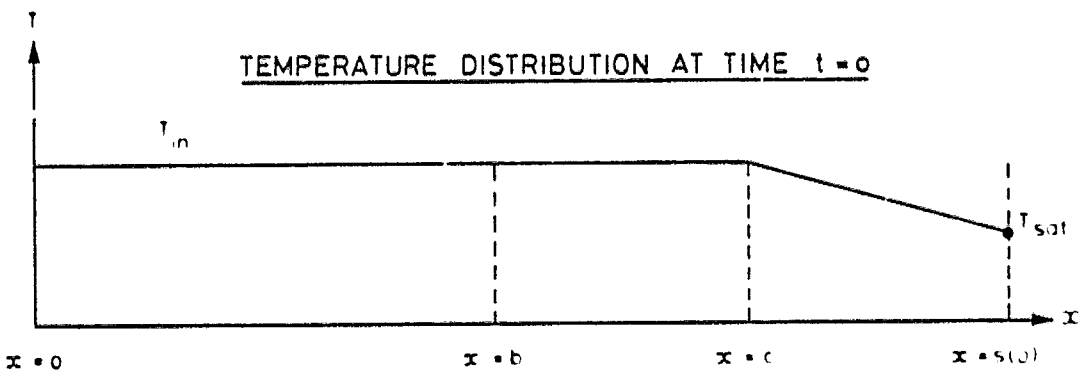

FIG A18.1 DEFINITION OF MICROLAYER CONDUCTION PROBLEM

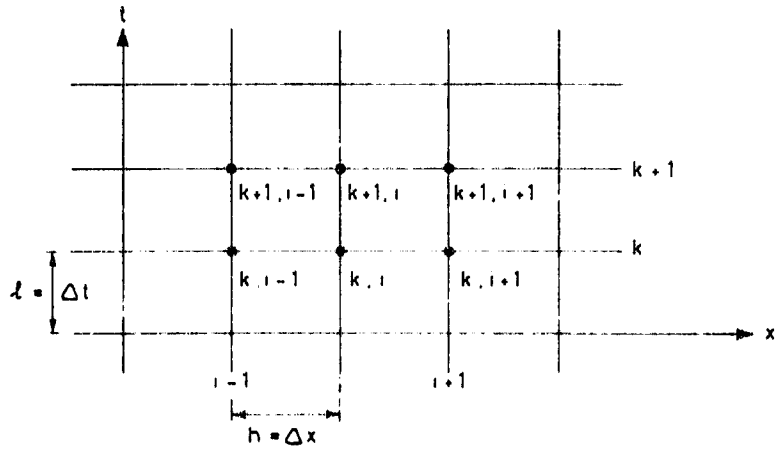

FIG. A18.2 INCREMENTS AND NODE NOTATION ON x - t PLANE.

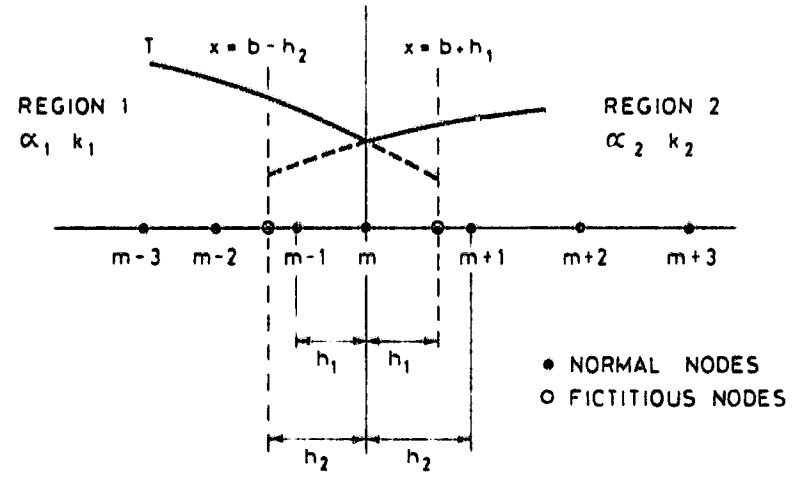

FIG. A18.3 FICTITIOUS NODES AT BOUNDARY BETWEEN REGIONS 1 AND 2.

$$-0,5\ T_{i-1,k+1} + (\xi + 1)T_{i,k+1} - 0,5\ T_{i+1,k+1}$$

$$= 0,5\ T_{i-1,k} + (\xi - 1)T_{i,k} + 0,5\ T_{i+1,k} + Gh^2/\alpha \qquad (A18.5)$$

where

$$\xi = h^2/\theta\alpha \qquad (A18.6)$$

The subdivision of the x - t plane and the relevant node points are shown in Figure A18.2.

The left-hand side of equation A18.5 contains the temperatures for the (k + 1)th time step, which require to be solved, and the right-hand side the temperatures for the k th step, already solved or known from the initial conditions.

For N internal node points along each time row (and with linear boundary conditions) the successive application of equation A18.5 to each node point (i = 1, 2, 3 ... N) results in N simultaneous linear equations for the N unknown temperatures as follows:

$$\begin{aligned}
B_1T_1 + C_1T_2 &= D_1 \\
A_2T_1 + B_2T_2 + C_2T_3 &= D_2 \\
&\vdots \qquad (A18.7) \\
A_i\ T_{i-1} + B_iT_i + C_i\ T_{i+1} &= D_i \\
&\vdots \\
A_N\ T_{N-1} + B_N\ T_N &= D_N
\end{aligned}$$

where the subscript (k+1) is omitted. Solution of the linear equations A18.7 advances the solution of the conduction problem by one time step. Successive application of the procedure for each time step gives the overall solution of the problem.

In the present study the linear equations were solved by an extremely rapid algorithm, derivable from Gauss elimination, the so-called Thomas algorithm [201].

Equation A18.5 was applied to the internal node points of all three regions, with physical properties and increment sizes appropriately evaluated, and with the heat generation term set to zero in regions 1 and 3.

A18.2 INTERNAL BOUNDARIES AT x = b AND x = c

The treatment of internal boundaries is illustrated for x = b (i = m), that is, the boundary between regions 1 and 2.

Continuity of temperature and heat flux at x = b gives (see equations 9.6 and 9.8):

$$T(b-0,t) = T(b+0,t) \qquad \text{(A18.8)}$$

$$k_1 \partial T(b-0,t)/\partial x = k_2 \partial T(b+0,t)/\partial x \qquad \text{(A18.9)}$$

Equation A18.9 requires to be approximated by a finite-difference equation of discretisation error no larger than that of the Crank-Nicolson equation itself. Thus a central-difference approximation is required [205]. This is derived below using Saulyev's method of fictitious nodes [205].

Figure A18.3 shows the contact of regions 1 and 2. Each region is imagines to extend by one x-increment beyond the boundary at x = b. At the fictitious nodes $x = b + h_1$ and $x = b - h_2$ the temperatures are denoted $T^*_{m+1,k}$ and $T^*_{m-1,k}$ (k = 0, 1, 2 ...). Assuming the possibility of the smooth extrapolation of T from one region into another over a small distance h (see dotted curves in Figure A18.4), the central difference approximation of equation A18.9 is

$$k_1 \frac{T^*_{m+1,k+1} - T_{m-1,k+1}}{2h_1} = k_2 \frac{T_{m+1,k+1} - T^*_{m-1,k+1}}{2h_2} \qquad (A18.10)$$

Application of the Crank-Nicolson equation to regions 1 and 2 at x = b (i = m) gives

$$-0,5\ T_{m-1,k+1} + (\xi_1 + 1)T_{m,k+1} - 0,5T^*_{m+1,k+1}$$

$$= 0,5\ T_{m-1,k} + (\xi_1 - 1)T_{m,k} + 0,5T^*_{m+1,k} \qquad (A18.11)$$

and

$$-0,5\ T^*_{m-1,k+1} + (\xi_2 + 1)T_{m,k+1} - 0,5T_{m+1,k+1}$$

$$= 0,5T^*_{m-1,k} + (\xi_2 - 1)T_{m,k} + 0,5T_{m+1,k} + Gh_2^2/\alpha_2 \qquad (A18.12)$$

Using equations A18.11 and A18.12 the fictitious temperatures in equation A18.10 may be eliminated to give the final node equation at i = m as follows:

$$-X_{12}\ T_{m-1,k+1} + (X_{12}\xi_1+\xi_2+X_{12}+1)\ T_{m,k+1} - T_{m+1,k+1}$$

$$= 0,5\ X_{12}T_{m-1,k} + (X_{12}\xi_1+\xi_2-X_{12}-1)\ T_{m,k} + 0,5T_{m+1,k}$$

$$+ 0,5\ T^*_{m-1,k} + 0,5\ X_{12}T^*_{m+1,k} + Gh_2^2/\alpha_2 \qquad (A18.5)$$

where

$$X_{12} = k_1h_2/k_2h_1 \qquad (A18.4)$$

and the fictitious temperatures for time step k (obtained from equations A18.11 and A18.12 with (k+1) replaced by k) are:

$$T^*_{m+1,k} = -T_{m+1,k} + (2\xi_1 + 2)T_{m,k} - T_{m-1,k-1}$$

$$- (2\xi_1 - 2)T_{m,k-1} - T^*_{m+1,k-1} \qquad (A18.15)$$

$$T^*_{m-1,k} = (2\xi_2 + 2)\, T_{m,k} - T_{m+1,k} - T^*_{m-1,k}$$

$$- (2\xi_2 - 2)\, T_{m,k-1} - T_{m+1,k-1} - 2\, Gh_2^2/\alpha_2 \qquad (A16)$$

where the fictitious temperatures $T^*_{m-1,k-1}$ and $T^*_{m+1,k-1}$ are known from the previous time step or from the initial conditions.

A similar procedure, applied to the boundary between regions 2 and 3, that is, to x = c (i = n), results in

$$-X_{23}\, T_{n-1,k+1} + (X_{23}\xi_2+\xi_3+X_{23}+1)\, T_{n,k+1} - T_{n+1,k+1}$$

$$= 0{,}5\, X_{23}\, T_{n-1,k} + (X_{23}\xi_2+\xi_3-X_{23}-1)\, T_{n,k} + 0{,}5\, T_{n+1,k}$$

$$+ 0{,}5\, T^*_{n-1,k} + 0{,}5\, X_{23}\, T^*_{n+1,k} + X_{23}\, Gh_2^2/\alpha_2 \qquad (A18.17)$$

where

$$X_{23} = k_2 h_3/k_3 h_2 \qquad (A18.18)$$

and

$$T^*_{n+1,k} = -\, T_{n+1,k} + (2\xi_2 + 2)\, T_{n,k} - T_{n-1,k-1}$$

$$- (2\xi_2 - 2)\, T_{n,k-1} - T^*_{n+1,k-1} - 2\, Gh_2^2/\alpha_2 \qquad 19)$$

$$T^*_{n-1,k} = (2\xi_3 + 2)\, T_{n,k} - T_{n+1,k} - T^*_{n-1,k-1}$$

$$- (2\xi_3 - 2)\, T_{n,k-1} - T_{n+1,k-1} \qquad (A18.20)$$

A18.3 BOUNDARY AT x = 0

The required conditions at x = 0 follow from Chapter 9 (equations 9.10 and 9.11) as:

$$T(0,t) = T_{in} \tag{A18.21}$$

$$\partial T(0,t)/\partial x = 0 \tag{A18.22}$$

Equation A18.21 was satisfied by the following Crank-Nicolson nett equation for the first internal node (i = 1):

$$(\xi_1+1)\, T_{1,k+1} - 0{,}5\, T_{2,k+1} = T_{in} + (\xi_1-1)\, T_{1,k} + 0{,}5\, T_{2,k} \tag{A18.23}$$

Equation A18.22 was satisfied by making region 1 sufficiently thick to maintain the inequality $(T_{in} - T_1) < 0{,}001\ ^{o}C$.

A18.4 BOUNDARY AT x = s

The evaporation boundary condition at x = s (i = p) follows from Chapter 9 (equation 9.12) as:

$$-k_3 \frac{\partial T}{\partial x} = \left[\frac{\eta\lambda}{1-\frac{1}{2}\eta}\right]\left[\frac{M}{2\pi R}\right]^{\frac{1}{2}} \left[\frac{p^{o}_{s}}{T_s^{\frac{1}{2}}} - \frac{p}{T_{sat}^{\frac{1}{2}}}\right] \tag{A18.24}$$

For each problem to be solved the following quantities are constants:

$$C_1 = \left[\frac{\eta\lambda}{k_3(1-\frac{1}{2}\eta)}\right]\left[\frac{M}{2\pi R}\right]^{\frac{1}{2}} \tag{A18.25}$$

$$C_2 = p/T_{sat}^{\frac{1}{2}} \tag{A18.26}$$

From the Clausius-Clapeyron equation the saturation vapour

pressure of the evaporating surface, P_s^o, may be written as

$$P_s^o = \exp\{C_3 - C_4/T_s\} \qquad \text{(A18.27)}$$

where C_3 and C_4 are constants for each liquid.

Equation A18.24 may thus be rewritten as

$$-\partial T/\partial x = C_1\left[\exp\{C_3-C_4/(T_s + 273,2)\}\Big/(T_s + 273,2)^{\frac{1}{2}} - C_2\right] \qquad \text{(A18.28)}$$

or

$$-\partial T/\partial x = \phi(T_s) \qquad \text{(A18.29)}$$

In terms of central differences at x = s (i = p), using fictitious nodes as before, equation A18.29 may be approximated (for time steps k+1 and k) as follows:

$$-(T^*_{p+1,k+1} - T_{p-1,k+1})\Big/2h_3 = \phi(T_{p,k+1}) \qquad \text{(A18.30)}$$

$$-(T^*_{p+1,k} - T_{p-1,k})\Big/2h_3 = \phi(T_p,k) \qquad \text{(A18.31)}$$

The Crank-Nicolson equation at x = s (i = p) is

$$-T_{p-1,k+1} + (2\beta_3 + 2)\, T_{p,k+1} - T^*_{p+1,k+1}$$

$$= T_{p-1,k} + (2\beta_3 - 2)\, T_{p,k} + T^*_{p+1,k} \qquad \text{(A18.32)}$$

Elimination of the fictitious temperatures via equations A18.30 and A18.31 gives the final node equation at x = s (i = p) as

$$-2T_{p-1,k+1} + (2\xi_3 + 2)\, T_{p,k+1} + 2h_3\phi(T_{p,k+1})$$

$$= 2T_{p-1,k} + (2\xi_3 - 2)\, T_{p,k} - 2h_3\phi(T_{p,k}) \qquad \text{(A18.33)}$$

where from the foregoing

$$\phi(T) = C_1\left[\exp\{C_3 - C_4/(T + 273,2)\}\Big/(T_s + 273,2)^{\frac{1}{2}} - C_2\right] \qquad \text{(A18.34)}$$

and the constants are defined by equations A18.25 to A18.27.

Equation A18.33 is non-linear in $T_{p,k+1}$. All other node equations were linear. In order to maintain overall linearity and thus to profit from the fast Thomas algorithm an iterative procedure, adapted from Young [201], was followed: First, $\phi(T_{p,k+1})$ in equation A18.33 was replaced with $\phi(T_{p,k})$; solution of the nett equations led to the first estimate of $T_{p,k+1}$, that is, $(T_{p,k+1})_1$. Now $\phi(T_{p,k+1})$ was replaced with $\phi\left[\frac{1}{2}\{(T_{p,k}) + (T_{p,k+1})_1\}\right]$ to give $(T_{p,k+1})_2$ and the iteration continued until $(T_{p,k+1})_n$ differed by less than 0,01 ^{o}C from $(T_{p,k+1})_{n-1}$. (Differences as low as 0,0001 ^{o}C were tested in trial computations, but gave essentially identical evaporation rates.) Convergence was rapid.

Movement of the boundary was given in Chapter 9 (equation 9.13) as

$$ds/dt = (k_3/\lambda\rho_L).\partial T(s,t)/\partial x \qquad \text{(A18.35)}$$

which in terms of the ϕ function of equation A18.34 is

$$ds/dt = -(k_3/\lambda\rho_L)\,\phi(T_s) \qquad \text{(A18.36)}$$

In difference form this becomes

$$(S_{k+1} - S_k)/\ell = -(k_3/\lambda\rho_L)\,\phi(T_{p,k}) \qquad \text{(A18.37)}$$

or finally

$$s_{k+1} = S_k + \ell\,(k_3/\lambda\rho_L)\;\phi(T_{p,k}) \qquad \text{(A18.38)}$$

With a constant number of x increments (N_3 in region 3), h_3, the size of the x increments in region 3, had to be recalculated for each time step (k = 1, 2, 3 ...), that is

$$h_{3,k} = (S_k - c)/N_3 \qquad \text{(A18.39)}$$

(In the foregoing net equations the notation $h_{3,k}$ was abbreviated to h_3.)

The entire computation was terminated when region 3 had shrunk to less than 5 per cent of its initial thickness.

A18.5 EXECUTION AND TESTING OF PROGRAM

The numerical procedures described above were incorporated into a double precision FORTRAN program and executed on an IBM System 370.

The problem was solved for the conditions of run M10. Thus the initial thickness of region 3 (methanol) was 0,332 μm (see also Section 9.2.3). The optical thickness of region 2 (SnO_2) was $\lambda/2$, that is, the physical thickness was 0,109 μm. The thickness of region 1 (glass) was established by trial computations such that the 'semi-infinite' boundary condition (equation A18.22) was satisfied; the resulting thickness was 100 μm.

Region 1 was subdivided into 20 increments and regions 2 and 3 into six increments each. Finer grid spacings were tested but led to essentially identical results.

The size of the time increments was coupled with the problem

of stability as discussed in Chapter 9. The normally unconditional stability of the Crank-Nicolson scheme (irrespective of the ratio $\alpha\ell/h^2$) was apparently destroyed by the non-linear boundary condition at x = s. In accordance with a suggestion of Starfield's [206] the time increments were made exceedingly small until a region of stable operation was found. A range of increment sizes within this region was tested and the effect on errors noted. The errors took the form of minor temperature perturbations at and near the internal boundaries (x = b and x = c). An increment size of $2,5 \times 10^{-5}$ ms was finally chosen. With this size the perturbations were limited to the late stages of the evaporation process (with region 3 shrunk to less than 20 per cent of its original thickness). Smaller time increments gave reduced temperature perturbations (and excessive computation time), but left the overall rate of evaporation essentially unchanged.

Since no analytical solution of the transient conduction-evaporation problem was available the program could not be fully tested. By setting the evaporation coefficient to zero, however, stationary-boundary transient conduction problems could be investigated. The case tested was that of the response of a plate initially at uniform temperature and with one face adiabatic, to a step change in temperature on the other face. The plate was treated as homogeneous by setting the physical properties identical in all three regions. The overall plate thickness and the x and t increments were approximately the same as those used in the solution of the microlayer problem. Agreement with the analytical solution [211] was excellent.

A18.6 PHYSICAL PROPERTIES

The physical properties used in the final computations are listed in Table A18.1 below. While the accuracy of some values, particularly for SnO_2, is open to doubt, it is sufficient for the order-of-magnitude estimates of evaporation rate required in Chapter 9.

TABLE A18.1

PHYSICAL PROPERTIES FOR CONDUCTION-EVAPORATION COMPUTATION

PHYSICAL PROPERTY				SOURCE
Thermal conductivity (W/m K)	k_1	glass	0,762	[51]
	k_2	SnO_2	27,6	[208]
	k_3	methanol	0,183	[137]
Density (kg/m^3)	ρ_1	glass	2710	[208, 209]
	ρ_2	SnO_2	6580	[208]
	ρ_3	methanol	759	Appendix 15
Heat capacity (kJ/kg K)	c_1	glass	0,837	[208]
	c_2	SnO_2	0,376	[208]
	c_3	methanol	2,747	[137]
Thermal diffusivity $k/\rho c$ (m^2/s)	α_1	glass	$3,36 \times 10^{-7}$	
	α_2	SnO_2	$1,12 \times 10^{-5}$	
	α_3	methanol	$8,78 \times 10^{-8}$	
Clausius-Clapeyron constants	C_3	methanol	21,007	Appendix 13
	C_4		4857	
Latent heat of vaporisation (kJ/kg)	λ	methanol	1082	[210]

APPENDIX 19

NON-LINEAR REGRESSION AND EVALUATION OF BUBBLE FORCES

The opening sections of this Appendix describe the Taylor linearisation technique for non-linear regression and the methods of obtaining confidence limits on the fitted parameters and on functions of these parameters. The remaining sections show how these techniques were applied in the evaluation of the bubble forces required in Chapter 9.

A19.1 NON-LINEAR REGRESSION BY TAYLOR LINEARISATION

The problem to be solved consists of the fitting of a non-linear function involving one independent variable and (in the present case) two parameters to a set of observations. (The procedure described may be readily extended to more parameters).

The observations are m pairs of values $\{y_i, x_i\}$ where y_i (but not x_i) are assumed to be subject to experimental error. The function is

$$f = f(x; \alpha_1, \alpha_2) \qquad (A19.1)$$

where the α's are the parameters to be optimised.

The vertical deviation between observed and fitted values for a particular x_i is

$$r_i = y_i - f_i = y_i - f(x_i; \alpha_1, \alpha_2) \qquad (A19.2)$$

According to the least squares criterion the parameters giving the best fit are those which minimise the sum of

the squares of these deviations, that is, those which minimise the sum

$$S^2 = \sum_{i=1}^{m} \varepsilon_i^2 \qquad \text{(A19.3)}$$

The minimisation is achieved by the following iterative procedure:

First, the function f is linearised [220, 221] by expanding it in a Taylor series in the parameters α_1 and α_2 about initial guesses α_1^o and α_2^o and by omitting terms with derivatives higher than first order:

$$f(x; \alpha_1, \alpha_2) = f(x; \alpha_1^o, \alpha_2^o) + (\partial f/\partial \alpha_1)^o \Delta\alpha_1 + (\partial f/\partial \alpha_2)^o \Delta\alpha_2 \qquad \text{(A19.4)}$$

(Superscripts on the partial derivatives indicate that their values are determined using α_1^o and α_2^o). Then

$$S^2 = \sum_{i=1}^{m} \{y_i - f(x_i; \alpha_1^o, \alpha_2^o) - (\partial f/\partial \alpha_1)^o \Delta\alpha_1 - (\partial f/\partial \alpha_2)^o \Delta\alpha_2\}^2 \qquad \text{(A19.5)}$$

By setting

$$a_i = y_i - f(x_i; \alpha_1^o, \alpha_2^o) \qquad \text{(A19.6)}$$

$$b_i = (\partial f/\partial \alpha_1)^o \qquad \text{(A19.7)}$$

$$c_i = (\partial f/\partial \alpha_2)^o \qquad \text{(A19.8)}$$

equation A19.5 becomes

$$S^2 = \Sigma (a_i - b_i \Delta\alpha_1 - c_i \Delta\alpha_2)^2 \qquad \text{(A19.9)}$$

The conditions for S^2 to be a minimum are determined by setting $\partial S^2/\partial(\Delta\alpha_1)$ and $\partial S^2/\partial(\Delta\alpha_2)$ equal to zero:

$$2 \Sigma (a_i - b_i\Delta\alpha_1 - c_i\Delta\alpha_2)(-b_i) = 0 \qquad \text{(A19.10)}$$

$$2 \Sigma (a_i - b_i\Delta\alpha_1 - c_i\Delta\alpha_2)(-c_i) = 0 \qquad \text{(A19.11)}$$

This leads to the linear equations

$$\Sigma b_i^2\Delta\alpha_1 + \Sigma b_i c_i\Delta\alpha_2 = \Sigma a_i b_i \qquad \text{(A19.12)}$$

$$\Sigma b_i c_i\Delta\alpha_1 + \Sigma c_i^2\Delta\alpha_2 = \Sigma a_i c_i \qquad \text{(A19.13)}$$

or, in matrix notation

$$[A]\{\Delta\alpha\} = \{g\} \qquad \text{(A19.14)}$$

If the determinant $|A| \neq 0$, the equation can be solved and

$$\{\Delta\alpha\} = [A]^{-1}\{g\} \qquad \text{(A19.15)}$$

The initial values of the parameters are now modified to give improved values:

$$\alpha_1^1 = \alpha_1^0 + \Delta\alpha_1 \qquad \text{(A19.16)}$$

$$\alpha_2^1 = \alpha_2^0 + \Delta\alpha_2 \qquad \text{(A19.17)}$$

(Here and below superscripts on α's refer to iterations, not powers of α.)

The procedure is repeated until the desired accuracy is achieved, say, after n iterations. The regression line is then

$$\hat{f} = f(x; \alpha_1^n, \alpha_2^n) = f(x; \{\hat{\alpha}\}) \qquad \text{(A19.18)}$$

The residual sum of squares is given by

$$(SS) = \Sigma (y_i - \hat{f}_i)^2 \qquad (A19.19)$$

and the quantity

$$s^2 = (SS)/(m - 2) \qquad (A19.20)$$

is an estimate of the variance about the regression based on (m - 2) degrees of freedom (2 being the number of parameters estimated). If the regression equation had been based on infinitely many observations, the true variance about regression, σ^2_{yx}, would have been obtained.

A19.1.1 Properties of the Fitted Parameters

For each x_i there exists an infinite population of observations that could have been made. The single observation y_i is considered a random sample drawn from this population. It is now assumed that (1) y_i and y_j are independent, that is, an error in one observation has no effect on the error in another observation, and (2) all distributions of y_i have the same (unknown) variance σ^2.

Then the variances (var) and covariances (cov) on the fitted parameters are given by $\sigma^2[A]^{-1}$ (using the $[A]^{-1}$ of the final iteration) as follows [221, 222]:

$$\sigma^2[A]^{-1} = \begin{bmatrix} \text{var}(\alpha_1) & \text{cov}(\alpha_1, \alpha_2) \\ \text{cov}(\alpha_2, \alpha_1) & \text{var}(\alpha_2) \end{bmatrix} \qquad (A19.21)$$

and $\sigma^2[A]^{-1}$ is known as the variance-covariance matrix.

In matrix notation:

$$\text{var}(\alpha_i) = \sigma^2 A^{-1}_{ii} \qquad \text{(A19.22)}$$

$$\text{cov}(\alpha_i, \alpha_j) = \sigma^2 A^{-1}_{ij} \qquad \text{(A19.23)}$$

The covariances $\text{cov}(\alpha_i, \alpha_j)$ and $\text{cov}(\alpha_j, \alpha_i)$ are equal since $[A]^{-1}$ is symmetrical.

If the postulated model described by the function f is the correct one then the variance σ^2 is equal to the variance σ^2_{yx}. The quantity s^2 in equation A19.20 is an estimate of σ^2_{yx}. Hence if $\sigma^2[A]^{-1}$ is replaced by $s^2[A]^{-1}$, then the elements of the matrix are estimated variances and covariances on the parameters.

A19.1.2 Confidence Limits on Fitted Parameters

In order to assign confidence limits to the fitted parameters it is necessary to make the additional assumption that for each x_i the population of y_i's is normally distributed. In real situations this is frequently the case [221].

In the case of a linear regression the true confidence limits could now be assigned to the fitted parameters. In the non-linear case, however, this is not generally possible since $\{\alpha\}$ is no longer normally distributed [221]. Non-linear confidence limits can still be defined by the expression applicable to the linear model, normal error situation, but the confidence will not be strictly known. The limits are then known as approximate confidence limits.

Thus, for example, approximate $100(1 - A)$ per cent confidence limits for parameter α_i are given by

$$\alpha_i \pm t_{(m-2,\ 1-0,5A)}\text{var}(\alpha_i) \qquad \text{(A19.24)}$$

where $\text{var}(\alpha_i)$ is the estimated variance on α_i and

$t_{(m-2,\ 1-0,5A)}$ is the (1-0,5A) percentage point on a t-distribution for (m-2) degrees of freedom. Values of the t-distribution are obtainable from standard tables [223]. A few illustrative values for a confidence level of 95 per cent are given below:

Degrees of freedom	t
∞	1,96
20	2,09
10	2,23
5	2,57
2	4,30
1	12,71

A19.1.3 Variance and confidence limits on functions of the fitted parameters

If p is the number of parameters estimated and ϕ is any function of the parameters (including the fitted function f), that is

$$\phi = \phi\ (x;\ \alpha_1,\ \alpha_2,\ \ \ldots\ \alpha_p) \qquad \text{(A19.25)}$$

then, from [224]

$$\text{var}(\phi) = \sum_{i=1}^{p} \left[(\partial\phi/\partial\alpha_i)^2\ \text{var}(\alpha_i)\right]$$

$$+ \sum_{i=1}^{p} \sum_{j=1, j\neq i}^{p} \left[(\partial\phi/\partial\alpha_i)(\partial\phi/\partial\alpha_j)\ \text{cov}(\alpha_i, \alpha_j)\right] \qquad \text{(A19.26)}$$

In the present case, with p = 2, this becomes

$$\mathrm{var}(\phi) = (\partial\phi/\partial\alpha_1)^2\,\mathrm{var}(\alpha_1) + (\partial\phi/\partial\alpha_2)^2\,\mathrm{var}(\alpha_2)$$

$$+ 2\,(\partial\phi/\partial\alpha_1)(\partial\phi/\partial\alpha_2)\,\mathrm{cov}(\alpha_1,\alpha_2) \qquad \text{(A19.27)}$$

where in the non-linear case var and cov signify estimated variances and covariances.

Approximate 100(1 - A) per cent confidence limits on ϕ are then given as before by

$$\phi \pm t_{(m-2,\ 1-0,5A)}\ \mathrm{var}(\phi) \qquad \text{(A19.28)}$$

A19.2 EVALUATION OF BUBBLE FORCES

The bubble forces (per unit area) required to be evaluated were the forces of inertia, viscosity, surface tension and gravity, given respectively by

$$P_i = \rho_L(R\ddot{R} + 1,5\,\dot{R}^2) \qquad \text{(A19.29)}$$

$$P_v = 4\mu\dot{R}/R \qquad \text{(A19.30)}$$

$$P_s = 2\sigma/R \qquad \text{(A19.31)}$$

$$P_g = (\rho_L - \rho_V)gR \qquad \text{(A19.32)}$$

where R is the equivalent spherical bubble radius and $\dot{R}$ and $\ddot{R}$ are the first and second derivatives of R with respect to time (t).

As discussed in Chapter 9, the experimental R vs t data were first hand-smoothed and normalised to the correct time base. Smoothing was essential to prevent erratic oscillations in the second derivative and thus the inertia force P_i. Data points $\{R_i, t_i\}$ were then read from the corrected and smoothed curves. A non-linear equation of the form

$$R = at^b \qquad \text{(A19.33)}$$

was fitted, by the regression methods outlined in Section A19.1, to overlapping groups of such data points. The first group of successive points, odd in number (3, 5, 7, 9 or 11), and starting with point 1 was fed to the regression program and the fitted values of the parameters a and b applied at the central point (for example, at point 3 for a 5-point fit); R was calculated from equation A19.33 and $\dot{R}$ and $\ddot{R}$ from equation A19.34 and A19.35

$$\dot{R} = abt^{(b-1)} \qquad \text{(A19.34)}$$

$$\ddot{R} = ab(b-1)t^{(b-2)} \qquad \text{(A19.35)}$$

The procedure was then repeated for the next group of points, this time starting with point 2 and, for a 5-point fit, giving R, $\dot{R}$ and $\ddot{R}$ at point 4. The procedure was successively applied to all data points and the bubble forces calculated from equations A19.29 to A19.32 at each point.

For each curve-fitting operation the regression program provided, in addition to the parameters a and b, their variance-covariance matrix, that is, values of var(a), var(b) and cov(a, b), as described in Section A19.1.1.

A19.2.1 Variance and Confidence Limits on Bubble Forces

From equation A19 27 it is seen that the estimated variance, var(P), on a bubble force P is given by

$$\text{var}(P) = (\partial P/\partial a)^2 \text{var}(a) + (\partial P/\partial b)^2 \text{var}(b) + 2(\partial P/\partial a)(\partial P/\partial b)\, \text{cov}(a, b) \qquad \text{(A19.36)}$$

The partial derivatives for the four bubble forces (and

for the bubble radius) were calculated as follows:

Radius:

$$R = at^b \tag{A19.37}$$

$$(\partial R/\partial a) = t^b \tag{A19.38}$$

$$(\partial R/\partial b) = at^b \ln t = R \ln t \tag{A19.39}$$

Inertia:

$$P_i = \rho_L \{at^b . ab(b-1)t^{(b-2)} + 1{,}5(abt^{(b-1)})^2\} \tag{A19.40}$$

$$(\partial P_i/\partial a) = \rho_L \{2a(b^2-b)t^{(2b-2)} + 3\, ab^2 t^{(2b-2)}\} \tag{A19.41}$$

$$(\partial P_i/\partial b) = \rho_L \left[a^2 t^{(2b+2)} \{2b^2-b) \ln t + 2b-1\}\right.$$

$$\left. + 3a^2 bt^{(2b-2)} (b \ln t+1)\right] \tag{A19.42}$$

Viscosity:

$$P_v = 4\mu bt^{-1} \tag{A19.43}$$

$$(\partial P_v/\partial a) = 0 \tag{A19.44}$$

$$(\partial P_v/\partial b) = 4\mu t^{-1} \tag{A19.45}$$

Surface tension:

$$P_s = 2\sigma t^{-b}/a \tag{A19.46}$$

$$(\partial P_s/\partial a) = -2\sigma/a^2 t^b \tag{A19.47}$$

$$(\partial P_s/\partial b) = -2\sigma \ln t/at^b \tag{A19.48}$$

Gravity:

$$P_g = g(\rho_L - \rho_V)at^b \qquad \text{(A19.49)}$$

$$(\partial P_g/\partial a) = g(\rho_L - \rho_V)t^b \qquad \text{(A19.50)}$$

$$(\partial P_g/\partial b) = g(\rho_L - \rho_V)at^b \ln t \qquad \text{(A19.51)}$$

Thus for each fitted point equation A19.36 gave the variances var(R), var(P_i), var(P_v), var(P_s) and var(P_g).

Approximate confidence limits were obtained from these variances as shown in Section A19.1.3. For example, approximate 95 per cent confidence limits on the inertia force, P_i, were given, for the case of a 5-point fit, by

$$P_i \pm t_{(3;\ 0,975)}\ \mathrm{var}(P_i) = 3,182\ \mathrm{var}(P_i) \qquad \text{(A19.52)}$$

Here, 3,182 is the 0,975 (= 1 - 0,5A) fraction point on a t-distribution for 3 degrees of freedom (5 observations minus 2 parameters).

Since the regressions were based on the smoothed R vs t data, rather than on the original experimental data, the calculated confidence limits were not meaningful in the normal sense. They were useful, however, in determining the most suitable number of points per fit (3, 5, 7 ...) as shown further below.

A19.2.2 Scatter, Confidence Limits and Number of Points Per Fit

In discussing the scatter in the final forces vs time data the example of the inertia force, evaluated via a 5-point fitting procedure, is considered.

From data points 1 to 5 a P_i value was obtained at point 3 based on certain 'best' values of the parameters a and b. From data points 2 to 6 a P_i value was obtained at point 4 based on different 'best' values of a and b. Thus the P_i values at points 3 and 4, and similarly for all other points, were not related by a continuous function. Scatter in the (smoothed) R vs t data was reflected, and magnified by the double derivative, in the P_i vs t data. This scatter could be reduced by increasing the number of points per fitting operation.

Confidence limits on P_i at point 3 are related to the 'goodness of fit' of the regression on points 1 to 5. A different 'goodness of fit' obtains over points 2 to 6, and similarly for all other points. Thus the magnitude of the confidence interval on P_i must be expected to vary irregularly from point to point, as was indeed observed.

Increasing the number of points per fitting operation influences the confidence intervals in a twofold fashion; firstly, it reduces the 'goodness of fit', thus increasing var(P_i) and hence increasing the confidence intervals, and secondly, it decreases the value of the t-distribution (see Section A19.1.2), thus decreasing the confidence intervals. In the range of values of the present work the second effect predominated.

A large number of points per fit thus both smoothed the forces output data and reduced the confidence intervals. However, it also caused loss of information; for example, in an 11-point fitting procedure the first and last five data points of the total set are lost.

Trial computations established the most suitable number of points per fit for each bubble force, as illustrated in the example below.

A19.2.3 Example

The entire regression and force evaluation procedure and the choice of the number of points per fit are illustrated for the case of Run M10.

Figure A19.1 shows the 44 experimental points of R against uncorrected t. The hand-smoothed dotted line through the points is shown extrapolated to R = ∞. Time was corrected such that R = 0 and t = 0 coincided, and 61 values of R were read from the corrected curve as follows: for the period 7 to 43 ms at 1,0 ms intervals, from 3 to 7 ms at 0,5 ms intervals and during the first 3 ms at 0,1 to 0,3 ms intervals. The solid curve in Figure A19.1 connects the R vs t points resulting from regression with 7 points per fitting operation. The truncation resulted from the loss of 3 points at each end of the curve. Confidence limits of R cannot be shown, the 95 per cent and even the 99 per cent intervals being of the order of magnitude of the thickness of a pencil line.

Figure A19.2 shows the calculated points for the four bubble forces. The 95 per cent confidence intervals on P_v, P_s and P_g are again too small to be shown; the confidence limits on P_i are dealt with in the next group of figures.

The effect of the number of points per fit on the scatter and confidence limits for the inertia force P_i is shown in Figures A19.3 to A19.5. A 3-point procedure (Figure A19.3) resulted in unacceptable scatter and excessive confidence intervals. A 5-point, and 7-point procedure (Figure A19.4) gave better results and an 11-point procedure (Figure A19.5) was considered ideal. A larger number of points per fit would have resulted in an excessive loss of points at the two ends of the curve.

Plots similar to Figures A19.3 to A19.5 for the viscosity,

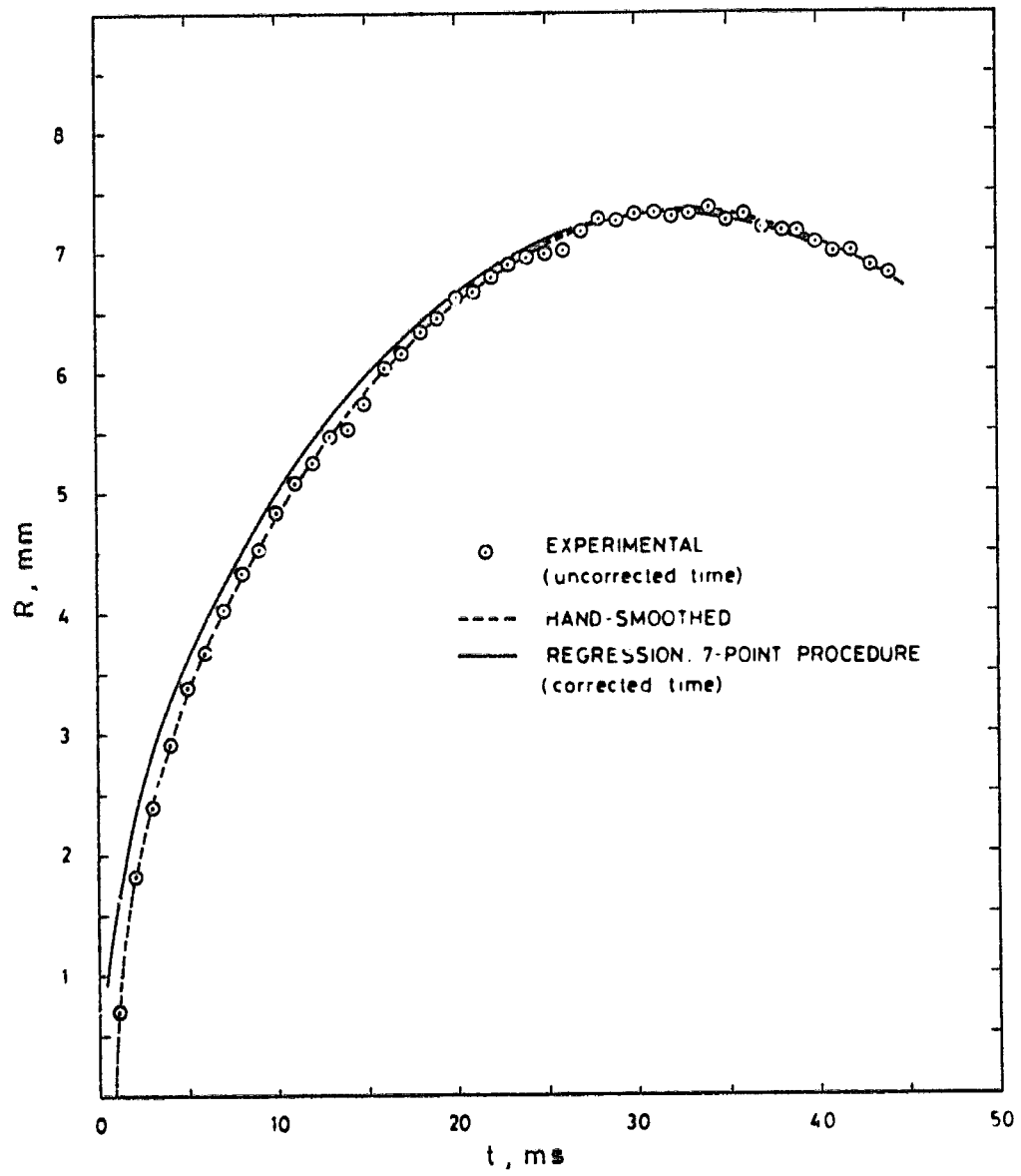

FIG. A19.1 EXPERIMENTAL AND FITTED BUBBLE RADIUS. RUN M10.

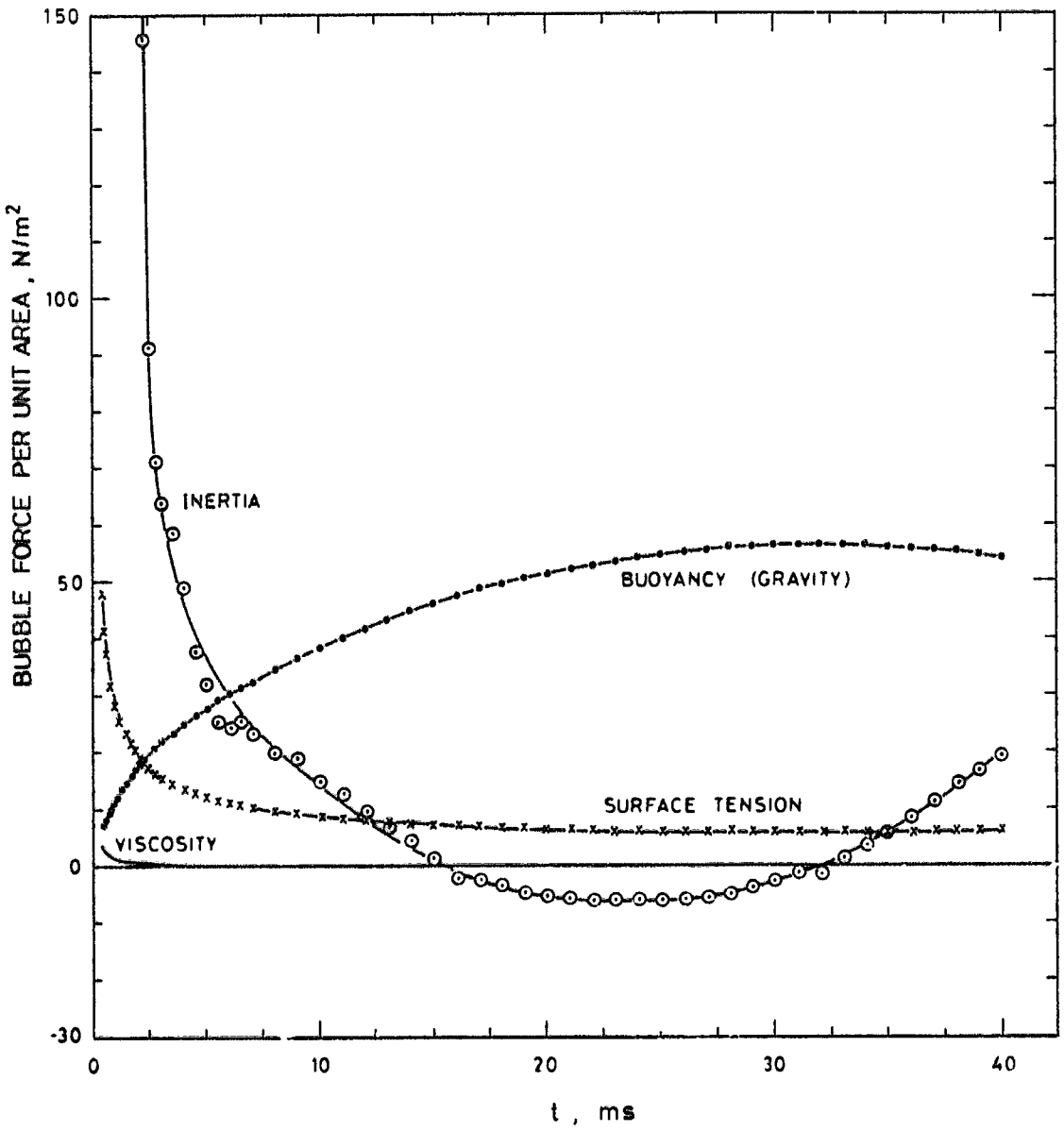

FIG. A19.2 BUBBLE FORCES. RUN M10.
7-point fitting procedure

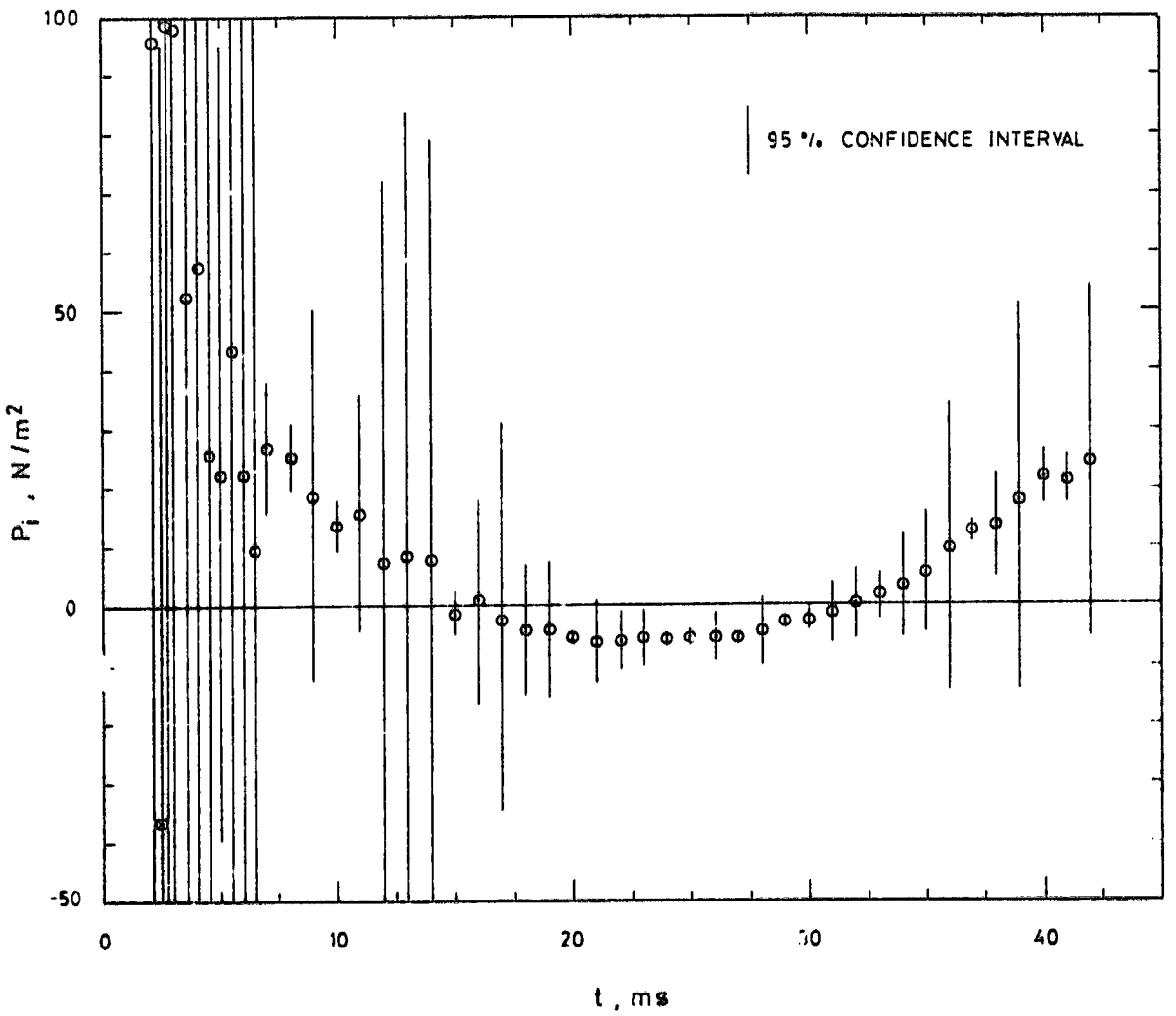

FIG. A19.3 INERTIA FORCE AND CONFIDENCE INTERVALS. RUN M10
3 - point fitting procedure

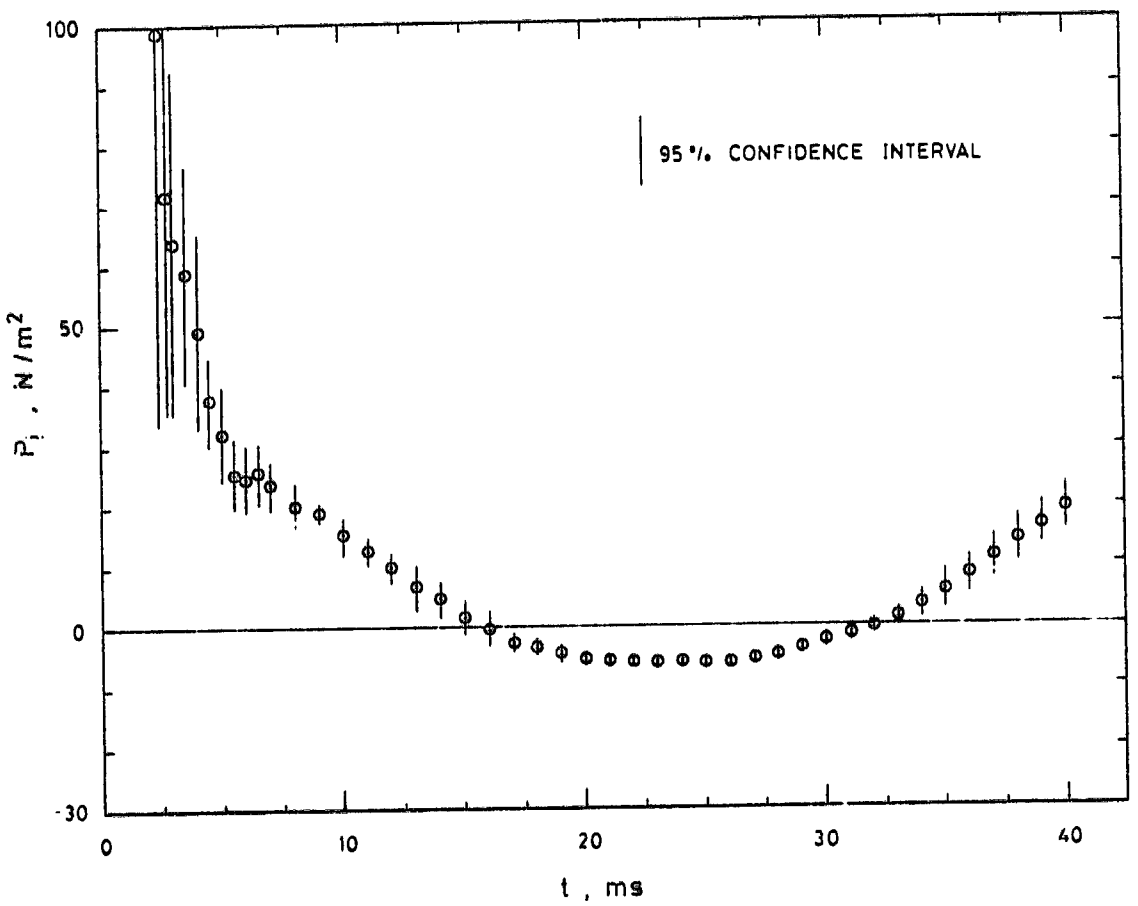

FIG. A19.4 INERTIA FORCE AND CONFIDENCE INTERVALS. RUN M10.
7-point fitting procedure

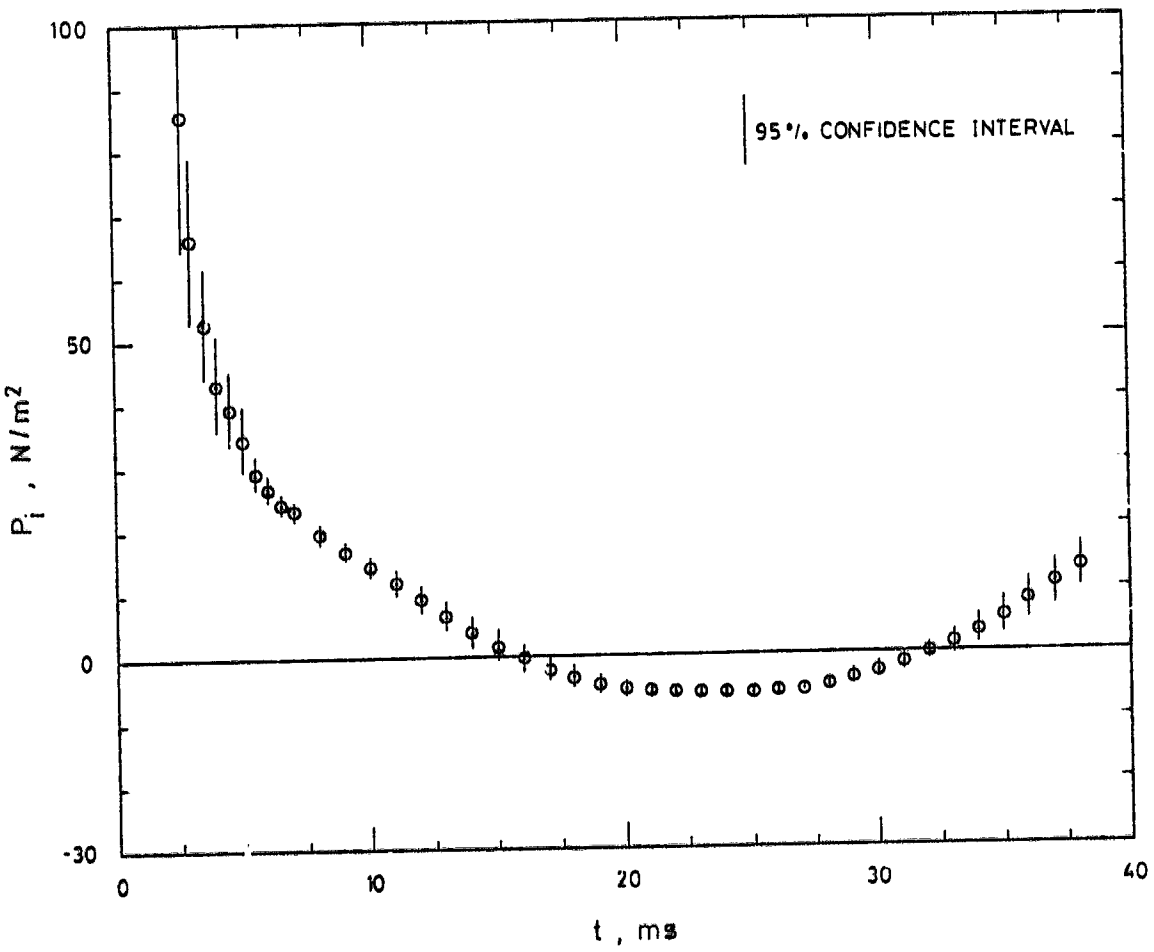

FIG. A19.5 INERTIA FORCE AND CONFIDENCE INTERVALS. RUN M10.
11-point fitting procedure

surface tension and gravity forces showed that these could be satisfactorily evaluated using 3-point or 5-point fitting procedures; the 95 per cent confidence intervals were again too small to be worth plotting.

In all final computations reported in Chapter 9 an 11-point procedure was used for the evaluation of inertia forces and a 3-point procedure for the remaining forces.

REFERENCES

1. C J RALLIS, R V GREENLAND and A KOK, Stagnant pool nucleate boiling from horizontal wires under saturated and sub-cooled conditions, S. Afr. Mech. Engr 10, 171-186 (1961).

2. C J RALLIS and H H JAWUREK, Latent heat transport in saturated nucleate boiling, Int. J. Heat Mass Transfer 7, 1051-1068 (1964).

3. C J RALLIS and H H JAWUREK, The mechanism of nucleate boiling, Paper A/CONF. 28/P/600, 3rd U.N. Int. Conf. Peaceful Uses Atomic Energy, Geneva (1964)

4. H H JAWUREK, A latent-heat-based correlation of nucleate pool boiling heat transfer, Proceedings S.75, Conference: 'Heat transfer and the design and operation of heat exchangers' Sponsored: S.A. Inst. Chem. Engrs, S.A. Inst. Mech. Engrs, C.S.I.R.; Johannesburg (1974).

5. ANON., An analysis of the AEB power reactor concept PELINDUNA, Vol. 6: Summary of reports. S.A. Atomic Energy Board Report PEL 117, Pelindaba (1967).

6. ANON., The International Metric System (SI), Publication M55a, S. Afr. Bureau of Standards, Pretoria (1973). ISBN-0-626-01216-3.

7. M JAKOB, Heat Transfer Vol. 1. Wiley, New York (1949).

8. F C GUNTHER and F KREITH, Photographic study of bubble formation in heat transfer to subcooled water, Proc. Heat Transfer and Fluid Mech. Institute, pp 113-138. Amer. Soc. Mech. Engrs (1949); also: Jet Propulsion Lab. Progr. Report 4-120, California Inst. Techn., Pasadena (1950).

9. W M ROHSENOW and J A CLARK, A study of the mechanism of boiling heat transfer, Trans. Amer. Soc. Mech. Engrs 73, 609-620 (1951).

10. W H McADAMS, W E KENNEL, C S MINDEN, C RUDOLF, P M PICORNELL and J E DEW, Heat transfer at high rates to water with surface boiling, Ind. Engng Chem. 41, 1945-1953 (1949).

11. P C ZMOLA, Discussion of paper by Rohsenow and Clark [9], Trans. Am. Soc. Mech. Engrs 73, 618-619 (1951).

12. S G BANKOFF, W J COLAHAN and D R BARTZ, Summary of conference on bubble dynamics and boiling heat transfer, Jet Propulsion Lab. Memo. 20-137, California Inst. Techn., Pasadena, (1956).

13. D K EDWARDS, The rôle of interphase mass transfer in the mechanism of nucleate boiling, M.S. Thesis, University of California, Berkley (1956).

14. M S PLESSET, Note on the flow of vapour between liquid surfaces, J. Chem. Phys. 20, 790-793 (1952).

15. O KNACKE and I N STRANSKI, The mechanism of evaporation, Progr. Metal Phys. 6, 181-235 (1956).

16. B PAUL, Compilation of evaporation coefficien ~, J. Amer. Rocket Soc. 32, 1321-1328 (1962).

17. N ZUBER and E FRIED, Two-phase flow and boiling heat transfer to cryogenic liquids, J. Amer. Rocket Soc. 32, 1332-1341 (1962).

18. G LEPPERT and C C PITTS, Boiling, Advances in Heat Transfer (eds T I Irvine and J P Hartnett) Vol. 1, pp 185-266. Academic Press, New York (1964).

19. L S TONG, Boiling Heat Transfer and Two-phase Flow. Wiley, New York (1965).

20. W ROHSENOW, A method of correlating heat transfer data for surface boiling of liquids, Trans. Amer. Soc. Mech. Engrs 74, 969-976 (1952).

21. H K FORSTER and N ZUBER, Dynamics of vapour bubbles and boiling heat transfer, Amer. Inst. Chem. Engrs J. 1, 531-535 (1955).

22. S S KUTATELADZE, Fundamentals of Heat Transfer, (ed. R D Cess), p 362. Academic Press, New York (1963).

23. W FRITZ, Berechnung des Maximalvolumens von Dampfblasen, Phys. Z. 36, 379 (1935).

24. M T CICHELLI and C F BONILLA, Heat transfer to liquids under pressure, Trans. Amer. Inst. Chem. Engrs 41, 755-787 (1945).

25. J N ADDOMS, Sc. D. Thesis in Chem. Engng, Massachusetts Inst. Tech. (1948); summarised in McAdams [51].

26. C W FROST and K W LI, On the Rohsenow pool-boiling correlation, J. Heat Transfer C93, 232-234 (1971).

27. C CORTY and A S FOUST, Surface variables in nucleate boiling, Chem. Engng Progr. Symp. Ser. 51, No. 17, 1-12 (1955).

28. H M KURIHARA and J E MYERS, The effects of superheat and surface roughness on boiling coefficients, Amer. Inst. Chem. Engrs J. 6, 83-91 (1960).

29. B STOCK, Observations on transition boiling heat transfer phenomena, Argonne National Lab. Report ANL-6175, Argonne, Ill. (1960).

30. P J BERENSON, Experiments on pool-boiling heat transfer, Int. J. Heat Mass Transfer 5, 985-999 (1962).

31. I S HALL and A P HATTON, The influence of surface roughness and a wetting additive on pool boiling on horizontal rods, Paper 1, Inst. Mech. Engrs Symposium on Boiling Heat Transfer, Manchester (1965).

32. R I VACHON, G E TANGER, D L DAVIS and G H NIX, Pool boiling on polished and chemically etched stainless-steel surfaces, J. Heat Transfer C90, 231-238 (1968).

33. R I VACHON, G H NIX and G E TANGER, Evaluation of constants for the Rohsenow pool-boiling correlation, J. Heat Transfer C90, 239-247 (1968).

34. K YAMAGATA, F HIRANO, K NISHIKAWA and H MATSUOKA, Nucleate boiling of water on the horizontal surface, Memoirs Fac. Engng, Kyushu Univ. 15, No. 1, 99-163 (1955).

35. R F GAERTNER and J W WESTWATER, Population of active sites in nucleate boiling heat transfer, Chem. Engng Progr. Symp. Ser. 56, No. 30, 39-48 (1960).

36. K NISHIKAWA and K YAMAGATA, On the correlation of nucleate boiling heat transfer, Int. J. Heat Mass Transfer 1, 219-235 (1960).

37. N ZUBER, Nucleate boiling. The region of isolated bubbles and the similarity with natural convection, Int. J. Heat Mass Transfer 6, 53-78 (1963).

38. C L TIEN, A hydronamic model for nucleate pool boiling, Int. J. Heat Mass Transfer 5, 533-540 (1962).

39. C L TIEN, Erratum, Int. J. Heat Mass Transfer 8, 972 (1965).

40. R F BOEHM and J H LIENHARD, Transient effects in Tien's nucleate boiling model, Amer. Soc. Mech. Engrs Paper No. 64-WA/HT-34 (1964).

41. K E FORSTER and R GREIF, Heat transfer to a boiling liquid, mechanism and correlations, J. Heat Transfer C81, 43-53 (1959).

42. C Y HAN and P GRIFFITH, The mechanism of heat transfer in nucleate pool boiling. Parts 1 and 2, Int. J. Heat Mass Transfer 8, 887-914 (1965).

43. Y Y HSU and R W GRAHAM, An analytical and experimental study of thermal boundary layer and ebullition cycle in nucleate boiling, Techn. Note NASA TN-D-594, Lewis Research Centre, Cleveland, Ohio (1961).

44. K STEPHAN, Mechanismus und Modellgesetz des Wärmeübergangs bei der Blasenverdampfung, Chemie - Ing. Technik 35, 775-778 (1963).

45. E RUCKENSTEIN, Remarks on nucleate boiling heat transfer from a horizontal surface, Int. J. Heat Mass Transfer 9, 229-237 (1966).

46. Y HELED, J RICKLIS and A ORELL, Pool boiling from large arrays of artificial nucleation sites, Int. J. Heat Mass Transfer 13, 503-516 (1970).

47. B B MIKIC and W M ROHSENOW, A new correlation of pool boiling data including the effect of heating surface characteristics, J. Heat Transfer C91, 245-250 (1969).

48. P GRIFFITH and J D WALLIS, The rôle of surface conditions in nucleate boiling, Chem. Engng Progr. Symp. Ser. 56, No. 30, 49-65 (1960).

49. R COLE and W M ROHSENOW, Correlation of bubble departure diameters for boiling of saturated liquids, Chem. Engng Progr. Symp. Ser. 65, No. 92, 211-213 (1969).

50. R COLE, Bubble frequencies and departure volumes at sub-atmospheric pressures, Amer. Inst. Chem. Engrs J. 13, 779-783 (1967).

51. W H McADAMS, Heat Transmission, 3rd ed. McGraw Hill, New York (1954).

52. M BÉHAR and R SÍMÉRIA, La strioscopie appliquée à l'étude de l'ébullition et du dégazage, La Houille Blanche No. 6, 687-691 (1963).

53. M BÉHAR and R SÍMÉRIA, Sur la mise en évidence par strioscopie de certain mécanismes d'échanges thermiques dans le dégazage et l'ébullition de l'eau, Comptes Rendus Acad. Sc. Paris 257, 2801-2803 (1963).

54. R SÍMÉRIA, Les échanges thermiques en ébullition nucléée, Publication Scientifiques et Techniques du Ministère de l'Air, No. 417 (1963).

55. H MONDIN, P LAVIGNE and R SÍMÉRIA, Some fundamental aspects of boiling in nuclear reactors, Paper A/CONF.28/P/55, 3rd U.N. Int. Conf. Peaceful Uses Atomic Energy, Geneva (1964).

56. N ISSHIKI and H TAMAKI, Photographic study of boiling heat transfer mechanism, Bul. Japan Soc. Mech. Engrs 6, 505-513 (1963).

57. A BÄHR, Bedeutung der von Dampfblasen erzeugten Mikokonvektion für die Wärmeübertragung beim Sieden, Chemie-Ing. Technik 38, 922-925 (1966).

58. H BRAUER, Schlierenoptische Beobachtungen bei der Wärmeübertragung, Chemie-Ing. Technik 34, 73-78 (1962).

59. T HARA, The mechanism of nucleate boiling heat transfer, Int. J. Heat Mass Transfer 6, 959-969 (1963).

60. T B BENJAMIN and A T ELLIS, The collapse of cavitation bubbles and the pressure thereby produced against solid boundaries, Phil. Trans. Roy. Soc. London A260, 221-240 (1966).

61. C BONNET, E MACKE, R MORIN and J SALOMON, Fluctuations de temperature dans la paroi chauffante et dans le liquide au cours de l'ébullition nucléée, Report EUR 3162 f, Euratom Research Centre, Ispra (1966).

62. R SÍMÉRIA and J C FLAMAND, Utilisation d'un micro-thermocouple pour l'etude de l'ébullition locale de l'eau en convection libre, Report T.T. No. 81, Centre d'Etude Nucléaires, Grenoble (1967).

63. S J D VAN STRALEN and W M SLUYTER, Local temperature fluctuations in saturated pool boiling of pure liquids and binary mixtures, Int. J. Heat Mass Transfer 12, 187-198 (1969).

64. J D JACOBS and A H SHADE, Measurements of temperatures associated with bubbles in subcooled pool boiling, J. Heat Transfer C91, 123-128 (1969).

65. S J D VAN STRALEN, The mechanism of nucleate boiling in pure liquids and binary mixtures, Parts 1 and 2: Int. J. Heat Mass Transfer 9, 995-1046 (1966); Parts 3 and 4: Int. J. Heat Mass Transfer 10, 1469-1498 (1967).

66. R L JUDD and H MERTE, Influence of acceleration on subcooled nucleate pool boiling, Paper B8.7, 4th Int. Heat Transfer Conf., Versailles (1970).

67. F D MOORE and R B MESLER, The measurement of rapid surface temperature fluctuations during nucleate boiling of water, Amer. Inst. Chem. Engrs J. 7, 620-624 (1961).

68. D A RENDIERSKY, A special thermocouple for measuring transient temperatures, Mech. Engng 75, 117-121 (1953).

69. S G BANKOFF and R B MESSELL, Bubble growth rates in highly subcooled nucleate boiling, Chem. Engng Progr. Symp. Ser. 55, No. 29, 95-102 (1959).

70. S G BANKOFF, On the mechanism of subcooled nucleate boiling, Parts 1 and 2, Chem. Engng Progr. Symp. Ser. 57, No.32, 156-172, (1961).

71. S G BANKOFF and J P MASON, Heat transfer from the surface of a steam bubble in turbulent subcooled liquid stream, Amer. Inst. Chem. Engrs J. 8, 30-33 (1962).

72. S G BANKOFF, A note on latent heat transport in nucleate boiling, Amer. Inst. Chem. Engrs J. 8, 63-65 (1962).

73. M E ELLION, A study of the mechanism of boiling heat transfer, Jet Propulsion Lab. Memo. 20-28, California Inst. Techn. (1954).

74. F C GUNTHER, Photographic study of surface boiling heat transfer to water with forced convection, Trans. Amer. Soc. Mech. Engrs 73, 115-123 (1951).

75. N W SNYDER and T T ROBIN, Mass transfer model in subcooled nucleate boiling, J. Heat Transfer C91, 404-412 (1969).

76. T T ROBIN and N W SNYDER, Theoretical analysis of bubble dynamics for an artificially produced vapour bubble in a turbulent stream, Int. J. Heat Mass Transfer 13, 523-536 (1970).

77. W G COURTNEY, Recent advances in condensation and evaporation, Amer. Rocket Soc. J. 31, 751-756 (1961).

78. T T ROBIN and N W SNYDER, Bubble dynamics in subcooled nucleate boiling based on the mass transfer mechanism, Int. J. Heat Mass Transfer 15, 305-318 (1970).

79. R L SÉMÉRIA, An experimental study of the characteristics of vapour bubbles, Paper 7, Inst. Mech. Engrs Symposium on Two-Phase Fluid Flow, London (1962).

80. R L SÉMÉRIA, Quelques résultats sur le méchanisme de l'ébullition, Question II, Rapport No. 3, VII ème Journéés de l'Hydrolique, Soc. Hydrotech. de France, Paris (1962).

81. R F GAERTNER, Photographic study of nucleate pool boiling on a horizontal surface, General Electric Co. Research Lab. Report 63-RL-3357C, Schenectady (1963).

82. H H JAWUREK, The definition of mean bubble frequency and mean bubble volume at departure in nucleate boiling, S. Afr. Mech. Engr 13, 47-48 (1963), (obscure because of misprints); corrected version: Dep. Mech. Engng Report 25, University of the Witwatersrand, Johannesburg (1964).

83. R V GREENLAND, An investigation into stagnant pool nucleate boiling from horizontal sires for saturated and sub-cooled conditions, M.Sc. Thesis in Mech. Engng, University of the Witwatersrand, Johannesburg (1969).

84. M M NOVAKOVIĆ, L L JOVANOVIĆ, M S STEFANOVIĆ and N C NINIĆ, Nucleation from a mercury surface, Proc. 3rd Int. Heat Transf. Conf. 3, 213-218, Chicago (1966).

85. M NOVAKOVIĆ and M STEFANOVIĆ, Boiling from a mercury surface, Int. J. Heat Mass Transfer 7, 801-807 (1964).

86. C F BONILLA and C W PERRY, Heat transmission to boiling binary liquid mixtures, Trans. Amer. Inst. Chem. Engrs 37, 685-705 (1941).

87. R F GAERTNER, Distribution of active sites in the nucleate boiling of liquids, Chem. Engng Progr. Symp. Ser. 59, No. 41, 52-61 (1963).

88. D L J ANDERSON, R L JUDD and H MERTE, Site activation phenomena in saturated nucleate boiling, Amer. Soc. Mech. Engrs Paper No. 70-HT-14 (1970).

89. W H McADAMS, J N ADDOMS, P M RINALDO and R S DAY, Heat transfer from single horizontal wires, Chem. Engng Progr. 44, 639-646 (1948).

90. H J IVEY and D J MORRIS, Critical heat flux of saturated and sub-cooled pool boiling in water at atmospheric pressure, Proc. 3rd Int. Heat Transf. Conf. 3, 129-142, Chicago (1966).

91. R SIEGEL, Effects of reduced gravity on heat transfer, Advances in Heat Transfer (eds T F Irvine and J P Hartnett) Vol. 4, pp 143-228. Academic Press, New York (1967).

92. N ZUBER, On the stability of boiling heat transfer, Trans. Amer. Soc. Mech. Engrs 80, 711-720 (1958).

93. R SIEGEL and E G KESHOCK, Effects of reduced gravity on nucleate boiling bubble dynamics in saturated water, Amer. Inst. Chem. Engrs J. 10, 509 (1964).

94. E G KESHOCK and R SIEGEL, Forces acting on bubbles in nucleate boiling under normal and reduced gravity conditions, Techn. Note NASA TN D-2299 Lewis Research Centre, Cleveland, Ohio (1964).

95. R L JUDD and H MERTE, Evaluation of nucleate boiling heat flux predictions at varying levels of subcooling and acceleration, Int. J. Heat Mass Transfer 15, 1075-1096 (1972).

96. T F ROGERS and R B MESLER, An experimental study of surface cooling by bubbles during nucleate boiling of water, Amer. Inst. Chem. Engrs J. 10, 656-660 (1964).

97. R C HENDRICKS and R R SHARP, Initiation of cooling due to bubble growth on a heating surface, Techn. Note NASA TN D-2290, Lewis Research Centre, Cleveland, Ohio (1964).

98. C BONNET, E MACKE and R MORIN, Visualization of bubble formation at atmospheric pressure and related measurement of the wall temperature variations, Report EUR 1622 e, Euratom Research Centre, Ispra (1965).

99. M G COOPER and A J P LLOYD, Transient local heat flux in nucleate boiling, Proc. 3rd Int. Heat Transf. Conf. 3, 193-203, Chicago (1966).

100. M G COOPER and A J P LLOYD, The microlayer in nucleate pool boiling, Int. J. Heat Mass Transfer 12, 895-913 (1969).

101. N B HOSPETI and R B MESLER, Vaporization at the base of bubbles of different shape during nucleate boiling of water, Amer. Inst. Chem. Engrs J. 15, 214-219 (1969).

102. D M FONTANA, Simultaneous measurements of bubble growth rate and thermal flux from the heating wall to the boiling fluid near the nucleation site, Int. J. Heat Mass Transfer 15, 707-720 (1972).

103. N B HOSPETI and R B MESLER, Deposits formed beneath bubbles during nucleate boiling of radioactive calcium sulphate solution, Chem. Engng Progr. Symp. Ser. 62, 72-76 (1966).

104. R R SHARP, The nature of liquid film evaporation during nucleate boiling, Techn. Note NASA TN D-1997, Lewis Research Centre, Cleveland, Ohio (1964).

105. K TORIKAI, M HORI, M AKIYAMA, T KOBORI and H ADACHI, Boiling heat transfer and burnout mechanism in boiling water cooled reactors, Paper A/CONF. 28/P/580, 3rd U.N. Int. Conf. Peaceful Uses Atomic Energy, Geneva (1964).

106. K TORIKAI and T YAMAZAKI, The contact area of boiling bubbles on the heating surface, Bull. Jap. Soc. Mech. Engrs 8, 660-669 (1965).

107. K TORIKAI and T YAMAZAKI, Photographic study for boiling heat transfer mechanism, Proc. 3rd Int. Heat Transf. Conf. 3, 239-244, Chicago (1966).

108. Y KATTO and S YOKOYA, Experimental study of nucleate pool boiling in case of making interference-plate approach to the heating surface, Proc. 3rd Int. Heat Transf. Conf. 3, 219-227, Chicago (1966).

109. Y KATTO and S YOKOYA, Principal mechanism of boiling crisis in pool boiling, Int. J. Heat Mass Transfer 11, 993-1002 (1968).

110. H J VAN OUWERKERK, The rapid growth of a vapour bubble at a liquid-solid interface, Int. J. Heat Mass Transfer 14, 1415-1431 (1971).

111. H J VAN OUWERKERK, Burnout in pool boiling. The stability of boiling mechanisms, Int. J. Heat Mass Transfer 15, 25-34 (1972).

112. N MADSEN, Temperature fluctuations at a heated surface supporting pool boiling of water, Paper 14, Inst. Mech. Engrs Symposium on Boiling Heat Transfer, Manchester (1965).

113. S G BANKOFF, Ebullition from solid surfaces in the absence of a pre-existing gaseous phase, Trans. Amer. Soc. Mech. Engrs 79, 735-740 (1957).

114. H B CLARK, P S STRENGE and J W WESTWATER, Active sites for nucleate boiling, Chem. Engng Progr. Symp. Ser. 55, No. 29, 103-110 (1959).

115. Y HELED and A OREL, Characteristics of active nucleation sites in pool boiling, Int. J. Heat Mass Transfer 10, 553-554 (1967).

116. J P NAIL, R I VACHON and J MOREHOUSE, An SEM study of nucleation sites in pool boiling from 304 stainless steel, J. Heat Transfer C 96, 132-137 (' 74).

117. S G BANKOFF, Entrapment of gas in the spreading of a liquid over a rough surface, J. Amer. Inst. Chem. Engrs 4, 24-26 (1958).

118. J R HOWELL and R SIEGEL, Incipience, growth and detachment of boiling bubbles in saturated water from artificial nucleation sites of known geometry and size, Proc. 3rd Int. Heat Transf. Conf. 4, 12-23, Chicago (1966).

119. J R HOWELL and R SIEGEL, Activation, growth and detachment of boiling bubbles in water from artificial nucleation sites of known geometry and size, Techn. Note NASA TN D-4101, Lewis Research Centre, Cleveland, Ohio (1967).

120. A P HATTON and I S HALL, Photographic study of boiling on prepared surfaces, Proc. 3rd Int. Heat Transf. Conf. 4, 24-37, Chicago (1966).

121. M SHOUKRI and R L JUDD, Nucleation site activation in saturated boiling, J. Heat Transfer C97, 93-98 (1975).

122. Y Y HSU, On the size range of active nucleation cavities on a heating surface, J. Heat Transfer C84, 207-216 (1962).

123. D L J ANDERSON, A photographic investigation of saturated nucleate boiling, M. Eng. Thesis in Mech. Engng, McMaster University, Hamilton, Ontario (1969).

124. H H JAWUREK, Nucleation during boiling with special reference to its cessation at low pressure, M.Sc. Thesis in Chem. Engng, University of Cape Town, Rondebosch (1962).

125. H J IVEY, Relationships between bubble frequency, departure diameter and rise velocity in nucleate boiling, Int. J. Heat Mass Transfer 10, 1023-1040 (1967).

126. B E STANISZEWSKI, Nucleate boiling bubble growth and departure, Techn. Rept. No. 16, Div. Sponsored Res., Massachusetts Inst. Techn., Cambridge, Mass. (1959).

127. R COLE and H L SHULMAN, Bubble departure diameters at subatmospheric pressures, Chem. Engng Progr. Symposium Ser. No. 64, 62, 6-16 (1966).

128. G W PRECKSHOT and V E DENNY, Exploration of surface and cavity properties on the nucleate boiling of carbon tetrachloride, Canad. J. Chem. Engng 45, 211-246 (1967).

129. H S PERKINS and J W WESTWATER, Measurements of bubbles formed in boiling methanol, Amer. Inst. Chem. Engrs J. 2, 471-476 (1956).

130. R L NICKELSON and G W PRECKSHOT, Observations on boiling carbon tetrachloride from surfaces, J. Chem. Engng Data 5, 310-315 (1960).

131. P W McFADDEN and P GRASSMANN, The relation between bubble frequency and diameter during nucleate pool boiling, Int. J. Heat Mass Transfer 5, 169-173 (1962).

132. R SÉMÉRIA, Caractéristiques des bulles de vapeur sur une paroi chauffante dans l'eau en ébullition à haute pression, Compt. Rend. Acad. Sci. Paris 256, 1227-1230 (1963).

133. W WANNINGER, Dynamik von Dampfblasen in Propan, Chemie-Ing. Techn. 37, 939-943 (1965)

134. V I TOLUBINSKY and J N OSTROVSKY, On the mechanism of boiling heat transfer (vapour bubbles growth rate in the process of boiling of liquids, solutions and binary mixtures), Int. J. Heat Mass Transfer 9, 1463-1470 (1966).

135. M FISHENDEN and O M SAUNDERS, Heat Transfer. University Press, Oxford (1950).

136. H GRÖBER, S ERK and U GRIGULL, Die Grundgesetze der Wärmeübertragung, 3rd ed. Springer, Berlin (1961).

137. VEREIN DEUTSCHER INGENIEURE, VDI-Wärmeatlas. VDI-Verlag, Düsseldorf (1963).

138. S T HSU and F W SCHMIDT, Measured variations in local surface temperatures in pool boiling of water, J. Heat Transfer C83, 254-260 (1961).

138a. A KOVACS and R B MESLER, Making and testing small surface thermocouples for fast response, Rev. Sci. Instruments 35, 485-488 (1964).

139. M A JOHNSON, J DE LA PEÑA and R B MESLER, Bubble shapes in nucleate boiling, Amer. Inst. Chem. Engrs J. 12, 344-348 (1966).

140. R MORIN, What is boiling? Euratom 5, 109-117 (1966).

141. R B ROEMER, Surface temeprature fluctuations during steady state boiling, Int J. Heat Mass Transfer 13, 985-995 (1970).

142. S J D VAN STRALEN, R COLE, W M SLUYTER and M S SOHAL, Bubble growth rates in nucleate boiling of water at subatmospheric pressures, Int. J. Heat Mass Transfer 18, 655-669 (1975).

143. S J D VAN STRALEN, M S SOHAL, R COLE and W M SLUYTER, Bubble growth rates in pure and binary systems: combined effect of relaxation and evaporation microlayers, Int. J. Heat Mass Transfer 18, 453-467 (1975).

144. M G COOPER and A J P LLOYD, Miniature thin film thermometers with rapid response, J. Sci. Instrum. 42, 791-793 (1965).

145. G E FOLTZ and R B MESLER, The measurement of surface temperatures with platinum films during nucleate boiling of water, Amer. Inst. Chem. Engrs J. 16, 44-48 (1970).

146. F A JENKINS and H E WHITE, Fundamentals of Optics, 3rd ed. McGraw-Hill, New York (1957).

147. R R OLANDER and R G WATTS, An analytical expression of microlayer thickness in nucleate boiling, J. Heat Transfer C91, 178-180 (1969).

148. J G KNUDSEN and D L KATZ, Fluid Dynamics and Heat Transfer, Chap.10. McGraw-Hill, New York (1958).

149. L E SCRIVEN, On the dynamics of phase growth, Chem. Engng Sci. 10, 1-13 (1959).

150. R L JUDD, Comparison of experimental microlayer thickness results, Trans. Canad. Soc. Mech. Engng 1, 168-170 (1972).

151. C M VOUTSINOS and R L JUDD, Laser interferometric investigation of the microlayer evaporation phenomenon, J. Heat Transfer C97, 88-92 (1975).

152. H H JAWUREK, Simultaneous determination of microlayer geometry and bubble growth in nucleate boiling, Int. J. Heat Mass Transfer 12, 843-848 (1969).

153. L HOLLAND, Vacuum Deposition of Thin Films. Chapman and Hall, London (1958).

154. D B KIRBY and J W WESTWATER, Photography from below: nucleate boiling on electrically heated horizontal glass plates, Chem. Eng. Sci. 18, 469 (1963).

155. Y Y HSU, Gradual transition of nucleate boiling from discrete bubble regime to multi-bubble regime, Chem. Engng Progr. Symp. Ser. 61, No.59, 290-298 (1965).

156. LIBBEY-OWENS-FORD GLASS COMPANY Electrically conducting films and method of application, British Patent 632256, (Oct. 1942).

157. R E AITCHISON, Transparent semi-conducting oxide films, Australian J. Appl. Sci. 5, 10-17 (1954).

158. LIBBEY-OWENS-FORD GLASS COMPANY Controlling resistivity of electrically conducting films, British Patent 671767 (Ap. 1949).

159. LIBBEY-OWENS-FORD GLASS COMPANY Light transmissive electrically conducting optical articles suitable for use as a lens, a window or windshield or the like, British Patent 682264 (Ap. 1949).

160. LIBBEY-OWENS-FORD GLASS COMPANY Transparent electrically conducting films, British Patent 682342 (July 1949).

161. LIBBEY-OWENS-FORD GLASS COMPANY Electrode connections to conducting films on vitreous surfaces, British Patent 686280 (Dec. 1949).

162. R B BELSER, A technique of soldering to thin metal films, Rev. Sci. Inst. 22, 180 (1954).

163. H H MANKO, Solders and Soldering, p.100-105. McGraw-Hill (1964).

164. R B BELSER, Indium - a versatile solder to metals and non-metals. The Indium Corporation of America (Undated; probably 1952). (Copy obtained from author).

165. M S TARNOPOL, Treatment of films with liquid, U.S. Patent 2606566 (1952).

166. W J KARPLUS, Analogue Simulation, Chap.5. McGraw-Hill, New York (1958).

167. C J RALLIS, N H FREED and C L SUZMAN, Conducting sheet analogue for solution of potential problems, Dep. Mech. Engng Report 1/60 University of the Witwatersrand, Johannesburg (1960).

168. L YOUNG, Anodic oxide films, pp 193,216. Academic Press, London (1961).

169. G HASS, On the preparation of hard oxide films with precisely controlled thickness on evaporated aluminium mirrors, J. Opt. Soc. Amer. 39, 532-540 (1949).

170. J J SPADARO, H L I VIX and E A GASTROCK, Simple automatic control for vacuum systems, Ind. Engng Chem. (Anal. Secn). 18, 214 (1946).

171. D K CRAIG, Barometers and barometer calibrations, J. Mine Ventilation Soc. S.Africa 11, No.2, 25-42 (1958).

172. M. FRANÇON, Optical Interferometry, Chap. 3. Academic Press, New York (1966).

173. A VASÍCEK, Optics of Thin Films. North Holland, Amsterdam (1960).

174. N A LANGE (ed.), Handbook of Chemistry. McGraw-Hill, New York (1961).

175. Y KATTO and M SHOJI, Principal mechanism of micro-liquid-layer formation on a solid surface with a growing bubble in nucleate boiling, Int. J. Heat Mass Transfer 13, 1299-1311 (1970).

176. ANON., Forced cooled super-high mercury lamps. Brochure 10.077 BE 2/60. Philips, Eindhoven (1960).

177. ANON., Lamp Catalogue, Brochure 15.002 BE 5/65, p 119. Philips, Eindhoven (1965).

178. H K BOURNE, Discharge Lamps for Photography and Projection. Chapman and Hall, London (1948).

179. J W GATES, Interferometry with lasers, Paper 38, Conference 'Lasers and their Applications', Inst. Elec. Engrs, London (1964).

180. J TERRIEN, The visibility of two-beam interference, its measurement and its spectroscopic interpretation, Paper 5-5, Nat. Phys. Lab. Symposium No.11 'Interferometry'. Her Majesty's Stationery Office, London (1960).

181. D W HOLDER and R J NORTH Schlieren Methods, (Nat. Phys. Lab. Notes on Appl. Science No. 31) p 35-58. Her Majesty's Stationery Office, London (1963).

182. R F SAXE High-speed Photography, Chap. 2. Focal Press, London (1966).

183. W G HYZER, Engineering and Scientific High-speed Photography. MacMillan, New York (1962).

184. M G COOPER, The microlayer and bubble growth in nucleate pool boiling, Int. J. Heat Mass Transfer 12, 915-933 (1969).

185. M S PLESSET and J A ZWICK, The growth of vapour bubbles in superheated liquids, J. Appl. Phys. 25, 193-500 (1954).

186. H K FORSTER and N ZUBER, Growth of a vapour bubble in a superheated fluid, J. Appl. Phys. 25, 474-488 (1954).

187. K SCHREBER, Der Vorgang der Dampfentwicklung, Z. Techn. Physik 14, 81-85 (1933).

188. H MACHE, Der Verdampfungskoeffizient des Wassers und zwei Verfahren zu seiner Bestimmung, Z. Physik 107, 310-321 (1937).

189. H MACHE, Weitere Versuche über den Verdampfungskoeffizienten des Wassers, Z. Physik 110, 189-196 (1938).

190. W PRÜGER, Die Verdampfungsgeschwindigkeit der Flüssigkeiten, Z. Physik 115, 202-244 (1940).

191. T ALTY and C A MacKAY, The accommodation coefficient and the evaporation coefficient of water, Proc. Roy. Soc. (London) 149A, 104-116 (1935).

192. R W SCHRAGE, A Theoretical Study of Interphase Mass Transfer, Chaps 2, 3. Columbia Univ. Press, New York (1953); authorised facsimile: University Microfilms, Ann Arbor (1969).

193. A F MILLS and R A SEBAN, The condensation coefficient of water, Int. J. Heat Mass Transfer 10, 1815-1827 (1967).

194. D G KRÖGER, Interphase mass and energy transfer during condensation, S. Afr. Chem. Processing 6, No. 2, 40-45 (1971).

195. H H WYLLIE, Evaporation and the surface structure of liquids, Proc. Roy. Soc. (London) 197A, 383-395 (1949).

196. L J DELANEY, N J PSALTIS and L C EAGLETON, The rate of vaporization of methanol, Chem. Engng Sci. 20, 607-620 (1965).

197. H BUCKA, Über den Kondensationskoeffizienten von Äthylalkohol und ein Verfahren zur Bestimmung von Kondensationskoeffizienten, Z. Physikalische Chemie 195, 260-269 (1949).

198. L VON FOGDANDY, H G KLEIST and O KNACKE, Die Verdampfungsgeschwindigkeit von Äthylalkohol, Tetrachlorkohlenstoff und Zinn (II) - Chlorid, Z. Elektrochemie 59, 460-462 (1955).

199. L SLEGERS and R A SEBAN, Nusselt condensation of n-butyl alcohol, Int. J. Heat Mass Transfer 12, 237-239 (1969).

200. P A KICSKA and W R SMITH, Vapour condensation in a shock tube; condensation coefficient for sec-butyl alcohol, J. Chem. Phys. 47, 1418-1427 (1967).

201. D YOUNG, The numerical solution of elliptic and parabolic partial differential equations, Survey of Numerical Analysis (ed. J Todd), Chap. 11. McGraw-Hill, New York (1962).

202. G D SMITH, Numerical Solution of Partial Differential Equations, Chaps. 1-3. Oxford University Press, London (1965).

203. W D MURRAY and F LANDIS, Numerical and machine solutions of transient heat-conduction problems involving melting or freezing, J. Heat Transfer C81, 106-112 (1959).

204. W L HEITZ and J W WESTWATER, Extension of the numerical method for melting and freezing problems, Int. J. Heat Mass Transfer 13, 1371-1375 (1970).

205. V K SAULYEV, Integration of Equations of Parabolic Type by the Method of Nets, (International Series of Monographs on Pure and Applied Mathematics, Vol. 54). Pergamon Press, Oxford (1964).

206. A M STARFIELD, Department of Applied Mathematics, Computer Science and Statistics, University of the Witwatersrand, Johannesburg. Personal communication (1975).

207. J H TALBOT, Talbot Research, P O Box 56290, Pinegowrie, 2125 South Africa. Personal communication (1976).

208. A GOLDSMITH, T E WATERMAN and H J HIRSCHHORN, Handbook of Thermal Properties of Solid Materials, Vol 3. MacMillan, New York (1961).

209. W M ROHSENOW and C CHOI, Heat Mass and Momentum Transfer. Prentice-Hall, Englewood Cliffs N.J. (1961).

210. E W WASHBURN (ed.), International Critical Tables, McGraw-Hill, New York (1926).

211. H S CARSLAW and J C JAEGER, Conduction of Heat in Solids 2nd ed. University Press, Oxford (1959).

212. M S PLESSET and R B CHAPMAN, Collapse of an initially spherical vapour cavity in the neighbourhood of a solid boundary, J. Fluid Mech. 47, 283-290 (1971).

213. R C REID and T K SHERWOOD, The Properties of Gases and Liquids. McGraw-Hill, New York (1958).

214. R C WEAST (ed.), Handbook of Chemistry and Physics, 52nd ed. Chemical Rubber Co., Cleveland, Ohio (1971).

215. O A HOUGEN, K M WATSON and R A RAGATZ, Chemical Process Principles, Part 2, 2nd ed. Chap. 14. John Wiley, New York (1959).

216. J H PERRY (ed.), Chemical Engineers' Handbook, 3rd ed. McGraw-Hill, New York (1950).

217. ANON., Comparative physical properties and refrigerant characteristics of DAIFLON compounds, Daikin Kogyo Co., Ltd., Osaka, Japan (undated).

218. S GLASSTONE, Textbook of Physical Chemistry, 2nd ed., pp 494-499 and 526. Van Nostrand, Princeton (1946).

219. R C REID and T K SHERWOOD, The Properties of Gases and Liquids, 2nd ed. McGraw-Hill, New York (1966).

220. P G GUEST, Numerical Methods of Curve Fitting, p. 336. Cambridge University Press, London (1961).

221. N R DRAPER and H SMITH, Applied Regression Analysis, pp 55-56, 267-273. Wiley, New York (1966).

222. G F DE VRIES, 'PELSQ', 'n FORTRAN-program vir kleinste kwadrate berekenings, S.A. Atomic Energy Board Report PIN 12(BR), Pelindaba (1968).

223. E L CROW, F A DAVIS and M W MAXFIELD, Statistics Manual. Dover, New York (1960).

224. O L DAVIES, Statistical Methods in Research and Production. Oliver and Boyd, London (1958).